VIBRATION ANALYSIS OF A HAND-HELD PERCUSSION TOOL COUPLED WITH THE HAND-ARM SYSTEM

Shu Wang

A Thesis

in

The Department

of

Mechanical and Industrial Engineering

Presented in Partial Fulfillment of the Requirements
for
The Degree of Master of Applied Science
at
Concordia University
Montreal, Quebec, Canada

June 2014

© Shu Wang 2014

CONCORDIA UNIVERSITY

SCHOOL OF GRADUATE STUDIES

This is to certify that the Thesis prepared,

By: **Shu Wang**

Entitled: **"Vibration Analysis of a Hand-Held Percussion Tool Coupled with the Hand-Arm System"**

and submitted in partial fulfillment of the requirements for the Degree of

Master of Applied Science (Mechanical Engineering)

complies with the regulations of this University and meets the accepted standards with respect to originality and quality.

Signed by the Final Examining Committee:

_____ Chair
Dr. M. Paraschivoiu

_____ Examiner
Dr. M. Packirisamy

_____ Examiner
Dr. A. Bagchi   External
Building, Civil and Environmental Engineering

_____ Supervisor
Dr. S. Rakheja

_____ Co-Supervisor
Dr. P-E. Boileau

Approved by: _____
Dr. S. Narayanswamy, MASc Graduate Program Director
Department of Mechanical and Industrial Engineering

_____
Dr. C. Trueman, Interim Dean
Faculty of Engineering & Computer Science

Date: _____

ABSTRACT

**VIBRATION ANALYSIS OF A HAND-HELD PERCUSSION TOOL COUPLED
WITH THE HAND-ARM SYSTEM**

Shu Wang, Master of Applied Science

Concordia University, 2014

Exposure to hand-transmitted vibration (HTV) arising from hand power tools has long been associated with several disorders of the hand and arm, which are collectively termed as hand-arm vibration syndrome (HAVS). Owing to high prevalence of HAVS among the operators of the power tools, particularly the percussive tools, the desire to develop low vibration tool designs, has been widely recognized. The design of vibration isolators or assessment of vibration performance of tools necessitates development of dynamic model of the tool coupled with that of the hand-arm system (HAS) to account for energy absorption within the HAS.

This dissertation research is aimed at development of dynamic model of a percussive chipping hammer together with a biomechanical model of the hand-arm system. The model could serve as an essential tool for identifying effective vibration attenuation design features. The dynamic model of the tool is formulated considering identifications of various component contact pairs and the air flows between the primary piston and the striker. A tool tip-workpiece contact model is integrated to the tool model to describe the interactions between the tool and an energy dissipator. A biomechanical model of the hand-arm system is implemented to the tool model to develop a coupled hand-tool system, which could be applied to determine the hand vibration responses as a

function of the push force. The properties of different impact pairs are identified from the theory of visco-elastic collision between rigid bodies. The validity of the hand-tool model is examined on the basis of available measured data under selected levels of the hand push force. A simple model of an anti-vibration glove is further introduced to study its effectiveness in limiting the vibration exposure.

The simulation results show that the percussive tool model coupled with the biomechanical hand-arm model can yield reasonably good trends in view of the hand-transmitted vibration. The results suggest that the tool vibration transmitted to the hand is more sensitive to variations in push force and the operating speed. Slight increases in the diameter of the upper chamber orifices and the weight of the tool body, together with lower the striker mass, could yield notable reductions in the magnitudes of vibration transmitted to the hand-arm system. The results further show that the anti-vibration gloves yield very minimal vibration attenuation.

ACKNOWLEDGMENTS

I wish to express my sincere gratitude to my supervisors, Dr. Subhash Rakheja and Dr. Paul-Emile Boileau, for their guidance, encouragement, supervision and support during all stages of this research. The contributions and assistance of the Department of Mechanical and Industrial Engineering at Concordia University are also appreciated and acknowledged.

Appreciation is also due to my friends, Ning Zhou, Danying Zheng, Tengfei Han, Yuxiang Li and Yuming Yin, and my colleagues for their assistance during my study.

Finally, I would like to thank my parents, aunt, grandparents and other family members for their love, patience, understanding and support throughout this research. I sincerely appreciate everything you all did for me.

CONTENTS

LIST OF FIGURES

xii

LIST OF TABLES

LIST OF ABBREVIATIONS AND SYMBOLS

$A(8)$	Total daily vibration dosage
a_{hi}	Root mean square acceleration recorded at each center frequency
a_{hw}	Frequency-weighted R.M.S acceleration
A_{LC}	Effective cross section area of lower chamber
A_{LH}	Total cross section area of lower orifices
A_{UC}	Cross section area of upper chamber
A_{UH}	Total cross section area of upper orifices
bpm	Blow per minute
$c_1, c_2 \ldots$	Damping coefficients in relative hand arm models
C_a	Assumed damping coefficient of contact pair
C_{AU}	Fraction of upper orifices opening in upper chamber
C_b	Rotational damping coefficient of trunk
c_{BT}	Damping coefficient at impact bolt-tool tip contact pair
c_{CB}	Damping coefficient at tool body-impact bolt contact pair
c_e	Damping coefficient at elbow
C_e	Rotational damping coefficient at elbow
$c_g, c_{g1}, c_{g2},$	Damping coefficients of selected anti-vibration glove
C_P	Damping coefficient of workpiece plastic zone
c_s	Damping coefficient at shoulder
C_s	Rotational damping coefficient at shoulder
c_{SB}	Damping coefficient at striker-impact bolt contact pair
c_{FT}	Fluid friction coefficients at lubricant viscous layer between tool tip holder and tool tip

c_{FS}	Fluid friction coefficients at lubricant viscous layer between guide tube and striker
c_w	Damping coefficient at wrist
D_{LH}	Diameter of lower orifices
D_{UH}	Diameter of upper orifices
F_{BT}	Contact force between impact bolt and tool tip
F_{CB}	Contact force between tool body and impact bolt
$F_{dfinger}$	Dynamic finger force exerted by operator on tool handle
F_{dh}	Dynamic force exerted by operator's hand on tool handle
F_{dpalm}	Dynamic palm force exerted by operator on tool handle
F_{push}	Static push force exerted by operator's hand
F_{SB}	Contact force between striker and impact bolt
F_S	Restoring force generated by the spring wrapping around guide tube
$(F_S)_{min}$	Initial resorting spring force when the control bushing sits upon the lower control disk
$F_{sfinger}$	Static finger force exerted by operator on tool handle
F_{sh}	Static force exerted by operator's hand on tool handle
F_{spalm}	Static palm force exerted by operator on tool handle
F_{TG}	Contact force between tool tip and workpiece
F_{FT}	Idealized viscous friction between tool tip holder and tool tip
F_{FS}	Idealized viscous friction between guide tube and striker
g	Gravitational acceleration
h	Height of lumped trunk
$k_1, k_2 \ldots$	Stiffness coefficients in relative hand arm models

K_a	Assumed stiffness coefficient of contact pair
K_b	Torsional stiffness of trunk
k_{BT}	Stiffness coefficient at impact bolt-tool tip contact pair
k_{CB}	Stiffness coefficient at tool body-impact bolt contact pair
k_e	Stiffness coefficient at elbow
K_e	Torsional stiffness coefficient at elbow
$k_g,\ k_{g1},\ k_{g2},$	Stiffness coefficients of selected anti-vibration glove
K_P	Stiffness coefficient of workpiece plastic zone
K_E	Stiffness coefficient of workpiece elastic zone
k_s	Stiffness coefficient at shoulder
K_s	Torsional stiffness coefficient at shoulder
k_{SB}	Stiffness coefficient at striker-impact bolt contact pair
k_S	Stiffness coefficient of spring wrapping around control bushing
k_w	Stiffness coefficient at wrist
$(L_{BC})_{min}$	Displacement of impact bolt relative to tool body at their contact
$(L_{BS})_{min}$	Displacement of impact bolt relative to striker at their contact
$(L_{CBC})_{max}$	Displacement of control bushing relative to tool body when it sits on upper control disk
L_{CB}	Length of control bushing
l_{rod}	Effective length of connecting rod
$L_{SL},\ L_{SU}$	Length of lower and upper striker thicknesses
$(L_{SP})_{min}$	Displacement of striker relative to piston at their contact
$(L_{TB})_{min}$	Displacement of tool tip relative to impact bolt at their contact
L_{UCD}	Displacement of impact bolt relative to control bushing when control bushing is supported by lower control disk

xviii

l_{ue}, l_{us}	Distances from the center of upper-arm mass to the joints of elbow and shoulder respectively
L_{UH}, L_{LH}	Relative displacements of upper and lower orifices
$m_1, m_2 \ldots$	Equivalent masses in relative hand arm models
M_b	Mass of impact bolt
m_b	Lumped mass of trunk
M_c	Lumped mass of tool body
m_f	Lumped mass of fingers
m_{fa}	Lumped mass of fore-arm
m_p	Lumped mass of palm
M_s	Mass of striker
M_t	Mass of tool tip
m_{tf}	Lumped mass of finger tissue
m_{tfg}	Lumped mass of finger tissue and glove material
m_{tp}	Lumped mass of palm tissue
m_{tpg}	Lumped mass of palm tissue and glove material
m_{ua}	Lumped mass of upper arm
P_a	Atmospheric pressure
P_{LC}	Air pressure of lower chamber
P_{UC}	Air pressure of upper chamber
r_c	Effective crank radius
t	Time
V_{app}	Approaching velocity
V_{UE}	Outward flow velocity for upper chamber

V_{UI}	Inward flow velocity for upper chamber
V_{sep}	Velocity of separation
w_i	Defined weighting factor for related one-third-octave band
x_h, y_h, z_h	ISO defined coordinate system
z_{BC}	Displacement of impact bolt relative to tool body
z_C	Displacement of tool body
z_{CBC}	Displacement of control bushing relative to tool body
z_E	Displacement of workpiece elastic zone lower end
z_f	Displacement of fingers
z_{fa}	Displacement of fore-arm
z_h	Static deflection of hand
z_p	Displacement of palm
z_{PC}	Displacement of piston relative to tool body
z_{SC}	Displacement of striker relative to tool body
z_{TC}	Displacement of tool tip relative to tool body
z_{ua}	Displacement of upper arm
$\dot{z}_{BC}$	Velocity of impact bolt relative to tool body
$\dot{z}_C$	Velocity of tool body
$\dot{z}_E$	Velocity of workpiece elastic zone lower end
$\dot{z}_f$	Velocity of fingers
$\dot{z}_{fa}$	Velocity of fore-arm
$\dot{z}_p$	Velocity of palm
$\dot{z}_{PC}$	Velocity of piston relative to tool body
$\dot{z}_{SC}$	Velocity of striker relative to tool body

$\dot{z}_{TC}$	Velocity of tool tip relative to tool body
$\dot{z}_{ua}$	Velocity of upper arm
γ	Adiabatic constant
ε	coefficient of restitution
ζ	Damping ratio
θ	Defined crank angle
θ_b	Angular displacement of trunk
θ_{ua}	Angular displacement of upper arm
τ	Impact duration
ω_C	Angular velocity of crank
ω_d	Damped frequency
ω_n	Natural frequency

CHAPTER 1
LITERATURE REVIEW AND OBJECTIVES

1.1 General

Hand-held power tools, widely used in the industrial sectors, are known to transmit substantial vibrations to the operator's hand and arm. Depending on the operating conditions and other related determinants, exposure to hand-transmitted vibration (HTV) has been associated with an array of adverse health effects, including vascular, neurological and musculoskeletal disorders, collectively termed as hand-arm vibration syndrome (HAVS) (Gemne and Taylor, 1983; Bovenzi, 1998). In the U.S.A, over one million workers are continually exposed to HTV (NIOSH, 1989; BLS, 2004). A Canadian study estimated that approximately 200,000 operators are occupationally subjected to HTV (Brammer, 1984).

Over the past few decades, substantial clinical and epidemiological efforts have been made to explore and comprehend the phenomenon of HAVS. In the U.S.A, NIOSH (1989) has reported that the HAVS prevalence among the vibrating tools operator population ranges from 6% to 100%, with an average of about 50%. A number of standardized methods have also evolved to assess the HTV exposure in view of probable risk of HAVS (ISO 5349, 1986; ISO 5349-1, 2001). Considerable efforts have also been made to characterize mechanical properties of the human hand arm system (HAS) in terms of driving-point mechanical impedance, vibration power absorption, and vibration transmissibility of different segments of the HAS (Goel and Kwan, 1987; ISO 10068, 1998; 2012; Rakheja et al., 2002c; Dong et al., 2005; Adewusi, 2009).

1

The diversity in physical characteristics of the operators and variabilities in the environmental conditions such as temperature have been judged as the contributory factors to HTV-induced health effects. The characteristics of HTV, however, such as frequency and magnitude, and the cumulative exposure, have been of the primary concern (Griffin, 1990; Pelmear and Wasserman, 1998). Considerable efforts have been towards designs of anti-vibration gloves (Gurram et al., 1994; Hewitt, 1998; Pinto et al., 2001; Dong et al., 2005; 2009) and handle vibration isolators (Suggs and Abrams, 1983; Strydom et al., 2002; Oddo et al., 2004; Ko et al., 2011). Control of vibration at the source through designs of low vibration tools, however, has been attempted in a very few studies. This is most likely due to highly compact tool designs, and complexities associated with modeling and characterization of highly nonlinear interactions among the tools' subsystems. Consequently, analytical design tools do not yet exist, particularly for hand-held percussion tools.

Analyses of vibration transmission properties of hand-held power tools involve characterizations of subsystems and their interactions together with an appropriate model of the human hand arm system. This dissertation research is aimed at development of an analytical model of a hand-held percussion tool coupled with a comprehensive HAS dynamic model. The model is developed for a chipping hammer through integration of various impact pair models. The properties of each impact pair are characterized in terms of equivalent stiffness and damping, which are identified from the elastic-plastic impact theory. A six degrees-of-freedom biomechanical model of the HAS is integrated to the tool handle, and the anti-vibration glove effect is incorporated assuming linear stiffness and damping properties of the glove. The validity of the model is also explored using the

data acquired with the tool operating in an energy dissipator. The variations in different design parameters on the vibration emission characteristics of the tool are finally investigated to seek essential design guidance.

1.2 Literature Review

The study of vibration emission properties of a hand-held power tool encompasses various challenges in assessments of HTV, hand-arm vibration syndrome, tool design and tool subsystems' characterization and modeling, vibration isolation mechanisms and vibration absorption characteristics of the HAS. The reported relevant studies are thus reviewed to build essential background and knowledge on appropriate methods and the design issues. These, grouped under the relevant topics, are summarized below.

1.2.1 The Hand-Arm Vibration Syndrome (HAVS)

Continuous exposure to hand-transmitted vibration (HTV) can induce excessive stress and deformations in the substructures of the hand-arm system (HAS) such as nerve cells, tissues and bones, which may cause several disorders or injuries. Numerous epidemiological and clinical investigations have reported high prevalence of vascular, neural and musculoskeletal disorders among hand-tools operators (Brammer and Taylor, 1982; Brammer, 1984; NIOSH, 1997). The complex biological properties of the HAS and wide variations in HTV, together with various confounders such as working posture, hand forces, and types of tool and task, make it very difficult to identify specific causative factors of the HAVS. The reported studies have classified HAVS into four

groups of disorders, namely, vascular, neurological, muscular, and bones and joints disorders.

Intermittent episodes of blanching in the fingers and palm were reported as the early signs of vascular disorders associated with HTV coupled with exposure to cold (Iwata, 1968; Miyashita et al., 1983; Brubaker et al., 1986; Taylor, 1988). Increased frequency and severity of such episodes have been reported with continued HTV exposure. When exposed to cold temperatures, the vibration-induced contraction changes in muscles and vessels may markedly limit or completely block the blood supply towards the affected segment, resulting in severe pain and white finger (Pyykkö et al., 1976 and 1978; Griffin, 1990; Bovenzi et al., 2000). Such symptoms have been typically termed as the Raynaud's syndrome (Griffin, 1990; Bovenzi, 1998). Owing to such pathology, vibration-induced white finger (VWF) has the greatest prevalence in regions where the risk of exposure to cold is the highest (Riera et al., 1993; Maricq et al., 1993 and 1997; Bovenzi, 1998). Due to the dynamic strains from HTV, the distorted shapes of capillaries and blood vessels may lead to partial reductions in the blood flow, which is regarded as one of the contributory factors of Raynaud's syndrome, while the effects of other confounders such as gender, age, tobacco, and general health have not yet been understood (Palesch et al., 1999; Fraenkel al., 1999).

The typical symptoms of the peripheral neural disorder have been mostly referred to as pins and needles like tingling. The potentially affected segments can mostly be fingers, while palm or wrist may also be affected. Along with episodic swelling, operators may temporally experience the reduction in the sense of temperature, touch and manual sensitivity (Hjortsberg et al., 1989; Bovenzi, 1998). The growth in the intensity as

4

well as the daily dosage of HTV tends to enhance such symptoms with decrease or loss in sensory perception, manipulative dexterity and tactile sensibility, which are more resistant than the vascular ones (Bovenzi, 1998). Clinical and epidemiology studies have indicated that operators using chipping hammers or grinders have higher prevalence of neurological disorders (Griffin 1990; Gemne et al., 1993).

It has been also suggested that disorders of the central nervous system may be a products of the prolonged HTV exposure. Several central nervous symptoms such as over-activity of the cardiovascular responses (Hyvärinen et al., 1973), autonomic dysfunction (Banister and Smith, 1972), headache and insomnia (Watanabe, 1966) have been widely reported. However, owing to the complexity of the central nervous system and the inadequate prevalence data, the primarily causative factor is not yet clearly known.

Prolonged and excessive HTV exposure may likewise cause serious muscular disorders known as muscle fatigue, perennial muscular weakness and muscle force degeneration. High occurrences of muscle fatigue in the hands and arms of forest workers have been reported in various studies (Matsumoto et al., 1977; Farkkila et al., 1982), which are attributed to inadequate muscle contraction under extensive dosage of HTV. Associated with vibration-induced digital neural disorder or direct mechanical injury, these muscular disorders can lead to a remarkable reduction in the manipulative dexterity such as decrease of hand and finger-grip strength (Bannister et al., 1972). In some extreme cases, these muscle disorders can even become a form of disability such as chronic disturbance or even loss of fine motor control ability.

5

High prevalence of bone injuries among vibration-exposed operators, such as decalcification, vacuoles and cysts in hands and wrists, has also been reported in some early radiology studies. A relatively higher risk of ossifications in elbow tendon insertion and elbow arthritis exists among the coal miners, metal working workers and road construction workers, who are exposed to low-frequency but high magnitude vibration (Gemne and Saraste, 1987). Other studies, however, reported this risk to be only slightly higher than the manual workers, when the influence of age is taken into account (Härkönen et al., 1984; Bovenzi et al., 1987). Accordingly, it has been suggested that apart from HTV, awkward hand-arm position, overload due to heavy manual work in joints and other bio-mechanical factors can also contribute to higher prevalence of bone and joint disorders (Taylor and Brammer, 1982; Härkönen et al., 1984; Bovenziet al., 1987; Gemne and Saraste, 1987). Consequently, at present, a definite pathology of vibration-induced bone and joint disorders has not yet been identified.

1.2.2 Hand-Transmitted Vibration (HTV) and Exposure Assessments

Owing to the well-established correlations between the HTV exposure and various health disorders, considerable efforts have been made towards measurements and assessment of HTV. The International Organization for Standardization (ISO) has defined standardized methods for measurements, evaluations and risk assessments of HTV. The standard, ISO 5349-1 (2001), defines a dose-response relation for assessing probable vibration-induced white finger (VWF) risk of HTV exposure, and frequency weighting to determine the exposure, often expressed by eight-hour energy-equivalent vibration total value. The standard also provides vibration measurement method apart from guidance for assessing risk of VWF. The ISO 5349-2 (2001) recommends practical

regulations for measurements at the workplace such as the measurement procedure and the measurement uncertainty. Laboratory methods for measurements of HTV of different hand-held power tools have been described in ISO 8662 standards (1988; 1999).

The vast majority of hand-held power tools transmit vibration along multi-axes. The standard ISO 5348 (1998) defines two coordinate systems, basicentric and biodynamic, which provide guidance for mounting of transducers and measurements for handgrip and flat palm postures, respectively. Figure 1.1 shows the proposed handgrip position coordinate systems.
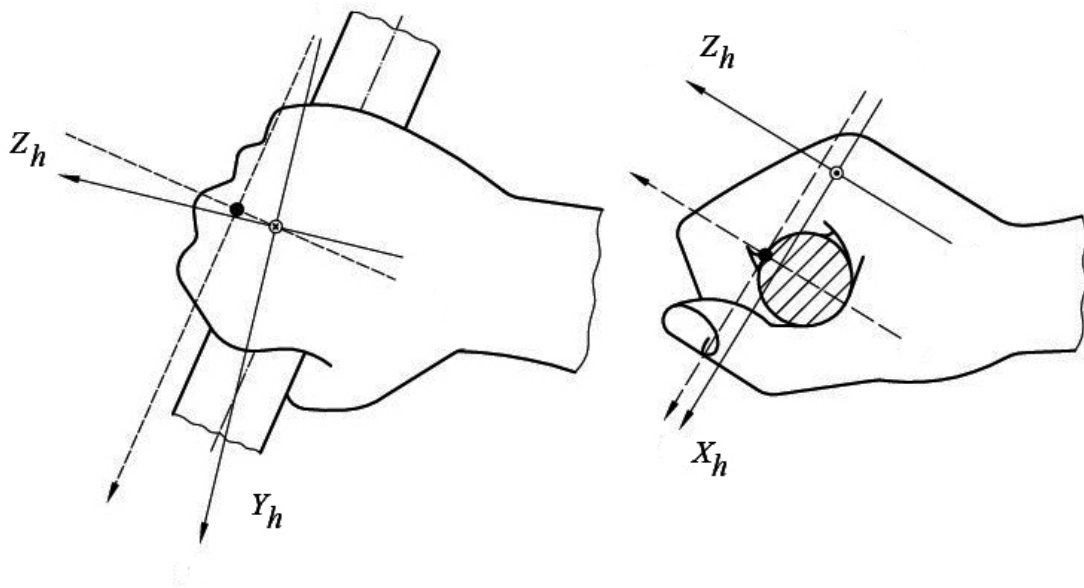
a) ------ Biodynamic coordinate system; and b) —— Basicentric coordinate system
Figure 1.1 : Coordinate systems for the human hand-arm (ISO 5348, 1998)

The HTV is measured along each orthogonal axis simultaneously, while the defined frequency-weighting and band-limiting filters are used to obtain HTV exposure in terms of frequency-weighted root-mean-square (r.m.s.) acceleration or eight-hour

equivalent energy for assessing the exposure risk (ISO 5349, 1986; 2001). Figure 1.2 illustrates the frequency-weighting, W_h, defined in ISO-5349-1 (2001).

The frequency-weighted r.m.s. acceleration, a_{hw}, due to vibratrion exposure, is obtained from:

$$a_{hw} = \sqrt{\sum_i (a_{hi} w_{hi})^2}$$ (1.1)

where a_{hi} is the r.m.s. acceleration due to vibration in the ith center frequency, f_i, of the one-third-octave band and w_{hi} is the weighting factor corresponding to the center frequency f_i.
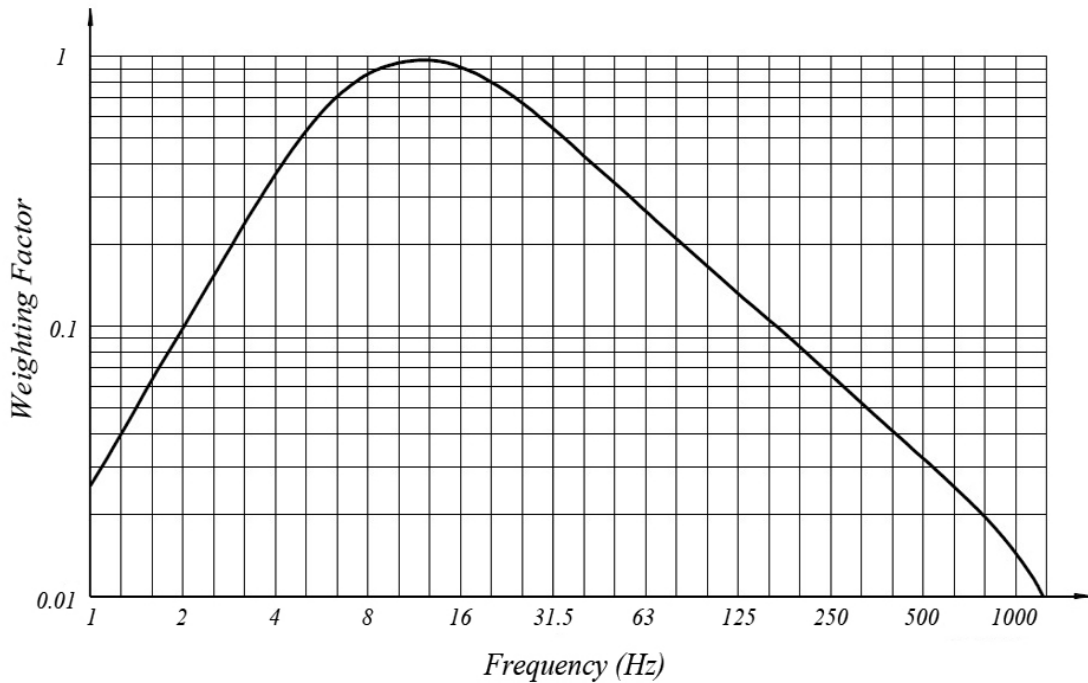
Figure 1.2 : Frequency-weighting curve for hand-transmitted vibration (ISO 5349-1, 2001)

The standard assumes identical frequency weighting along each orthogonal axis to compute the total value of vibration exposure as the vector sum of weighted accelerations

along the three axes, and the total daily vibration dosage in terms of eight-hour energy, A(8) (ISO 5349-1, 2001).

This proposed guidance for assessing the HTV exposure risk has been further adopted by the directive of the European Union (EU, 2002) and the ANSI (ANSI S2.70, 2006). The EU directive limits exposure value for hand-arm vibration to no greater than 5 m/s^2. The directive also recommends a daily exposure action value of 2.5 m/s^2 as the threshold of hand-transmitted vibration induced syndrome. Accordingly, appropriate HTV-protections are recommended to attenuate the vibration exposure exceeding 2.5 m/s^2.

Despite their wide usage, the dose-response relation and the frequency-weighting defined in ISO 5349-1 (2001) have been broadly criticized. A number of studies have shown substantial deviations between the recommended method and the actual prevalence observed in the field (Brubaker et al., 1986; Tasker, 1986; Walker et al., 1986; Dandanell and Engstrom, 1986; Engstrom and Dandanell, 1986; Bovenzi et al., 1980 and 1988; Bovenzi, 1998; Seppalainen et al., 1986; Starck and Pyykkö, 1986; Pelmear et al., 1989; Tominaga, 1993; Griffin et al., 2003). These studies have suggested various limitations of both the w_h-weighting filter and exposure limit values. This may in-part be attributed to limited knowledge on the human hand-arm bio-dynamics and roles of various operational factors such as hand grip and push forces, working posture, tool-type and individuals' work habits. The frequency weighting could potentially overestimate the adverse effects of vibration in the low frequency range, and underestimate the risks under exposure to high frequency vibrations (Dong et al., 2001; 2005c; and 2006). The prevalence of VWF syndrome reported in several epidemiological studies also suggests

9

considerable bias in the standardized health risk assessment guides. Griffin (2003) and Bovenzi (2010) suggested that the un-weighted vibration dose may yield a better prediction of VWF than the equivalent weighted vibration dose.

Griffin (2004) further stated that the exposure action and limit values, recommended by the EU, may underestimate the risks associated with short term exposure to extremely high-magnitudes vibrations. Operators exposed to such vibration, commonly encountered in the construction industry, may suffer from a high prevalence of VWF even when their vibration doses are below the recommended action value. Owing to lack of agreements with the standardized dose-response relation, frequency-weighting, and limiting dose values, the need for further epidemiologic and pathological studies has been widely recognized. Irrespective of the disagreements on the standards, the control of HTV is considered most essential for the prevention of vibration-induced injuries and health risks.

1.2.3 HTV Control Strategies

The nature of hand transmitted vibration (HTV) strongly depends upon many operating factors, such as tool speed, hand-grip and push forces, hand-arm posture and the type of task, apart from the tool and handle designs. The HTV exposure could be limited by limiting the tool speed and the daily exposure duration, irrespective of the tool design, nature of the task and the other operating conditions (Mallick, 2008; 2010). Such an approach, however, may not be generally acceptable in view of the reduced work rate. Furthermore, it is difficult to control the vast majority of the operating factors considering wide variations in the workplace environment, the tasks and individuals' working habits.

It is thus vital to limit the HTV exposure through designs of low vibration tools and handles in addition to the anti-vibration gloves.

Control of HTV while operating a hand-held vibrating tool may be realized through:

i) Isolating hands from the vibrating handles using anti-vibration materials or gloves;

ii) Isolating tool handles from the vibration source through designs of handle vibration isolators; and

iii) Designs of power tools integrating effective vibration control mechanisms.

The current design practice is primarily based on the isolation of the hands from the vibrating handles using either anti-vibration materials covering the tool handle or anti-vibration gloves or a combination of the two. Different resilient materials with visco-elastic properties are normally applied to the handle to achieve some degree of vibration attenuation. Suggs and Abrams (1983) investigated the vibration transmissibility of two plastic foams wrapped tool handles under a white noise excitation. Both the materials provided substantial vibration reduction, while the thinner and softer foam material resulted in greater reduction of vibration in the lower frequency range. The vibration isolation performance of the soft foam, however, will be limited under high magnitudes of grip and push forces due to excessive deformation of the foam. Moreover, thick foam layers may yield larger size of the handle and limit hand dexterity.

A wide range of anti-vibration gloves have been developed to realize suppression of HTV apart from protecting the operators' hands from cuts and cold/hot environments. Gloves have been designed with different vibration isolation materials such as gel, air bladders and rubber layers. The vibration isolation properties of different gloves have been extensively studied through laboratory experiments (Brown, 1990; Griffin, 1998;

Pinto et al., 2001; Dong et al., 2003; 2005; 2009; Rakheja et al., 2002a). These have shown that the vibration transmission characteristics of anti-vibration gloves are strongly dependent upon the nonlinear visco-elastic properties of the coupled hand-glove system (Griffin et al., 1982), hand forces and vibration excitation levels (Gurram et al., 1994; Griffin, 1998). The vibration attenuation characteristics of different gloves have been measured in the laboratory under vibration spectra of different tools apart from the M- and H-spectra recommended in ISO 10819 (1996) (Griffin, 1998; Pinto et al., 2001; Rakheja et al., 2002a). These studies have shown that vibration isolation effectiveness of a glove is not only tool-specific but also depends on the hand forces.

The laboratory methods involve design of an instrumented handles and measurement methods to assess anti-vibration effectiveness of gloves. The laboratory measurement method has been standardized in an International Standard (ISO 10819, 1996). The standardized method recommends assessments under medium (M) and high (H) frequency spectra, and the design of an instrumented palm-adapter for measurement of vibration transmitted to the palm of the hand. A number of studies have identified many technical problems with the standard method, namely, the recommended spectra and misalignments of the palm-adapter (Griffin, 1998; Hewitt, 1998; Dong et al., 2002; Welcome D.E. et al., 2012). Different laboratory studies of the same gloves thus resulted in widely different performance characteristics.

Rakheja et al. (2002c) attempted a systematic comparison between the vibration spectra defined in ISO 10819 and those measured from a series of power tools. It was shown that the vibration measured from a nut runner, a sander and a pneumatic chipping hammer were closer to the M-spectrum in view of the frequency contents, while the

magnitudes were substantially higher than those of the M-spectrum. The vibration spectra of a rivet gun, a chain saw and a pneumatic road breaker were comparable to the frequency range of the H-spectrum, while the spectral magnitudes were lower than the recommended values. The revised standard (ISO 10819, 2013) proposes the measurements under a single vibration spectrum in the 25 to 1600 Hz frequency range. The assessments, however, are required in the M- and H-frequency ranges. A glove is considered an anti-vibration, when its transmissibility magnitude in the M- and H-frequency ranges is ≤ 1.0 and ≤ 0.6, respectively.

Gurram et al. (1994) compared vibration transmissibility characteristics of nine different gloves and concluded that all of the gloves provided only very limited vibration reduction in specific frequency bands. Some of the gloves resulted in amplification of the handle vibration at frequencies below 100 Hz. Dong R. et al. (2009) proposed a dynamic model of the gloved hand-arm system using the five-DOF biodynamic model of the hand-arm system proposed by Dong J. et al. (2008) to predict vibration transmissibility of the gloves. The study concluded that the anti-vibration gloves may not provide effective attenuation of HTV at frequencies below 100 Hz, as stated by Gurram et al. (1994).

The reported studies have generally show anti-vibration effectiveness of gloves at relatively higher frequencies. The effectiveness of a glove may be enhanced by using thick vibration isolation materials, which could significantly impair the manual agility of the operator. A further concern associated with the use of anti-vibration gloves is the issue of durability. The effect of wear and tear on the glove's vibration attenuation performance remains uncertain (Hewitt, 1996; Pinto et al., 2001).

Alternatively, a few studies have proposed the isolation of the tool handles from the tool-generated vibration. A number of suspended handle designs have been proposed, where rubber or metal spring isolators are mounted between the tool body and the handles. The effectiveness of such handle isolators have been evaluated for different tools, such as chain saws, grass trimmer and rock drill (Suggs et al. 1968; Miwa, 1968; Brammer, 1975; Politschuk and Oblivin, 1975). Ko et al. (2011) evaluated the vibration attenuation performance of four different suspended anti-vibration handles installed on a petrol-driven grass trimmer. The study included a commercially available polymer material handle and three steel and aluminum handles of different lengths mounted on a grass trimmer through two rubber mounts. The study thus permitted the evaluations of the effect of spacing between two rubber mounts. The test results revealed that not all the rubber mounts can effectively reduce HTV. The mild steel handle with closely spaced rubber isolators revealed the best vibration isolation along all the three axes.

The effectiveness of rubber or metal spring handle vibration isolators mounted on chain saws was measured by Suggs et al. (1968). It was shown that such isolators are effective in limiting the transmission of high frequency vibrations (above 250 Hz), and may even amplify the low frequency vibrations. Such handle isolators would thus yield only limited isolation performance for tools powered by reciprocating engines or most types of pneumatic drills operating at relatively low frequencies around 35-45 Hz (Oddo et al., 2004).

Considering high magnitudes of HTV of jackleg drills in the vicinity of the blow frequency, Oddo et al. (2004) evaluated two different designs of anti-vibration suspended handles based on a robust spring-mass system. Parallel combinations of visco-elastic

14

mounts or helicoidal spring were tuned and employed as suspensions for attenuating tool vibrations. Owing to the high magnitudes of grip and push forces applied on the handle when initiating a drilling operation, relatively stiff suspended handles were designed so as to limit the deformations under push forces as high as 200 N. The measurements revealed superior vibration attenuation effectiveness of both the tuned handles in the low frequency range, especially around 35 Hz. The viscoelastic mounts resulted in enhanced vibration attenuation around the primary operating frequency of 35 Hz, whereas the helicoidal springs showed more linear character characteristics and considerable adaptability to the environment involving temperature variations or oil.

A few studies have also proposed dynamic vibration absorbers for attenuation of tool vibration. Strydom et al. (2002) proposed the design of a hydraulic vibration absorber for a rock drill, where the drill's percussion frequency was identified as the target absorber frequency. Through experiments, it was shown that tuning the fluid flow area could yield variable degree of vibration attenuation. Ko et al. (2011) investigated the effectiveness of a tuned vibration absorber for an electric grass trimmer within the frequency range of 1-1024 Hz. The resonance frequency of proposed vibration absorber was set to 220 Hz to match the grass trimmer's operating frequency, while the optimum mounting location of vibration absorber was evaluated analytically and experimentally. The field tests revealed up to 95% reduction in the acceleration due to HTV along the X_h axis. The tuned vibration absorber, however, would cause amplification of vibration during tool's idling or start-up, which was not addressed in the study.

Designs of low-vibration power tools are widely believed to be far more effective in limiting the HTV, compared to the gloves and handle isolators. Carefully optimizing

15

the design parameters of power tools, such as handle position, tool size, component materials, may yield control of HTV. However, owing to extremely complex interactions among tool components as well as highly compact tool designs, very few efforts have been attempted to optimize tools' design parameters for the purpose of HTV control, which are discussed in section 1.2.5.

1.2.4 Biodynamic Hand-Arm Models

Human hand-arm system (HAS) plays an essential role in the dynamics of integrated hand-tool-workpiece system. Owing to considerable absorption of the transmitted vibration in the HAS, it is essential to evaluate a tool design in the presence of coupling with a HAS model. Hence, the application of a valid biodynamic hand-arm model is critical and it can yield better understanding of the vibration transmission characteristics of the HAS under different excitations, vibration energy distributions, the developments in mechanical-equivalent simulators or test-rigs to estimate the dynamic performances of different vibrating tools, and evaluations of potential vibration reduction mechanisms (Mishoe and Suggs, 1977; Reyonlds and Falkenberg, 1982; 1984; Jahn and Hesse, 1986; Gurram et al., 1995; Rakheja et al., 2002c).

Considerable efforts have been made during the past few decades towards developments in effective mechanical-equivalent hand-arm vibration (HAV) models. However, since most of the hand-arm models have been derived from the laboratory-measured driving point mechanical impedances (DPMI), the excessive differences among measurements and laboratory test conditions can contribute to significant differences observed among the biodynamic responses of various hand-arm models (Mishoe, 1974; Rakheja et al., 2002c).

16

Accordingly, the reported analytical hand-arm models can be divided into three types, including the distributed-parameter biodynamic models, lumped-parameter biodynamic models and biomechanical models. Wood et al. (1978) proposed two distributed-parameter models for the hand-forearm system and the entire hand-arm system, respectively. These models presented the hand through two lumped masses coupled to a single driving point and two parallel combinations of stiffness and damping elements. The hand-forearm model consisted of radius and ulna bones and attached soft tissues described by two homogeneous flexural beams with distributed stiffness and damping. The entire HAS model integrated a single beam as the upper arm humerus bone to the hand-forearm model. Both the models considered 90° elbow angle and y_h axis vibration, while considerable deviations were reported in the DPMI response of the model when compared with the experimental data (Rakheja et al., 2002c).

The vast majority of the reported lumped-parameter HAV models consist of linear stiffness and damping elements. These include the single-DOF models by Abram (1971), Reynolds and Soedel (1972) and Abram and Suggs (1977); 2-DOF models by Miwa et al. (1979) and Mishoe and Suggs (1977); 3-DOF models by Mishoe and Suggs (1977), ISO 10068 (1998), Reynolds and Falkenberg (1982; 1984), Meltzer (1981), Daikoku and Ishikawa (1990), and Gurram et al. (1995); and 4-DOF models by Gurram (1993), Reynolds and Falkenberg (1984) and ISO 10068 (1998). Such lumped-parameter models do not describe the contributions due to hand push and grip forces, and the hand-arm posture. Furthermore, these models do not relate to the anatomical structure and properties of the HAS. Mishoe and Suggs (1977) proposed three different linear models corresponding to three different hand grip forces in order to account for the effect of grip

force on the biodynamic response. Gurram et al. (1996) proposed three and four-DOF HAS models with grip force-dependent stiffness and damping elements. The effect of hand push force, however, was ignored.

The vast majority of the lumped-parameter hand-arm models have been derived from laboratory-measured DPMI data using either curve-fitting techniques or error minimization methods. It has been suggested that the resulting models are not unique and multiple sets of model parameters could be identified that satisfy the measured DPMI data (Rakheja et al., 1993; 2002c; Adewusi, 2009). Moreover, the high-order lumped-parameter models defined in ISO 10068 (1998) exhibit very low masses and stiffness values, which limit their applications in tool models and in designs of hand-arm simulators (Rakheja et al., 2002c).

Rakheja et al. (2002c) performed relative evaluations of 12 reported hand-arm biodynamic models. Considering three criteria: (i) the static deflection of model under a static feed force of 50 N; (ii) the ability of the model to describe the DPMI characteristics of the HAS as per ranges defined in ISO 10068; and (iii) the natural frequencies and damping ratios of the models. The results revealed excessive static deflections of a number of reported models under a low-level of push force. This was particularly very high for the three- and four-DOF lumped parameter models. The single lumped-parameter models and the distributed-parameter models, however, revealed reasonably low static deflections in the static deflection test. The three- and four-DOF models revealed good agreements in the DPMI responses with the idealized ranges defined in ISO 10068, while the single DOF and distributed-parameter models showed considerable deviations. Furthermore, considerable differences were observed in the natural

frequencies and damping ratios of the reported models. It was concluded that none of the models is well-suited for applications in tool modeling and for developing HAS simulators.

In recent years, alternate HAS models employing two driving points (finger-handle and palm-handle interfaces) and biomechanical structure of the HAS have been proposed (Dong J. et al., 2008; Adewusi, 2009). These biomechanical models provide reasonable deformation responses and good predictions of vibration transmissibility apart from the DPMI. These models are thus considered more suited for integration in the tool model, and are described in section 2.2.

1.2.5 Hand-Held Power Tools and Modeling of Coupled System

The nature of vibration emitted by a tool strongly depends on many design and operating factors. For instance, the type of tool and task, rate of doing work, tool maintenance, hand-arm posture and hand forces contribute immensely to the magnitude and frequency components of HTV. The hand transmitted vibration of different tools have been generally characterized through field measurements.

Considering the diversity among the tool types, maintenance states, working speeds, treated materials, etc., a number of studies have suggested that the vibration frequencies of hand-held power tools are concentrated in the 20-1250 Hz frequency range, while the vibration magnitudes may vary from 10 m/s^2(weighted) to 2014 m/s^2(un-weighted) and the dominant vibration direction differs for different tools and the working postures. Table 1.1 and 1.2 summarize the range of magnitudes and dominant frequencies of vibration due to different tools (Gurram, 1993; Nemani, 2005). Wide variations in the

vibration characteristics of the power tools also contribute to broad differences in the prevalence of HAVS among the vibrating tool workers. The prevalence of vibration-induced white finger (VWF) associated with different power tools is also presented in Table 1.1.

A number of studies have reported the vibration exposure of specific tools, which have contributed to developments in the designs of vibration attenuation systems for those specific tools. For instance, a few studies have described the nature of vibration transmitted to the chain saw operators (Suggs et al., 1968; Abrams and Suggs, 1969 and 1977; Futatsuka and Ueno, 1985; Pitts et al., 2004). The primary sources of vibration have been identified as the drive and the cutting processes, which involve large magnitude dynamic forces and torques. It is shown that the magnitudes of vibration of a chain saw strongly depend on the cutting depth of the rotary chain. Excessive vibration, which is detrimental not only for the human hand-arm but also for the saw, may occur when the cutting gauge is too low. Furthermore, prolonged exposure to chain saw noise may contribute to mental disorders among the operators (Miyakita et al., 1987).

Table 1.1 : The ranges of magnitude of vibration and the associated VWF prevalence of different vibrating tools (Gurram, 1993; Nemani, 2005)

Tool Type	Magnitude of Vibration (m/s^2)	Prevalence of VWF Syndrome (%)
Chipping hammers	251-2014	47-80
Riveters	10*-1183	25-75
Jack-led drills	20*-362	45-80
Pavement breakers	195	10
Grinders	20-205	31-35
Chain saws	75	38

*weighted acceleration

Table 1.2 : Frequency ranges and direction of dominant vibrations of various hand-held power tools (Gurram, 1993)

Tool Type	Frequency Range (Hz)	Direction of Dominant Vibration
Chipping hammers	25-125	Z_h
Bush cleaner	100-150	X_h
Garden tool	63-80	X_h
Grinders	40-250	X_h, Y_h, Z_h
Orbital sanders	60-100	X_h, Y_h, Z_h
Chain saws	63-150	X_h, Y_h, Z_h

In a similar manner, a few studies have described the nature and sources of vibration of grinding tools (Agate et al., 1946; Hempstock and O'connor, 1975; Pelmear et al., 1974; Bovenzi et al., 1980; Reynolds et al., 1982; Starck et al., 1983; Daikoko and Ishikawa, 1990). Such tools can produce moderate levels of vibration attributed to unbalance of the grinding disk, and the offsets in the installation of associated mechanisms. Automatic balancing disks comprising moving balls within a guided race have been successfully implemented to reduce the effects of wheel unbalance (Rajalingham and Rakheja, 1998). Rotary tools, such as impact wrenches, electric screwdrivers, and nut runners, are the typical hand held torque tools used in the assembly and disassembly processes. These compact and light tools are mostly driven by pneumatic power to achieve high torques. Electric screwdrivers and nut-runners may not be as powerful as impact wrenches, but they can yield considerable levels of vibration as well as dynamic torque.

Compared with rotary tools, the percussive tools, such as chipping hammers, chisels, riveters and drillers, transmit considerably high magnitudes of dynamic forces and vibrations to the operator's hand-arm (Iwata, 1968; Matsumato et al., 1979; 1982;

Robert et al., 1977; Chatterjee et al., 1978; Taylor et al., 1981 and 1984; Behrens et al., 1984; Walker et al., 1985; Brubaker et al., 1986). Chipping hammers are widely used in the infrastructure or mining industry for crushing or drilling in hard materials. These tools are thus designed to produce high-magnitude impulses. Riveting hammers, mostly pneumatically powered, are designed in relatively compact size to install rivets in the aerospace industry. Needle-scalers are generally applied in the shipbuilding or automotive industry for the metal surface treatments such as rust, paint and loose scale cleaning.

The general operating principle of a percussive tool is very different from that of a rotary tool. Percussive tools develop high forces resulting from impacts between different components of the tool. Such impulses repetitively produce high magnitude cutting forces. The excessive impacts among tool components and between the tool tip and the work-piece are generally regarded as the major sources of harmful vibration. Such tools also emit higher magnitudes of HTV in the 20-125 Hz frequency range (Table 1.2). It has been suggested that percussive tool operators exhibit a relatively higher prevalence of VWF than operators of the other tools (Table 1.1).

A thorough understanding of dynamic characteristics of hand-held vibrating tools coupled with the human HAS is judged essential for design of low vibration tools and for identification of favorable operating conditions. The highly complex and compact designs of hand-held power tools together with highly nonlinear tool-workpiece interactions, however, pose difficult challenges in developing reliable analytical models. Despite the extensive studies on HAVS and the strong desire to limit the HTV dosage, the modeling of power tools and vibration isolation mechanisms has been attempted in a

22

very few studies. Abrams and Suggs (1969) experimentally investigated a vibration isolator for chainsaws and concluded that the isolator was particularly effective in attenuating high frequency vibration. Nemani (2005) proposed a multi-degree-of-freedom (DOF) analytical model of a hand-held angle grinder coupled with a gloved hand to evaluate the HTV along the three orthogonal axes in the presence of a rotating unbalance. The simulation results revealed that an increase in the grinding wheel unbalance would yield substantially higher levels of HTV along each axis. The study also showed considerable vibration attenuation by the anti-vibration glove, which was represented by a combination of linear spring and damping elements.

Golycheva et al. (2003; 2004) refined the analytical model of an electro-pneumatic hammer that was initially proposed by Babitsky (1998) to explore different vibration isolation mechanisms. The refinements involved considerations of the tool geometry and coupling with a single DOF hand-arm vibration model. Two vibration absorbers were introduced to the tool handle to limit HTV in two distinct frequency bands, together with a vibration isolator to suppress the high frequency handle vibration. The study showed superior effectiveness of vibration absorbers in limiting the low-frequency vibration. The acceleration response of the hand-mass, however, was observed to be highly asymmetric with negative acceleration peak substantially larger than the positive peak. This was most likely caused by the linear hand-arm system model. A nonlinear model of an electro-pneumatic percussive chipping hammer, coupled with the 3-DOF hand arm vibration model defined in ISO 10068 (1998), was developed by Rakheja et al. (2002b). The model involved many simplifying assumptions, associated with orifices geometry and air flows, while the simulation results revealed in reasonably good agreement only with respect to

23

the fundamental frequency of the tool. Considerable deviations were observed between the simulation results and the experimental data in terms of vibration magnitudes of the tool and the hand-arm system. The observed deviations from the measured data were attributed to very low stiffness of the standardized hand-arm vibration model, particularly the excessive static deflection under a 50 N push force (Rakheja et al., 2002c).

1.3 Scope and Objectives of the Dissertation Research

From the review of literature, it is evident that only minimal efforts have been made to develop reliable models of the hand-held power tools, which could serve as essential analytical means for design of low vibration power tools. Furthermore, despite considerable developments in anti-vibration gloves and handle vibration isolators, the need for developing low vibration emission tools has been widely emphasized. The primary objective of this dissertation research is thus to contribute towards development of a reliable analytical model of a hand-held percussive chipping hammer through considerations of components interactions in a systematic manner. The specific objectives include the following:

a. Develop an analytical model of a hand-held percussive tool through identifications of various contact pairs and the fluid flows between the primary piston and the striker;

b. Propose a tool tip-workpiece contact model to describe the energy dissipator used in experimental studies;

c. Integrate a biomechanical model of the hand-arm system to the tool model and evaluate hand-tool system responses under selected push forces;

d. Explore the model validity using the laboratory-measured data and identify desirable design parameters through parametric sensitivity analyses;

e. Investigate the effectiveness of an anti-vibration glove in controlling the tool vibration.

1.4 Dissertation Organization

This dissertation is organized in five chapters. The first chapter is devoted to the review of reported studies on health effects and assessment methods of hand transmitted vibration (HTV) exposure, developments in control strategies for HTV, and analytical models of the hand-arm system and power tools. The scope and the objectives of the dissertation research were formulated on the basis of the reviewed studies.

In the second chapter, a biomechanical model of the human hand-arm in the bent-arm posture (elbow angle=90°) reported by Adewusi (2009) is formulated and reviewed in terms of static deflections, natural frequencies, driving point mechanical impedance (DPMI) and vibration transmissibility responses, respectively. The hand-arm biodynamic model is subsequently refined to incorporate the model of an anti-vibration glove (ISO 10068, 2010) to study the vibration attenuation effectiveness of the anti-vibration glove.

An analytical model of a hand-held percussive power tool is formulated in Chapter 3 by integrating various subsystem models describing dynamics of different impact pairs. The parameters of these contact pairs (striker-impact bolt; impact bolt-tool body; and impact bolt –tool bit) are identified from the rigid body impact theory. A tool bit-workpiece impact model is also proposed on the basis of the available experimental data.

The equations of motion of the integrated hand-tool-workpiece system model with an anti-vibration glove are subsequently formulated.

In Chapter 4, the validity of the proposed integrated hand-tool-workpiece system model is examined using the available measured data in terms of tool handle and tool bit accelerations, and biodynamic responses of the hand-arm system without the glove. The simulations are performed to study vibration attenuation effects of various design-parameters. On the basis of the simulation results, a design guidance is proposed to reduce the magnitudes of HTV. The major conclusions and recommendations for future studies are finally presented in Chapter 5.

CHAPTER 2

BIOMECHANICAL MODEL OF THE HAND-ARM SYSTEM WITH ANTI-VIBRATION GLOVE

2.1 Introduction

Understanding of the biodynamic responses of the human hand-arm system (HAS) to HTV is considered vital for design of vibration isolation systems for power tools, and for derivations of alternate frequency weightings and vibration power flow analyses (Rakheja et al., 2002c). The biodynamic responses of the HAS have thus been extensively measured in many laboratory studies in terms of driving point mechanical impedance, vibration transmitted to different segments of the hand-arm and vibration power absorption (Mishoe and Suggs, 1977; Reyonlds and Falkenberg, 1982; 1984; Jahn and Hesse, 1986; Gurram et al., 1995). A few studies have proposed different mechanical-equivalent models of the HAS, ranging from single to many-degrees-of-freedom, to described the mean biodynamic responses to vibration and the vibration power distributions within the HAS (Rakheja et al., 2002c; Dong J., 2007; Adewusi, 2009). A few studies have also proposed hand-arm-vibration simulators on the basis of the biodynamic models for estimating the dynamic performances of different vibrating tools, and evaluations of potential vibration reduction mechanisms (Abrams and Suggs, 1969; Jahn and Hesse, 1986; Golysheva et al., 2004).

Rakheja et al. (2002c) performed a systematic comparison of 12 reported hand-arm vibration models considering three criteria: (i) ability to predict mechanical impedance properties; (ii) static deflections under a 50 N push force; and (iii) natural frequencies and damping ratios. The study concluded that none of the reported models were suited for

developing HAV simulators and assessment of coupled hand-tool systems. The lower order models revealed reasonably low static deflections under the specified push force but resulted in substantial deviations with respect to standardized DPMI ranges (ISO 10068, 1998). Conversely, the higher order models revealed good agreements in terms of the DPMI responses but showed excessive static deflections under a low-level of feed force. The study also concluded that the evaluated models yield no agreement in terms of the natural frequencies of the human HAS.

The reported lumped parameters do not represent anatomical structure of the HAS. Fritz (1991) and Cherian et al. (1996) proposed biomechanical models of the human HAS considering the elbow angles of 60^0 and 90^0, respectively, and the anatomical structures of the forearm and the upper-arm. Dong J. et al. (2008) proposed a hand-arm model comprising biomechanical structure of the hand, while the forearm and the upper-arm were represented by a lumped mass. Alternatively, Adewusi (2009) proposed two biomechanical models of the HAS considering two different postures with the elbow angles of 90^0 and 180^0, respectively, together with biomechanical structures of the hand and the arm. Furthermore, unlike the reported models that are based upon measured DPMI alone, the proposed models were identified using the simultaneously measured vibration transmissibility and DPMI responses.

The study of the vibration characteristics of a power tool necessitates the application of a HAS model to account for the energy absorption by the human HAS. It has been shown that application of the lumped-parameter models, recommended in ISO-10068 (1998), to the tool model yield poor predictions of the tool handle vibration due to excessive static deflection of the model (Rakheja et al., 2002b). In this study, the

biomechanical model, proposed by Adewusi (2009), is explored for the analysis of the couple hand-tool system vibration responses along the z_h- axis. The model reported for the bent-arm posture (elbow angle=90^0) is re-formulated and analyzed to assess its suitability for application to the tool model. This HAS model responses are assessed in terms of: (i) the static deflections under two different levels of the static push force (50 N and 75 N); (ii) the natural frequencies and normal modes of the model; (iii) the ability to predict DPMI characteristics of the HAS; and (iv) the ability to predict vibration transmissibility responses of HAS near the wrist, elbow and shoulder joints.

2.2 Biomechanical Model of the Hand-Arm System

The application of a valid biodynamic hand-arm model is critical to attain a better understanding of the dynamic characteristics of the HAS under the tool-generated vibrations, and evaluations of vibration performances of different hand-held power tools and vibration isolation mechanisms. Considering that the tools' vibrations generally dominate along the z_h- axis, the bent-arm biomechanical model of the HAS, proposed by Adewusi (2009), is investigated for its application to the power tool model. The reported studies have generally considered the bent-arm posture (elbow angle=90^0 and shoulder abduction=0^0) for the measurement of biodynamic responses and model development, which does not represent the postures observed in the field (Adewusi, 2009). Owing to the lack of models for more representative posture, the bent-arm biomechanical model is considered better suited for application to power tools as it describes the anatomical structure of HAS and yields relatively lower static deflection under a feed force.

Figure 2.1 illustrates the structure of the six-degrees-of-freedom HAS model. The model employs a clamp-like structure of the hand, as proposed by Dong et al. (2005), which permits considerations of the two driving points formed by the fingers-handle and palm-handle interfaces to describe corresponding dynamic interactions. The bones of the fingers and palm-wrist are represented by lumped masses, m_f and m_p, respectively. The masses of the skins and tissues overlaying the contacting areas between the hand and tool handle are designated by m_{tf} for the fingers and m_{tp} for the palm-wrist, while the visco-elastic properties of corresponding tissues are represented by linear damping and stiffness constants (c_1 and k_1), and (c_2 and k_2), respectively.

The visco-elastic properties of the carpals and metacarpals connecting the fingers to palm-wrist are also described by lumped damping and stiffness constants (c_3 and k_3). The masses due to the bones, tissues and skin of the forearm are represented by m_{fa}, while corresponding visco-elastic properties of the wrist and elbow joints are expressed by c_w and k_w, and c_e and k_e, respectively. Similarly, the lumped mass, m_{ua}, represents the sum of masses of the bones, tissues and skin of the upper-arm. Associated visco-elastic properties of the shoulder joint are shown as c_s and k_s. The entire trunk of the operator is represented by a lumped mass m_b of height h coupled to the shoulder joint, as shown in the Figure 2.1. Furthermore, based on experimental observations, rotary motions are considered at the elbow, shoulder and pelvic joints but are ignored at the wrist. Consequently, corresponding linear rotational visco-elastic properties of the elbow, shoulder and pelvic joints are described by (C_e and K_e), (C_s and K_s), and (C_b and K_b), respectively.

The motion of the tool handle coupled to the hand is represented by z_c along the z_h-axis. In a similar manner, z_i is used to denote the z_h-axis displacements of different substructures of the HAS, where the subscript i can be f, p, fa, ua, representing the fingers, palm-wrist, forearm and upper-arm, respectively. Moreover, the rotational motions of the upper-arm and trunk are designated by θ_{ua} and θ_b, respectively.
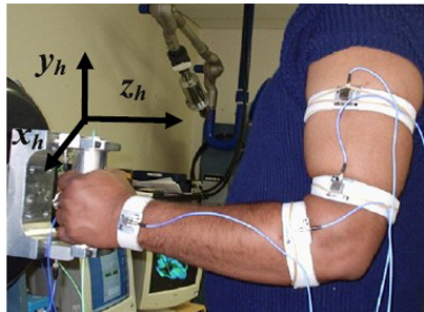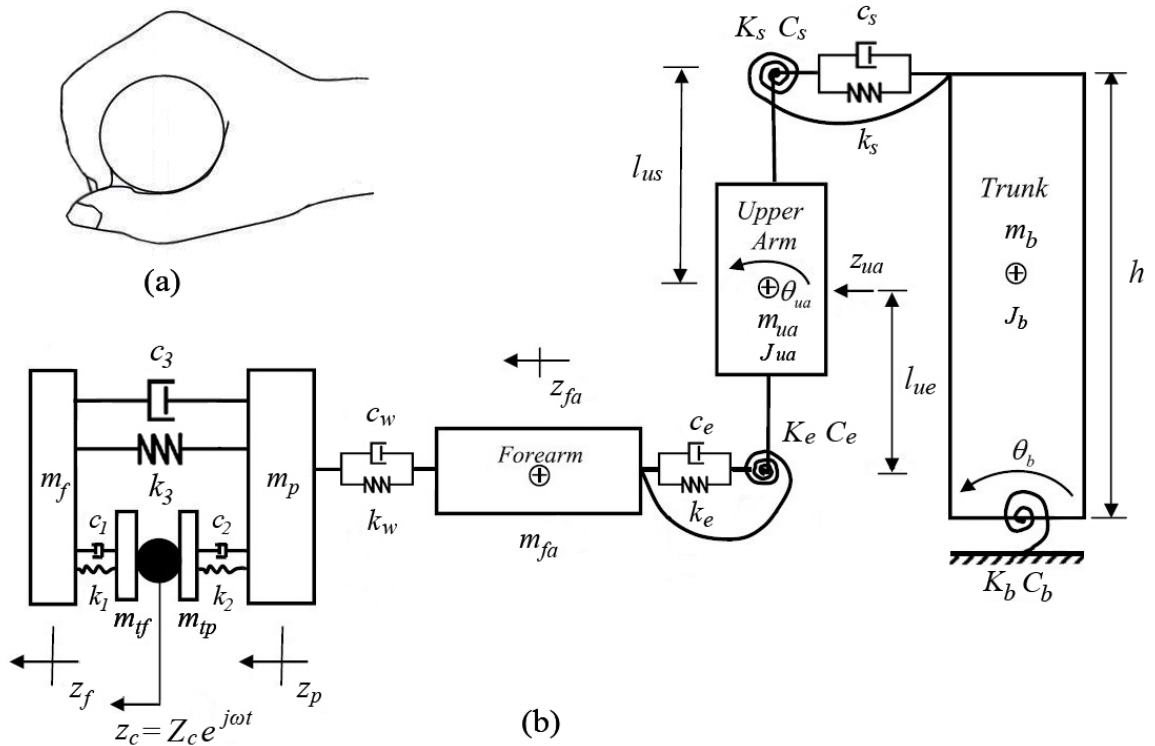
Figure 2.1 : (a) Schematic of the hand grasping the tool handle (b) schematic of the bent-arm model with 90° elbow angle; and (c) experimental set-up (Adewusi, 2009)

31

The equations describing the motions of the lumped fingers and palm-wrist masses are formulated as:

$$m_f \ddot{z}_f + k_1(z_f - z_c) + c_1(\dot{z}_f - \dot{z}_c) + k_3(z_f - z_p) + c_3(\dot{z}_f - \dot{z}_p) = 0 \qquad (2.1)$$

$$m_p \ddot{z}_p + k_2(z_p - z_c) + c_2(\dot{z}_p - \dot{z}_c) + k_3(z_p - z_f) + c_3(\dot{z}_p - \dot{z}_f)$$
$$+ k_w(z_p - z_{fa}) + c_w(\dot{z}_p - \dot{z}_{fa}) = 0 \qquad (2.2)$$

Similarly, the equation describing the motion of the forearm is formulated as:

$$m_{fa} \ddot{z}_{fa} + k_w(z_{fa} - z_p) + c_w(\dot{z}_{fa} - \dot{z}_p) + k_e(z_{fa} - z_{ua} + l_{ue}\theta_{ue})$$
$$+ c_e(\dot{z}_{fa} - \dot{z}_{ua} + l_{ue}\dot{\theta}_{ue}) = 0 \qquad (2.3)$$

The equations describing the z_h axis and rotational motions of the upper-arm are derived as:

$$m_{ua} \ddot{z}_{ua} + k_e(z_{ua} - l_{ue}\theta_{ue} - z_{fa}) + c_e(\dot{z}_{ua} - l_{ue}\dot{\theta}_{ue} - \dot{z}_{fa})$$
$$+ k_s(z_{ua} + l_{us}\theta_{ua} - h\theta_b) + c_s(\dot{z}_{ua} + l_{us}\dot{\theta}_{ua} - h\dot{\theta}_b) = 0 \qquad (2.4)$$

$$J_{ua} \ddot{\theta}_{ua} + K_e\theta_{ua} + C_e\dot{\theta}_{ua} + K_s(\theta_{ua} - \theta_b) + C_s(\dot{\theta}_{ua} - \dot{\theta}_b)$$
$$- l_{ue}[k_e(z_{ua} - l_{ue}\theta_{ua} - z_{fa}) + c_e(\dot{z}_{ua} - l_{ue}\dot{\theta}_{ua} - \dot{z}_{fa})]$$
$$+ l_{us}[k_s(z_{ua} + l_{us}\theta_{ua} - h\theta_b) + c_s(\dot{z}_{ua} + l_{us}\dot{\theta}_{ua} - h\dot{\theta}_b)] = 0 \qquad (2.5)$$

where J_{ua} denotes the mass moment of inertia of the upper-arm, and l_{ua} defines the length of the upper-arm. l_{ue} and l_{us} are the distances from the mass center of upper-arm to the elbow joint and the shoulder joint, respectively.

The equation describing the rotational motion of the trunk is derived as:

$$J_b \ddot{\theta}_b + K_b\theta_b + C_b\dot{\theta}_b + K_s(\theta_b - \theta_{ua}) + C_s(\dot{\theta}_b - \dot{\theta}_{ua})$$
$$- h[k_s(z_{ua} + l_{us}\theta_{ua} - h\theta_b) + c_s(\dot{z}_{ua} + l_{us}\dot{\theta}_{ua} - h\dot{\theta}_b)] = 0 \qquad (2.6)$$

32

where J_b is the mass moment of inertia of the trunk about the pelvic joint.

As shown in Figure 2.2, the total dynamic force (F_{dh}) developed at the tool handle interfaces can be formulated as:

$$F_{dh} = F_{dpalm} + F_{dfinger} \qquad (2.7)$$

where the dynamic hand forces developed at the finger side ($F_{dfinger}$), and palm side (F_{dpalm}) can be calculated from:

$$F_{dfinger} = k_1(z_f - z_c) + c_1(\dot{z}_f - \dot{z}_c) + m_{tf}\ddot{z}_c \qquad (2.8)$$

$$F_{dpalm} = k_2(z_p - z_c) + c_2(\dot{z}_p - \dot{z}_c) + m_{tp}\ddot{z}_c \qquad (2.9)$$
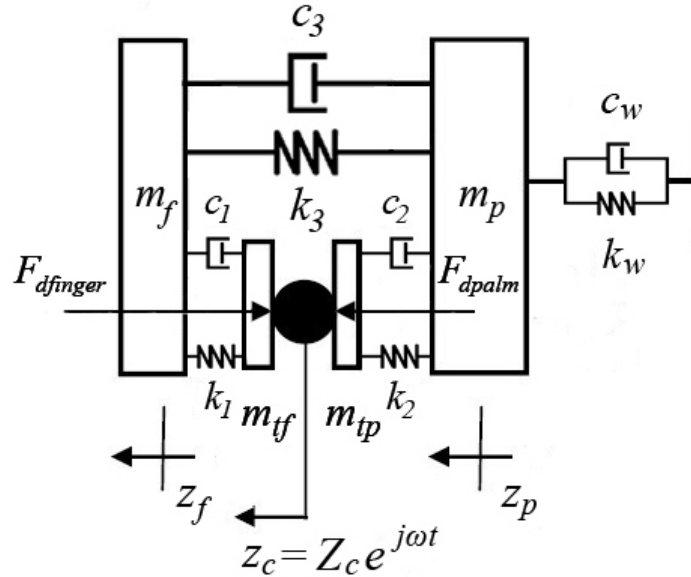
Figure 2.2 : Schematic of the dynamic hand forces

Eqs. (2.1) to (2.6) describe the motions of different segments of the hand-arm system subject to handle vibration. These equations also yield driving-point mechanical impedance responses at the two driving points formed by the fingers-handle and palm-handle interfaces, which are derived in section 2.7. It should be noted that the Eq. (2.5),

33

describing the rotational motion of the upper-arm, differed from that reported in Adewusi's study (2009). This difference was due to an error that was discovered in the reported equation.

2.3 Development of the Biomechanical Model of the Hand-Arm System Coupled with the Anti-Vibration Glove

As stated in section 1.2.3, the control of HTV can be realized through isolating hands from vibrating tool handles. Considerable efforts thus have been made towards designs of anti-vibration gloves (Brown, 1990; Griffin, 1998; Pinto et al., 2001; Dong et al., 2003; 2005; 2009; Rakheja et al., 2002a). Gloves with different vibration isolation materials have been widely proposed to obtain some degree of vibration suppression. Air bladder glove is one of the anti-vibration gloves utilized in the industrial sectors. The air enclosed in tiny plastic bladders provides vibration isolation effects between hands and tool handle under HTVs in specific frequency ranges (Dong et al., 2009). In this dissertation research, an air bladder anti-vibration glove model proposed by Dong et al. (2009) is integrated to the biomechanical model of HAS to investigate its vibration isolation effectiveness. The applied glove model exhibits different visco-elastic properties at two diving points formed by the finger- and palm-handle interfaces, respectively. Similar to the bent-arm posture model, the gloved hand-arm model is formulated upon consideration of the motions of the masses due to the tissues and glove materials covering the contacting areas between the hand and tool handle, as shown in Figure 2.3.

The equations describing the motions of the masses m_{tfg} and m_{tpg}, for the tissues and glove materials covering the finger and the palm-wrist, are formulated as:

$$m_{tfg}\ddot{z}_{tf} = k_1(z_f - z_{tf}) + c_1(\dot{z}_f - \dot{z}_{tf}) + k_{g1}(z_c - z_{tf}) + c_{g1}(\dot{z}_c - \dot{z}_{tf}) \tag{2.10}$$

$$m_{tpg}\ddot{z}_{tp} = k_2(z_p - z_{tp}) + c_2(\dot{z}_p - \dot{z}_{tp}) + k_{g2}(z_c - z_{tp}) + c_{g2}(\dot{z}_c - \dot{z}_{tp}) \tag{2.11}$$

where m_{tfg} and m_{tpg} are derived as:

$$m_{tfg} = m_{tf} + m_1 \tag{2.12}$$

$$m_{tpg} = m_{tp} + m_2 \tag{2.13}$$

m_1 and m_2 present the lumped glove material masses distributed at the finger- and palm-glove interfaces. Let k_{g1} and c_{g1}, and k_{g2} and c_{g2} denote the linear stiffness and damping properties of the anti-vibration glove covering the fingers and the palm, respectively.

The equation describing the motion of the fingers is derived as:

$$m_f\ddot{z}_f = k_1(z_{tf} - z_f) + c_1(\dot{z}_{tf} - \dot{z}_f) + k_3(z_p - z_f) + c_3(\dot{z}_p - \dot{z}_f) \tag{2.14}$$

Similarly, the equation describing the motion of the palm-wrist can be determined as:

$$\begin{aligned} m_p\ddot{z}_p &= k_2(z_{tp} - z_p) + c_2(\dot{z}_{tp} - \dot{z}_p) + k_3(z_f - z_p) \\ &+ c_3(\dot{z}_f - \dot{z}_p) + k_w(z_{fa} - z_p) + c_w(\dot{z}_{fa} - \dot{z}_p) \end{aligned} \tag{2.15}$$

As shown in Figure 2.4, the dynamic hand forces developed at the finger side $F_{dfinger}$, and palm side F_{dpalm} can be expressed as:

$$F_{dfinger} = k_{g1}(z_{tf} - z_c) + c_{g1}(\dot{z}_{tf} - \dot{z}_c) \tag{2.16}$$

$$F_{dpalm} = k_{g2}(z_{tp} - z_c) + c_{g2}(\dot{z}_{tp} - \dot{z}_c) \tag{2.17}$$

The total dynamic hand force (F_{dh}) developed on the tool-handle interfaces can be formulated as:

$$F_{dh} = F_{dpalm} + F_{dfinger} \qquad\qquad (2.18)$$
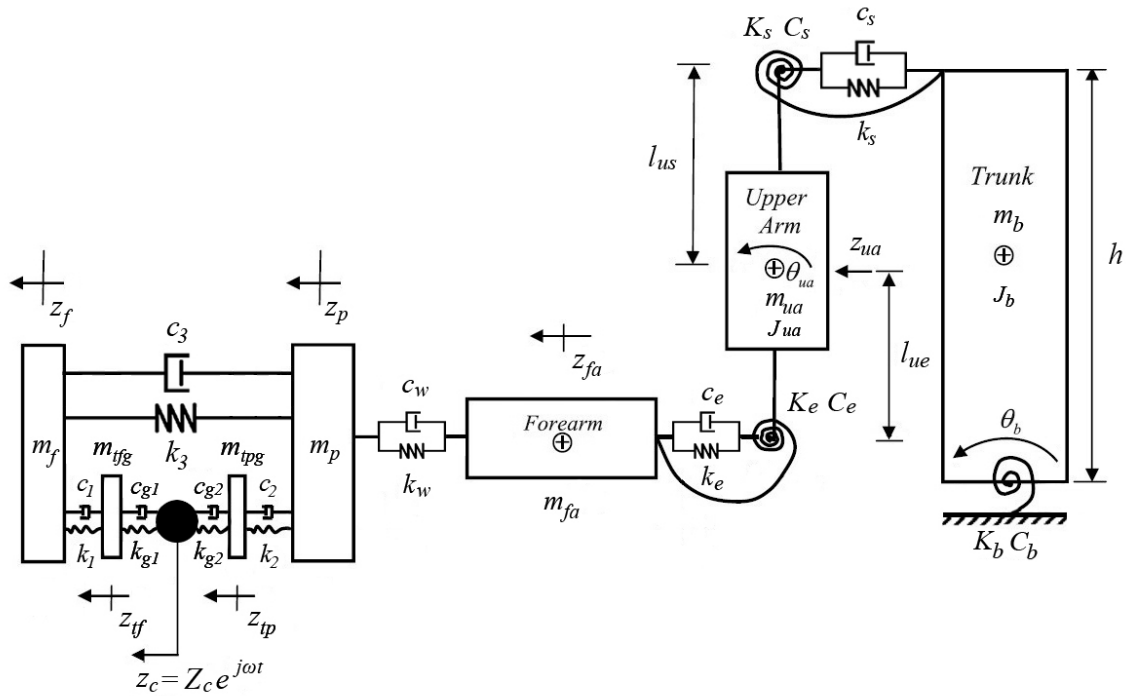
Figure 2.3 : Schematic of the gloved hand-arm model in bent-arm posture
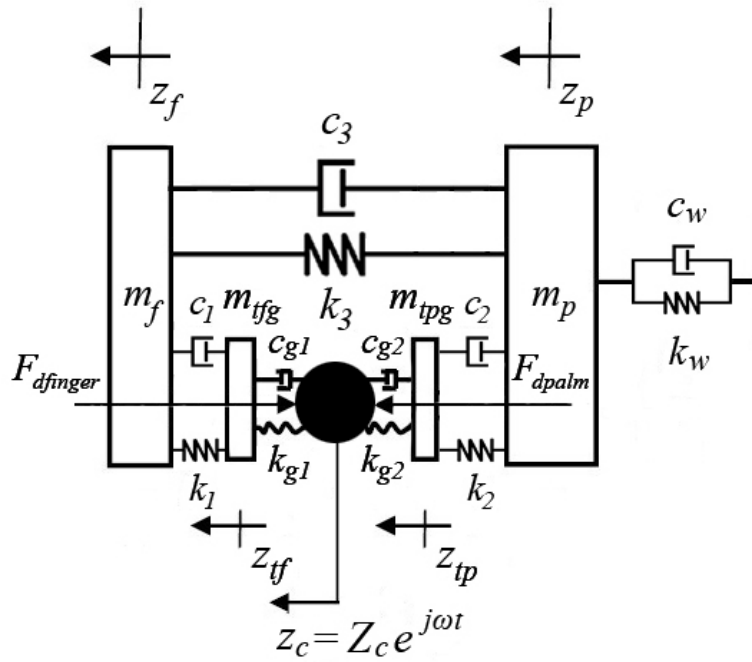
Figure 2.4 : The hand model integrating the glove model

The motions of the forearm, upper arm and trunk are identical to those formulated in Eqs. (2.3) to (2.6), and the model parameters of the air bladder glove along z_h- axis are tabulated in Table 2.1 (Dong et al., 2009).

Table 2.1 : Parameters of the air bladder glove model (Dong et al., 2009)

Parameter	Value
m_{g1} (kg)	0.02
k_{g1} (kN/m)	327.3
c_{g1} (Ns/m)	75.20
m_{g2} (kg)	0.0673
k_{g2} (kN/m)	177.4
c_{g2} (Ns/m)	88.80

2.4 Parameters of the Bent-Arm Model

The model parameters associated with different push forces (50 N and 75 N) and a constant grip force of 30 N were identified by minimizing the errors between the model and measured biodynamic responses in terms of DPMI and vibration transmissibility responses, respectively (Adewusi, 2009). The reported model parameters are tabulated in Table 2.2.

The comparison of the model parameters, as presented in Table 2.2, suggests an increase in the push force will increase vast majority of the visco-elastic coefficients of the bent-arm model. Increasing the push force from 50 N to 75 N yields substantial increases in the stiffness of the elbow joint (K_e increased by 237.5%), the pelvic joint (K_b increased by 122.2%) and the shoulder (k_s increased by 74.7%). The greatest percentage increase in the damping coefficients occurs at the elbow (c_e increased by 99.3%), followed by that for the tissue covering the palm (c_2 increased by 49.9%). These

percentage increases may be attributed to the tightening effect of the tendons or tissues in

the HAS when the push force is increased.

Table 2.2 : Parameters of the bent-arm model under different push forces (Adewusi, 2009)

Parameters	30 N Grip force	
	50 N Push force	75 N Push force
m_{tf} (kg)	0.02	
m_f (kg)	0.11	
m_{tp} (kg)	0.03	
m_p (kg)	0.47	
m_{fa} (kg)	1.09	
m_{ua} (kg)	1.73	
m_b (kg)	29.51	
l_{ue} (cm)	11.56	
l_{us} (cm)	8.94	
h (cm)	52.00	
J_{ua} (kgm²)	0.061	
J_b (kgm²)	2.6598	
c_1 (Ns/m)	103.14	109.10
c_2 (Ns/m)	33.68	50.48
c_3 (Ns/m)	2.09	1.05
c_w (Ns/m)	147.86	217.91
c_e (Ns/m)	103.99	207.25
c_s (Ns/m)	28.90	13.85
C_e (Nms/rad)	2.24	3.36
C_s (Nms/rad)	2.52	2.52
C_b (Nms/rad)	53.49	74.59
k_1 (N/m)	94714.0	96342.0
k_2 (N/m)	53750.0	86729.0
k_3 (N/m)	6478.0	3239.0
k_w (N/m)	14155.0	18566.0
k_e (N/m)	2763.6	449.1
k_s (N/m)	4467.0	7804.4
K_e (Nm/rad)	537.1	1812.7
K_s (Nm/rad)	605.3	828.7
K_b (Nm/rad)	1353.3	3007.7

An increase in the push force also yields considerable reductions in the stiffness of

the tissues coupling the fingers and palm (k_3 decreased by 50.0%) and the elbow (k_e

decreased by 83.7%). Similarly, the damping effects of the tissues coupling the fingers and palm, and the shoulder joint reduce by 49.8% and 52.1%, respectively. However, these reductions have not yet been explained. Generally, these observed percentage changes in the model parameters of the bent-arm model suggest that an increase in the push force will significantly affected the dynamic responses of the entire human hand arm system.

2.5 Natural Frequency Analysis

In this section, the natural frequencies of the bent-arm model are evaluated through the formulation and solution of an eigenvalue problem. The natural frequencies are identified for two different levels of the push force (50 N and 75 N), and a constant grip force of 30 N, using the model parameters presented in Table 2.2. The results are summarized in Table 2.3 together with the dominant deflection mode.

Table 2.3 : Natural frequency and dominate deflection mode of the bent-arm model under two different levels of push force

Hand forces	30 N Grip and 50 N Push	30 N Grip and 75 N Push	Dominate deflection mode
Natural Frequencies (Hz)	*4.05*	*5.42*	Trunk rotation
	10.13	*11.85*	Upper arm mass
	18.28	*19.06*	Forearm mass
	63.64	*76.94*	Palm-wrist mass
	71.33	*106.47*	Upper are rotation
	152.74	*151.46*	Finger mass

The computed natural frequencies revealed very good agreements with the resonant frequencies reported by Adewusi (2009), although slight differences were observed, which was attributed to the error discovered in Eq. (2.5) in the reported study. The highest natural frequencies (152.74 and 151.46 Hz), corresponding to the selected push

forces, were related to the lumped finger mass, while the lower frequencies (63.64 and 76.94 Hz) were associated with the lumped palm-wrist mass, and were referred to as the characteristic frequencies of the palm. The remaining frequencies for the two push forces (18.28 and 19.06 Hz, and 10.13 and 11.85 Hz) were related to the natural frequencies of the forearm and upper-arm masses. The whole body rotation occurred at a very low frequency (4.05 Hz) for the lower push force of 50 N, and it increased to 5.42 Hz with increase in the push force to 75 N. The upper arm rotation modes occurred at 71.33 and 106.47 Hz, for the 50 N and 75 N push force, respectively.

The comparison of the natural frequencies of the bent-arm model under two different push forces suggests that an increase in the push force tends to increase the characteristic frequencies of the entire human hand-arm system, especially at the palm (from 63.64 Hz at 50 N to 76.94 Hz at 75 N) and at the upper arm rotation (from 71.33 Hz at 50 N to 106.47 Hz at 75 N). These increases can be attributed to the fact that the associated muscles or tissues in the HAS tend to be stiffen when push force is increased. Consequently, the entire HAS becomes stiffer especially in the wrist, the elbow and the shoulder. The finger mass, however, formed an exception to this. The finger mode frequency decreased slightly with an increase in the push force.

2.6 Static Deflection Analysis

It has been shown that the vast majority of the reported HAS models exhibit large static deflections under a low level push force (Rakheja et al., 2002c). This is caused by the presence of a very low stiffness element of the models. Such models are thus not considered suited for applications in the coupled hand-tool system models. The total static deflection (deflection of the driving point with respect to the fixed support) of the

biomechanical model is evaluated by applying a static push force along the z_h-axis. The analysis is performed for the two hand grip and push force combinations, for which the model parameters were available. The push and grip force combinations may also be expressed in terms of finger- and palm-side forces using the definitions in ISO 15230 (2007), such that:

$$F_{sfinger} = F_{grip} \tag{2.19}$$

$$F_{spalm} = F_{push} + F_{grip} \tag{2.20}$$

where $F_{sfinger}$ and F_{spalm} refer to the static forces applied to the finger- and palm side driving points, respectively.

The static deflections were evaluated for the palm-wrist, elbow and the shoulder joints under the net static push forces of 50 and 75 N, as shown in Figure 2.5. The finger tissue deflection, however, was not of concern considering its high natural frequency. The static deflections of the reported low natural frequency single-DOF (Reynolds and Soedel, 1972) and the four-DOF (ISO 10068, 1998) hand-arm vibration models, shown in Figure 2.6, are also evaluated for comparison purposes. The parameters of these two biodynamic hand-arm vibration models along the z_h-axis are tabulated in Tables 2.4 and 2.5, respectively. It should be noted that the parameters off these models have not been related to the hand forces. Identical parameters are thus assumed for both the levels of the push force.

The static deflections of the palm-tissue (z_{tp}^S) and palm-wrist mass (z_p^S), forearm mass (z_{fa}^S), upper arm mass (z_{ua}^S), upper arm rotation (θ_{ua}^S), trunk rotation (θ_b^S) are evaluated from:

41

$$\{z_i^s\} = [K]^{-1}\{F\}$$
(2.21)

where

$$\{z_i^s\} = \begin{bmatrix} z_{tp}^s & z_p^s & z_{fa}^s & z_{ua}^s & \theta_{ua}^s & \theta_b^s \end{bmatrix}^T$$
(2.22)

$$\{F\} = \begin{bmatrix} F_{push} & 0 & 0 & 0 & 0 & 0 \end{bmatrix}^T$$
(2.23)
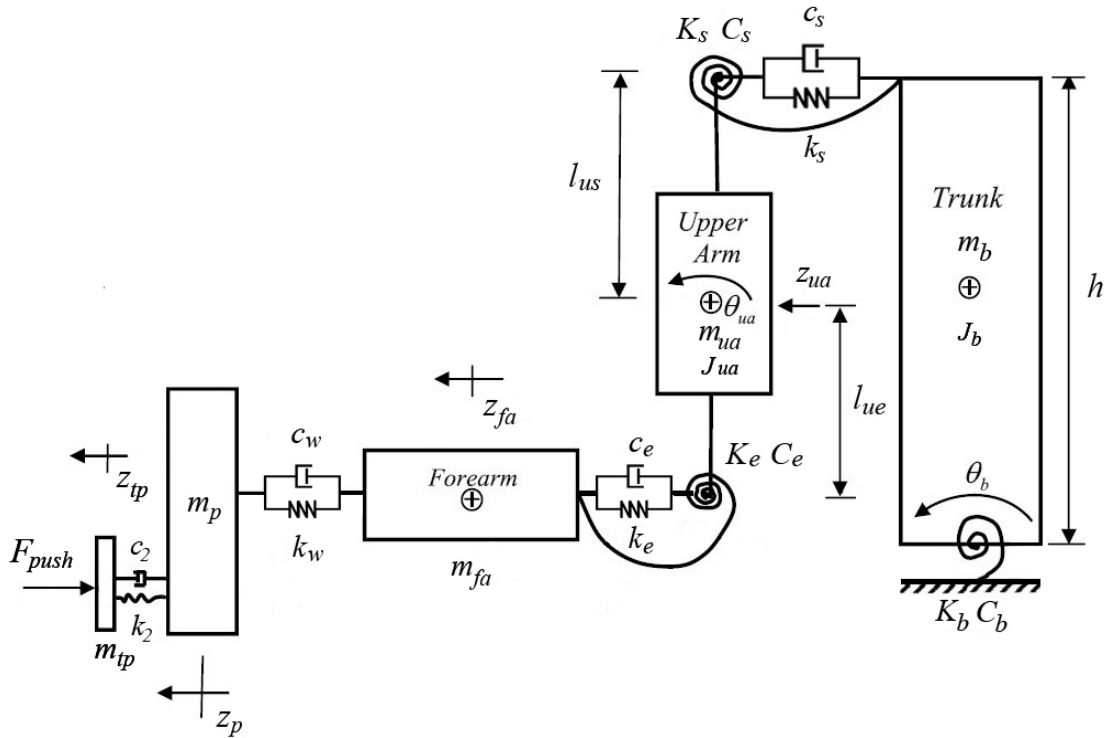
Figure 2.5 : Schematic of the biomechanical hand arm model under a static force

Table 2.6 compares the total static deflections of the biomechanical model with those of the two lumped parameter models (Figure 2.6) under two different levels of static push force. The total deflection of the biomechanical model refers to the deflection of the palm tissue mass with respect to the fixed body support. For the single and four-DOF models, it is defined as the deflection of the hand-handle contact mass (m_1) with respect to the fixed support. The single-DOF model yields the lowest static deflection

under the two push forces (13.70-20.55 mm), while the four-DOF model shows excessive static deflection (276.67 mm) under the 50 N push force and 415.00 mm under the 75 N push force. The lower deflection observed for the single-DOF model is considered more reasonable for the human HAS. The single-DOF model, however, yields poor prediction of the biodynamic response of the HAS. Moreover, the single-DOF model does not permit analyses of distributed vibration responses or power absorption of the HAS. The excessive static deflection responses of the four-DOF model, on the other hand, are judged inadequate for the developments of mechanical hand-arm simulator and coupled hand-tool system model, although this model yields good prediction of the biodynamic response (Rakheja et al., 2002c).
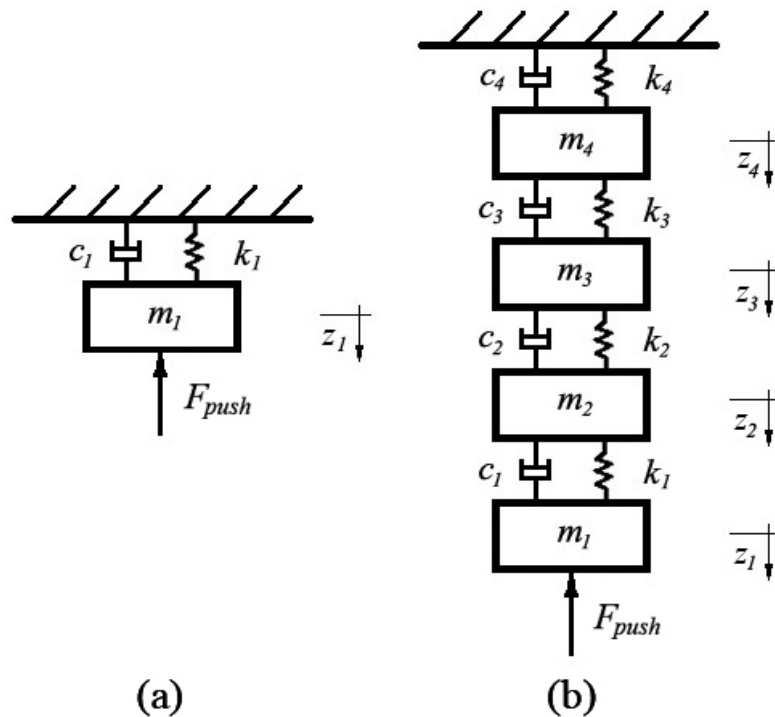
Figure 2.6 : Structure of the biodynamic hand-arm models: (a) single-DOF; and (b) four-DOF

Table 2.4 : Parameters of the single-DOF hand-arm vibration model (Reynolds and Soedel, 1972)

Parameter	Value (z_h axis)
m_1 (kg)	0.103
k_1 (N/m)	3.65e3
c_1 (Ns/m)	39.5

Table 2.5 : Parameters of the four-DOF hand-arm vibration model (ISO 10068, 1998)

Parameter	Value (z_h axis)
m_1 (kg)	0.019
m_2 (kg)	0.0947
m_3 (kg)	0.655
m_4 (kg)	4.290
k_1 (N/m)	3.00e5
k_2 (N/m)	6.80e4
k_3 (N/m)	1.99e2
k_4 (N/m)	2.04e3
c_1 (Ns/m)	591
c_2 (Ns/m)	203
c_3 (Ns/m)	199
c_4 (Ns/m)	239

Table 2.6 : Comparison of the total static deflection of the biomechanical model with those of the single- and four-DOF hand-arm vibration models

Hand-arm vibration model	Static deflection (mm)	
	50 N	75 N
Single DOF model (Reynolds and Soedel, 1972)	13.70	20.55
Four DOF model (ISO 10068, 1998)	276.67	415.00
Six DOF bent-arm model (Grip 30N Push 50N)	40.75	-
Six DOF bent-arm model (Grip 30N Push 75N)	-	187.06

The biomechanical model yielded reasonable static deflection responses under the lower push force of 50 N with total deflection being 40.75 mm. The total deflection under 75 N push force, however, was high (187.06 mm). The biomechanical model also showed reasonably good deformations for most of the individual HAS segments. For instance, the static deflections observed for the palm-wrist mass (x_p-x_{fa}) ranged from 3.53 to 4.04 mm under the two push forces, while the deflections of the forearm (x_{fa}-x_{ua}+$\theta_{ua}l_{ue}$) was relatively small (18.36 mm) under 50 N force, and it was quite large (167.33 mm) under the 75 N push forces. The high total deflections of the bent-arm model under 75 N force was attributed to the substantial decrease in the elbow joint stiffness (k_e decreased by 83.7%) with an increase in the push force, as evident in Table 2.2. The comparison in the static defections of different hand-arm models suggests that the biomechanical model is more suitable for the characterization of the distributed responses in the HAS, the simulation of coupled hand-tool system model, and for realizing a mechanical equivalent HAS simulator.

2.7 Biodynamic Responses Analysis

Occupational exposure to HTV can yield considerable dynamic stresses and deformations within the biological structures of human hand arm system (HAS), which may cause several health disorders. Due to the exceeding complexity of the human HAS, such stresses and deformations, directly acting on the tissues and cells, cannot be reliably measured (Dong J., 2007). Alternatively, the motion and force responses of the HAS have been widely characterized in terms of mechanical impedance and vibration transmissibility responses, which may be correlated with the vibration stresses and deformations (Dong et al., 2005f).

2.7.1 Diving Point Mechanical Impedance Response Analysis

The validity of the six-DOF biomechanical model of the HAS is firstly evaluated by comparing its driving-point mechanical impedance (DPMI) response with the reported measured data.

Referring to the model in Figure 2.1, the DPMI ($Z(j\omega)$) is derived from:

$$Z(j\omega) = \frac{F(j\omega)}{j\omega Z_c(j\omega)}$$ (2.24)

where $F(j\omega)$ denotes the total dynamic force developed at the driving-points at the excitation frequency ω. Since the applied bent-arm model employs two diving points, the dynamic forces developed at the two interfaces can be formulated in terms of the finger force F_f, and the palm force F_p. The dynamic force exerted on the finger-side can be expressed as:

$$F_f = k_1(z_c - z_f) + c_1(\dot{z}_c - \dot{z}_f) + m_{tf}\ddot{z}_c$$ (2.25)

In a similar manner, the dynamic force developed on the palm-side interface can be formulated as:

$$F_p = k_2(z_c - z_p) + c_2(\dot{z}_c - \dot{z}_p) + m_{tp}\ddot{z}_c$$ (2.26)

The total dynamic force, F_h, acting on the hand-handle interface is subsequently evaluated from the sum of the finger- and palm-side forces:

$$F_h = F_f + F_p$$ (2.27)

The mechanical impendences distributed at the finger- and the palm-sides can be computed from:

46

$$Z_{finger}(j\omega) = \frac{F_f(j\omega)}{j\omega Z_c(j\omega)} = \frac{(k_1 + j\omega c_1)(Z_c - Z_f)}{j\omega Z_c} + j\omega m_{tf} \qquad (2.28)$$

$$Z_{palm}(j\omega) = \frac{F_p(j\omega)}{j\omega Z_c(j\omega)} = \frac{(k_2 + j\omega c_2)(Z_c - Z_p)}{j\omega Z_c} + j\omega m_{tp} \qquad (2.29)$$

where $Z_{finger}(j\omega)$ and $Z_{palm}(j\omega)$ are the complex finger- and palm-side mechanical impedances, and Z_f, Z_p and Z_c are the magnitudes of motions of the finger mass, palm mass and handle, respectively.

The DPMI response of the entire hand-arm model, $Z_h(j\omega)$, can be subsequently determined from the sum of $Z_f(j\omega)$ and $Z_p(j\omega)$ (Dong J., 2007):

$$Z_h(j\omega) = \frac{F_h(j\omega)}{j\omega z_c(j\omega)} = \frac{F_f(j\omega) + F_p(j\omega)}{j\omega z_c(j\omega)} = Z_{finger}(j\omega) + Z_{palm}(j\omega) \qquad (2.30)$$

2.7.2 DPMI Responses of the Bent-Arm Model under Two Different Push Forces

Figures 2.7 and 2.8 show the comparisons of the DPMI responses of the bent-arm model along the z_h-axis with the mean measured responses. The measured DPMI responses, corresponding to 50 N and 75 N push forces, respectively, were attained through laboratory tests with six male subjects. The measured data were extracted for two hand grip/push forces combinations (30/50 N and 30/75 N), and broad band z_h-axis vibration in the 2.5 to 500 Hz frequency range (frequency-weighted r.m.s. acceleration=5.25 m/s^2).

The comparisons presented in Figures 2.7 and 2.8 show reasonably good agreements of model responses with the mean measured data for the two hand forces combinations (30 N grip, 50 N push; and 30 N grip, 75 N push). Some notable deviations

47

are also observed in nearly the entire frequency range. The DMPI phase responses of the bent-arm model also show good agreements with the mean measured responses with notable differences in the lower frequency range (2.5-9 Hz).
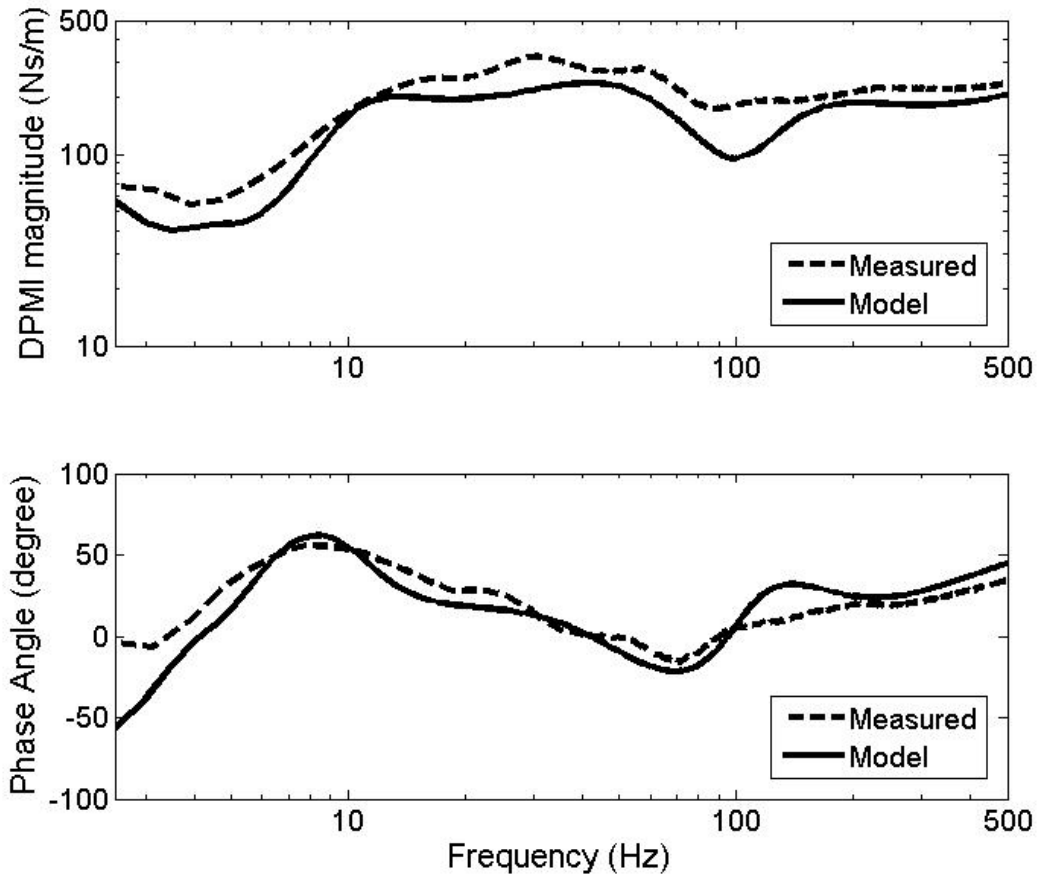
Figure 2.7 : Comparison of z_h-axis DPMI responses of the biomechanical model under 30 N grip force and 50 N push force with mean measured data (Adewusi, 2009)

It needs to be emphasized that the model parameters were identified through minimization of errors in both the DPMI and vibration transmissibility responses of different segments of the HAS model (Adewusi, 2009). While this approach offers a good compromise in predicting both the DPMI and the vibration transmissibility responses, it also contributes to notable errors in both the responses. Parameter identification on the basis of the DPMI along could yield lower error between the DPMI

responses of the model and the measured data. The observed deviations in the DPMI responses are thus believed to be caused by the method of parameters identification.
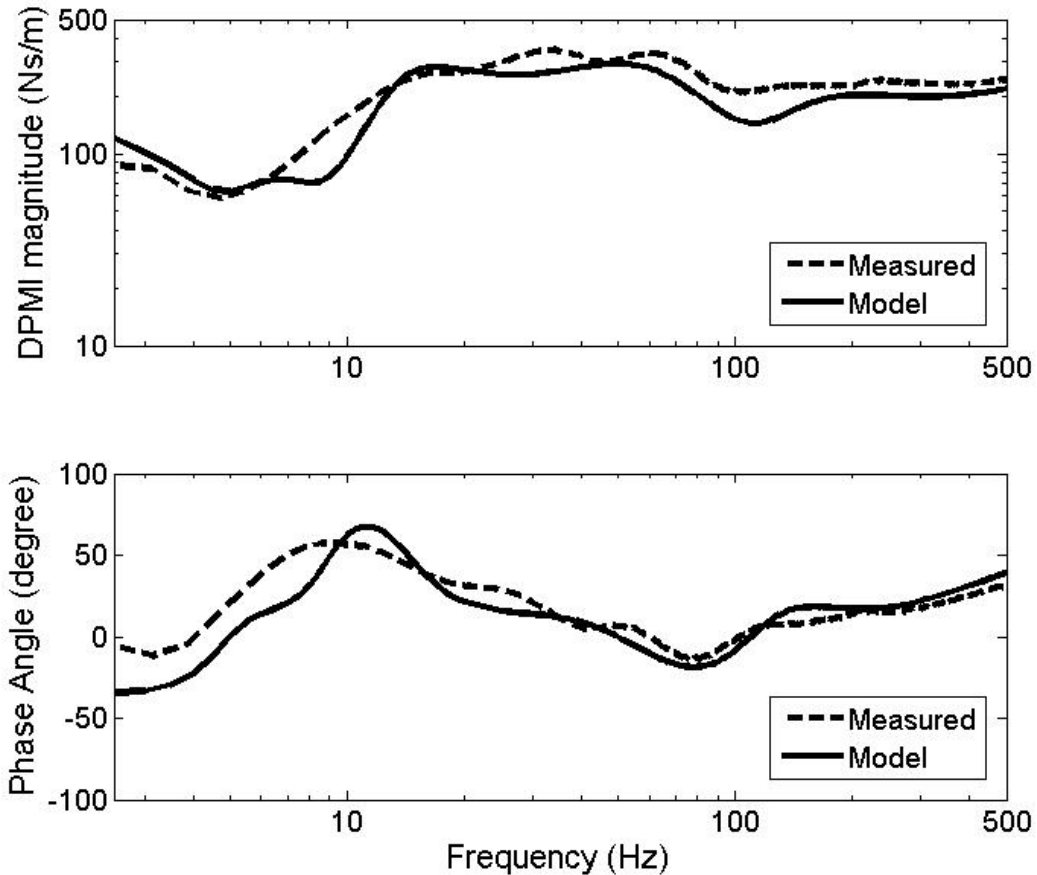
Figure 2.8 : Comparison of z_h-axis DPMI responses of the biomechanical model under 30 N grip force and 75 N push force with mean measured data (Adewusi, 2009)

2.7.3 Vibration Transmissibility Response Analysis

Apart from the DPMI response, a number of studies have also attempted to characterize the biodynamic response of the human hand-arm system (HAS) in terms of the vibrations transmitted to different segments of the HAS (Abrams and Suggs, 1969; Pyykkö et al., 1976; Griffin et al., 1982). Vibration transmissibility has been defined as the ratio of vibration measured a location of the HAS to the vibration measured at the tool handle along the z_h-axis. The validity of the bent-arm biomechanical model of the hand-

49

arm system is thus examined through comparisons of the segmental vibration transmissibility with the mean reported data.

In this dissertation, the z_h-axis vibration transmissibility responses distributed at the wrist, the elbow and the shoulder joint are obtained through solutions of the equations of motion for the bent-arm model, such that:

$$T_w(j\omega) = \frac{Z_p(j\omega)}{Z_c(j\omega)} \tag{2.31}$$

$$T_e(j\omega) = \frac{Z_{ua}(j\omega)}{Z_c(j\omega)} \tag{2.32}$$

$$T_s(j\omega) = \frac{Z_{ua}(j\omega) + l_{us}\theta_{ua}(j\omega)}{Z_c(j\omega)} \tag{2.33}$$

where $T_w(j\omega)$, $T_e(j\omega)$, and $T_s(j\omega)$ designate the vibration transmissibility responses at the wrist, the elbow and the shoulder joint, respectively, corresponding to excitation frequency ω.

The vibration transmissibility responses of the bare hand-arm model can be derived from:

$$\{T_i(j\omega)\} = \left[[K] - \omega^2[M] + j\omega[C]\right]^{-1}\{F(j\omega)\} \tag{2.34}$$

where $[M]$, $[K]$ and $[C]$ denote the mass, stiffness and damping matrices of the bare hand-arm model. $\{T_i(j\omega)\}$ is the vibration transmissibility vector, and $\{F(j\omega)\}$ denotes the forcing vector, given by:

$$\{F(j\omega)\} = [(k_1 + j\omega c_1) \quad (k_2 + j\omega c_2) \quad 0 \quad 0 \quad 0 \quad 0]^T \tag{2.35}$$

50

In a similar manner, the vibration transmissibility responses of the gloved hand-arm model are derived from the equation as:

$$\{T_{gi}(j\omega)\} = \left[\left[K_g\right] - \omega^2\left[M_g\right] + j\omega\left[C_g\right]\right]^{-1}\{F_g(j\omega)\} \qquad (2.36)$$

where $[M_g]$, $[K_g]$ and $[C_g]$ denote the mass, stiffness and damping matrices of the gloved hand-arm model, as formulated in section 2.3. $\{T_{gi}(j\omega)\}$ is the vibration transmissibility vector, and $\{F_g(j\omega)\}$ expresses the forcing vector of the gloved hand-arm system, given by:

$$\{F_g(j\omega)\} = \left[(k_{g1} + j\omega c_{g1}) \quad (k_{g2} + j\omega c_{g2}) \quad 0 \quad 0 \quad 0 \quad 0 \quad 0 \quad 0\right]^T \qquad (2.37)$$

2.7.4 Vibration Transmissibility Responses of the Bent-Arm Model with and without the Anti-Vibration Glove under Two Different Push Forces

Figures 2.9 to 2.14 show the comparisons of the vibration transmissibility responses of the bent-arm model with and without the anti-vibration glove with the mean measured data corresponding to two different levels of the push force (50 N and 75 N). The models consider a constant grip force of 30 N and the mean measured data were obtained from Adewusi (2009). The figures compare the vibration transmissibility responses at the wrist, elbow and shoulder, respectively.

Under the application of 50 N push force, the bent-arm model yields generally good agreements with the mean measured data, as shown in Figures 2.9 to 2.11. However, noticeable deviations are observed in the lower frequency ranges in the transmissibility responses at the wrist (8-30 Hz), at the elbow (2.5-100 Hz) and at the shoulder (2.5-50 Hz), respectively. The bent-arm model under 75 N push force also yields generally good

51

vibration transmissibility responses at all the joints, as shown in Figures 2.12 to 2.14. However, the increase in the push force generally tends to increase the deviations in all the transmissibility responses in the higher frequency range, and tends to decreases the errors observed in the lower frequency range. The observed deviations can be attributed to the minimization of errors in the DPMI and the vibration transmissibility responses for the model parameter identifications.

The comparisons of the vibration transmissibility of the bare-hand and the gloved hand models suggest that the anti-vibration glove under 30 N grip and 50 N push force yields minimal vibration attenuation effects at the elbow and the shoulder in nearly entire frequency range (Figures 2.10 and 2.11). The addition of the anti-vibration glove tends to amplify the vibration slightly around the primary peaks near 12 Hz. The glove, however, tends to attenuate wrist vibration in the 32 to 100 Hz frequency range, with slight amplification around 12 Hz. Similar trends are also evident in the model responses under 30 N grip and 75 N push forces. In this case, the addition of the glove causes relatively greater amplification of vibration transmitted to the wrist, elbow and the shoulder joints around 14 Hz. The results suggest that an anti-vibration glove may not yield effective vibration protection for the operators exposed to the low-frequency vibrations generated by hand-held tools, but could provide attenuation of medium frequency vibration transmitted to the wrist.
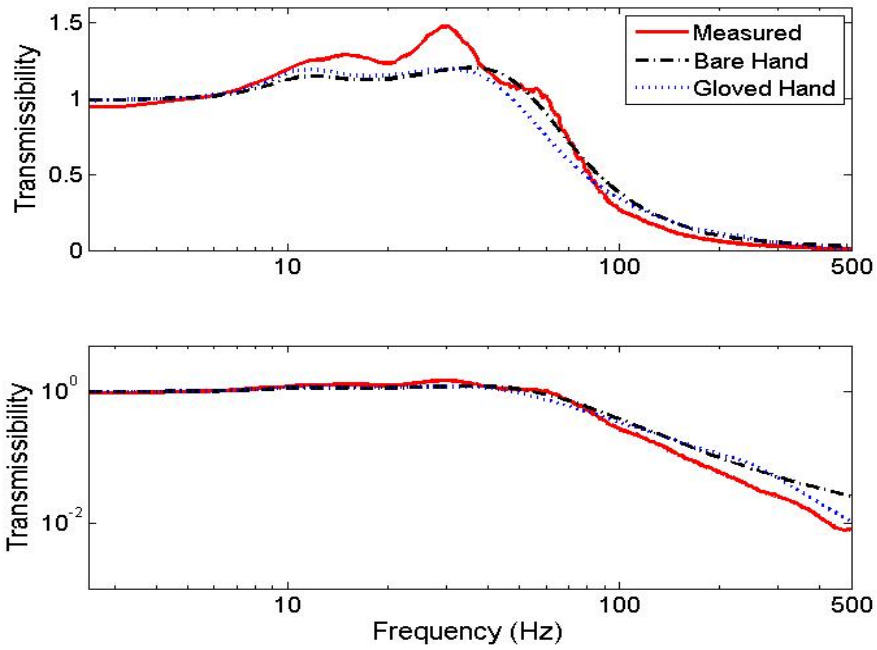
Figure 2.9 : Comparisons of z_h-axis vibration transmissibility responses of the bare and gloved hand-arm models at the wrist with the mean measured responses of the bare hand (grip force=30 N, push force=50 N)
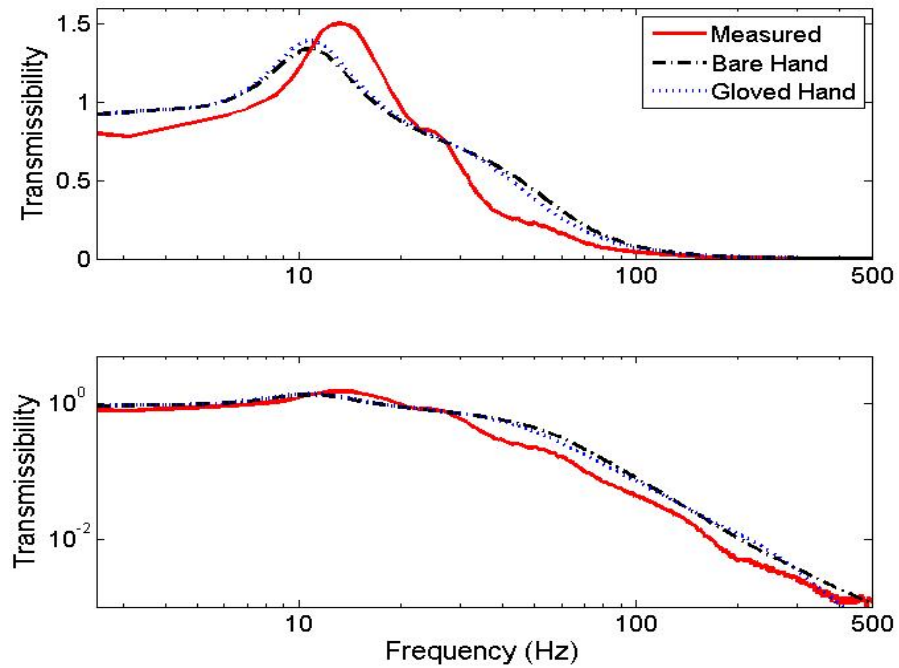
Figure 2.10 : Comparisons of z_h-axis vibration transmissibility responses of the bare and gloved hand-arm models at the elbow with the mean measured responses of the bare hand (grip force=30 N, push force=50 N)

53
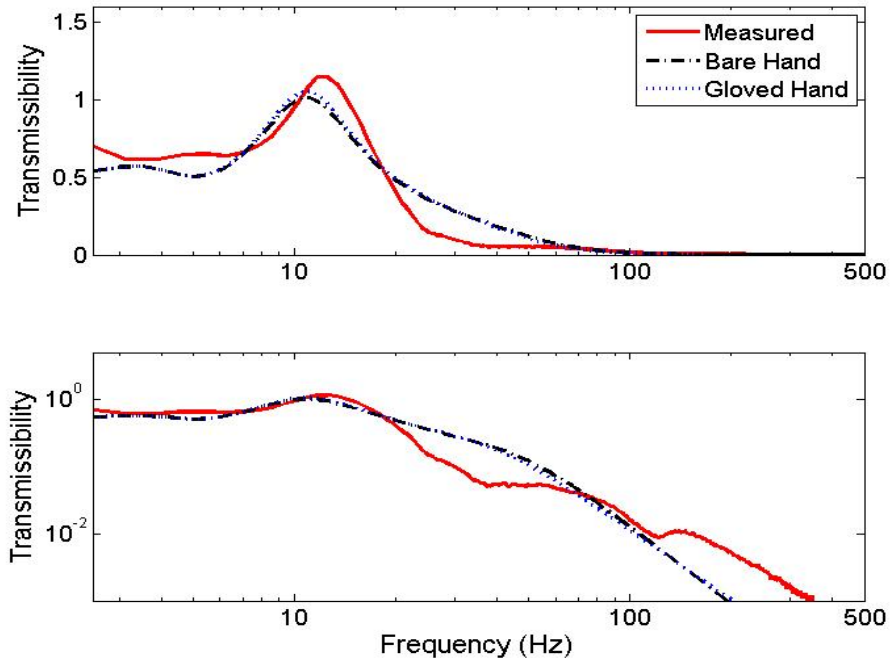
Figure 2.11 : Comparisons of z_h-axis vibration transmissibility responses of the bare and gloved hand-arm models at the shoulder with the mean measured responses of the bare hand (grip force=30 N, push force=50 N)
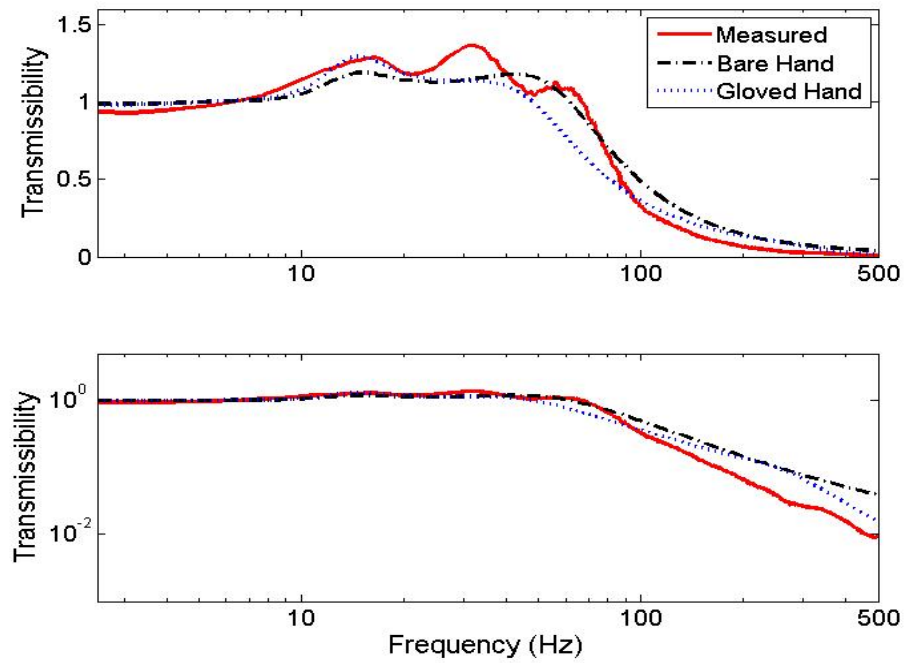
Figure 2.12 : Comparisons of z_h-axis vibration transmissibility responses of the bare and gloved hand-arm models at the wrist with the mean measured responses of the bare hand (grip force=30 N, push force=75 N)

54
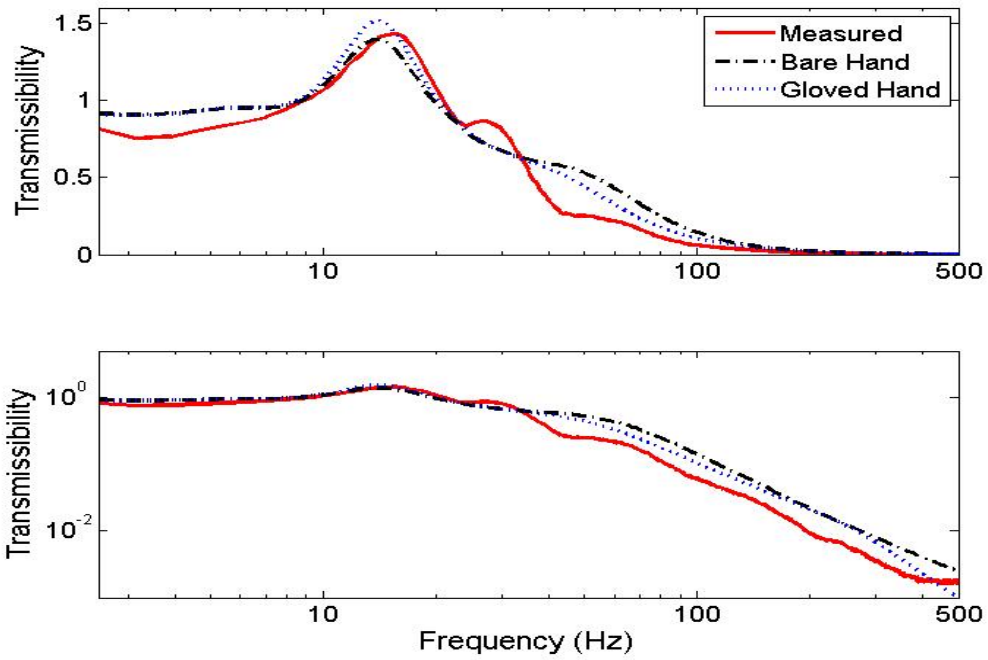
Figure 2.13 : Comparisons of z_h-axis vibration transmissibility responses of the bare and gloved hand-arm models at the elbow with the mean measured responses of the bare hand (grip force=30 N, push force=75 N)
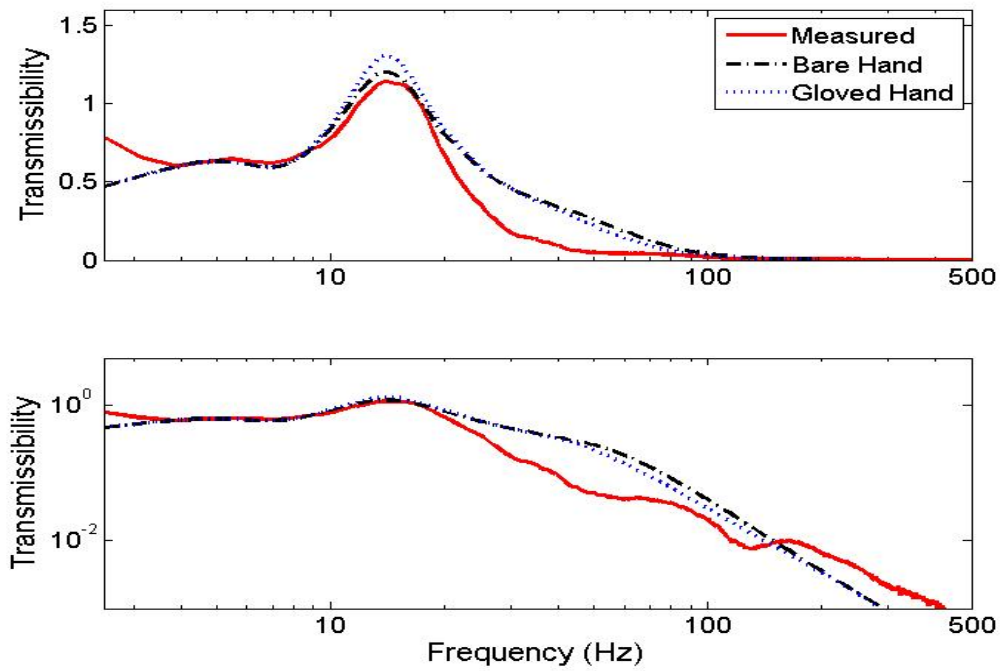
Figure 2.14 : Comparisons of z_h-axis vibration transmissibility responses of the bare and gloved hand-arm models at the shoulder with the mean measured responses of the bare hand (grip force=30 N, push force=75 N)

2.8 Summary

A six-DOF biomechanical model of the human hand-arm system (HAS) in a bent-arm posture is re-formulated and analyzed to assess its ability to predict the biodynamic responses of the HAS. It is shown that the model can yield reasonably good predictions of the responses in terms of driving point mechanical impedance and vibration transmissibility. Furthermore, the model yields reasonable deformations under 50 N push force, while the deformation under 75 N push force was considered to be high. A model of the HAS with an anti-vibration glove is further developed and analyzed. The hand-arm system model with and without the glove is judged suitable for implementation to the tool model. Corresponding coupled system models are further formulated in the following chapter.

CHAPTER 3
DEVELOPMENT OF ANALYTICAL MODELS OF PERCUSSIVE CHIPPING
HAMMER AND WORKPIECE

3.1 Introduction

Percussive chipping hammers, driven by pneumatic power, are broadly utilized in the infrastructure or mining industry. These tools are designed to pneumatically initiate impacts among tool components. Such impacts subsequently produce large-magnitude cutting forces at the tool tip for crushing or drilling in hard materials. However, substantial vibrations are also transmitted to the tool body and are subsequently absorbed by the operator's hand and arm through the tool handle. Percussive tools can emit excessive vibrations ranging from 251 to 2014 m/s^2, while the dominant frequency lies in the 25-125 Hz range (Gurram, 1993). As a result, percussive tool operators are more prone to suffer from a high prevalence of HAVS (Table 1.1).

Owing to high prevalence of HAVS among the percussive tools operators, the need for developing low vibration percussive tools or effective vibration isolation mechanism has been widely emphasized. The design of vibration isolators or assessment of vibration performance of different tools necessitates developments in dynamic models of the tools. Furthermore, a proven model of the hand-arm system (HAS) needs to be integrated to the tool model to account for energy absorption property of the HAS. However, owing to the extreme complexities associated with the compact tool designs, and wide variations in the tasks and workpiece properties, the developments in tools and integrated hand-tool-workpiece system models have been addressed in only a few studies (Rakheja et al., 2002b; Golycheva et al. 2003; 2004). These models were proposed to derive design

guidance for low vibration power tools and for identifying desirable operating factors, as described in section 1.2.5.

In this chapter, an analytical model of a percussive chipping hammer coupled with an idealized workpiece contact model, is systematically developed to estimate the effects due to the variations in operating factors, design parameters and hand-arm models on the dynamic performances of the integrated hand-tool-workpiece system.

3.2 Description of the Percussive Tool

A hand-held percussive chipping/demolition hammer, manufactured by BOSCH (11313 EVS), is considered in this study. A pictorial view of the tool is shown in Figure 3.1. The selected chipping hammer is driven by a 115 V AC electric motor and it can deliver up to 2600 blows per minute (bpm). The tool speed could be varied in the 1300 to 2600 bpm range, using the user-controlled speed dial. Two tool handles integrated with the tool housing, permit the operator to apply the desired feed force and guide the tool. The feed force is applied to the primary handle attached to the drive unit, which also houses the speed controller, as shown in Figure 3.1. The tool guidance is achieved by the operator using the secondary handle located above the tool bit holder.

The tool operation constitutes a series of impacts among the various tool components. Apart from the drive unit, the tool housing and the handles, the main components of the selected tool include the piston, the striker, the control disks, the guide tube, the control bushing, the impact bolt and the tool bit, as shown in Figure 3.2. The AC motor serves as the continuous drive for the piston via the slider-crank mechanism, while the piston motion is guided along the axial direction within the guide tube. A downward

piston motion compresses the air in the upper chamber bounded by the guide tube, the piston and the striker. The significant variations in the air pressure in the upper chamber subsequently cause a rapid axial motion of the striker, which further collides with the impact bolt, as shown in Figure 3.2. The impact bolt further impacts on the tool bit to transmit the energy to the tool bit and thereby the cutting force.

The air in the lower chamber, bounded by the guide tube, the striker and the lower control disk, is compressed by the striker. The air within the lower chamber offers a buffering effect between the striker and the impact bolt so as to eliminate direct impacts between the striker and the lower control disk. Moreover, two sets of orifices are provided within the upper and lower chambers for controlling the air pressure. The air flows through the orifices would also contribute to some damping. The flows through the upper chamber orifices are controlled by the relative positions of the control bushing and the striker, while the lower chamber orifices normally remain open. Furthermore, the annular clearance between the striker shaft and the control disks permits the flow of air from the lower chamber to the atmosphere. The air pressure in the lower chamber may thus be considered to be atmospheric. The light-weight control bushing could locate itself on the lower control disk, due to the preload on the spring supporting the control bushing. The upper chamber orifices may remain closed under static as well as during the compression cycle, and they may open either fully or partially during the rebound motion of the striker.

The collision between the striker and the impact bolt subsequently causes an impact between the impact bolt and the tool bit, while the rebound motion of the impact bolt causes the upper control disk to impact against the lower control disk, transmitting

vibrations to the tool body. Two elastomeric O-rings are mounted between the upper control disk and the impact bolt, and the impact bolt and the tool body, to achieve some degree of vibration isolation.

Figure 3.1 : Pictorial view of the BOSCH 11313EVS percussion chipping hammer
(BOSCH Co. Ltd.)
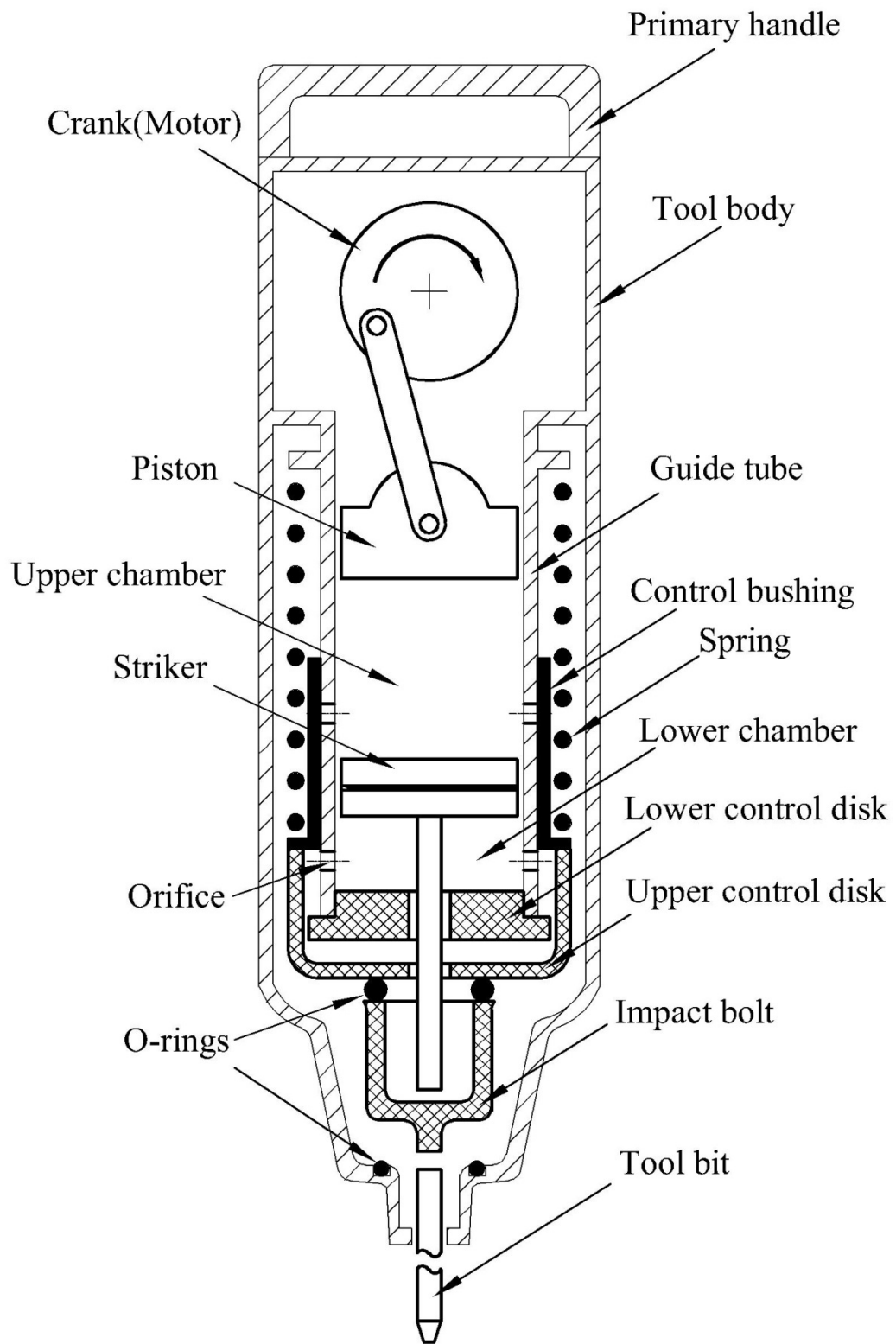
Figure 3.2 : Schematic of the chipping hammer illustrating the major components

3.3 Development of the Chipping Hammer Model

The operation of the chipping hammer involves a series of sequential impacts, namely, striker-impact bolt, impact bolt-tool bit, impact bolt-control discs-tool body and tool bit-tool body. Development of the tool model thus necessitates the modeling of these impact pairs and the identification of the impact model parameters. The subsystem models are systematically formulated in the following subsections, which are subsequently integrated with the hand-arm vibration models described in Chapter 2, so as to obtain the integrated hand-tool system model.

3.3.1 Displacement Coordinates

The coordinates of the different subsystems are initially defined for characterizing the interactions among different impact pairs considering the geometric constraints of the tool assembly. The crank center is designated as the origin of this coordinate system. The displacement of the crank center, z_C, is also utilized to describe the motion of the tool body as well as the handles. Figure 3.3 shows the relative positions of the piston, the striker, the impact bolt and the tool bit with respect to the origin as z_{PC}, z_{SC}, z_{BC} and z_{TC}, respectively. In this notation, for instance, z_{PC} denotes the relative displacement of the piston from the crank center. All the displacement coordinates are defined positive in the vertically downward direction.
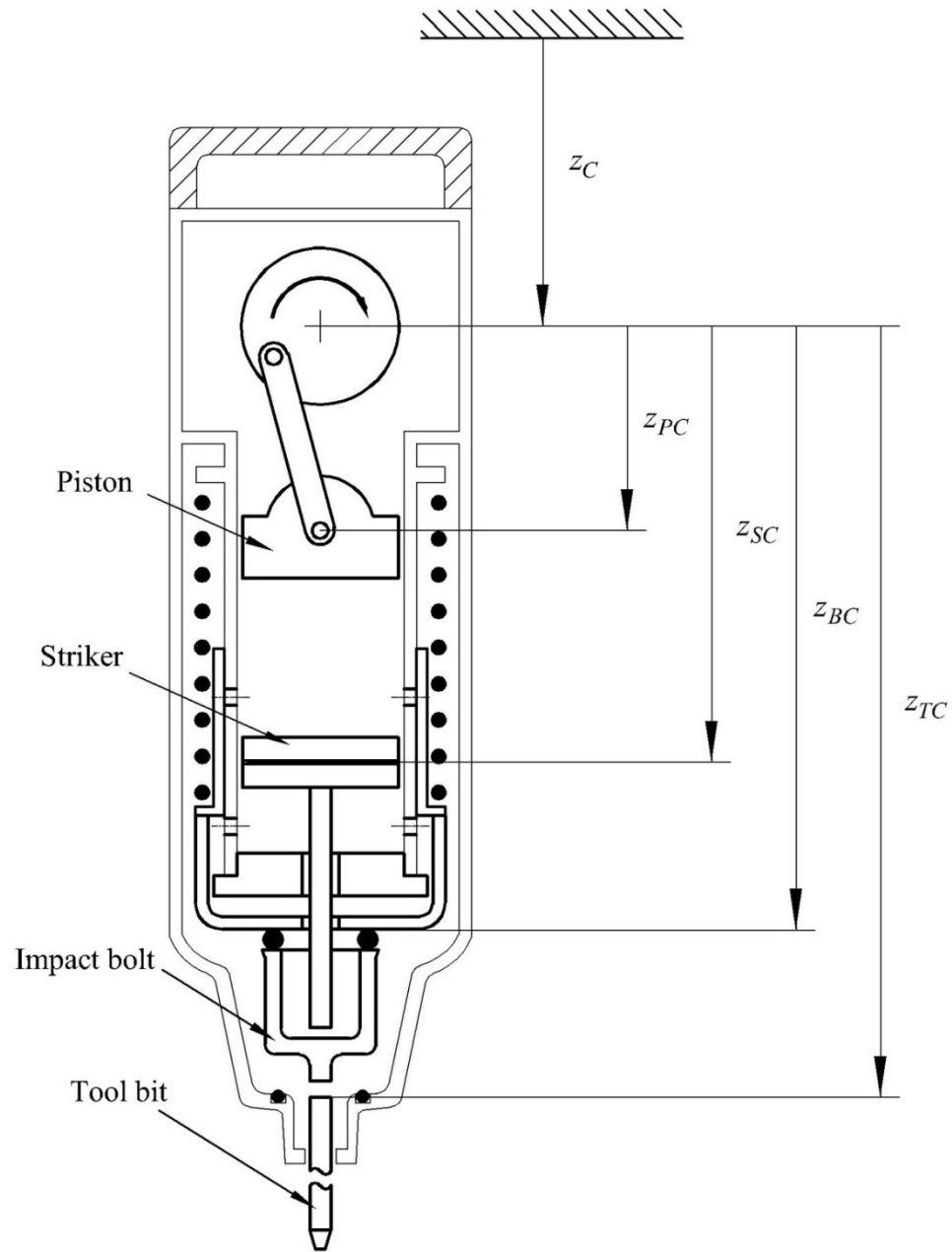
Figure 3.3 : Displacement coordinates used for modeling of different impact pairs

3.3.2 Piston Displacement

The displacement of the piston is obtained from the kinematics of the crank-slider mechanism, assuming negligible inertial effect of the mechanism and constant rotational

speed ω_c. Defining the crank rotation θ with respect to the top-dead center of the crank (Figure 3.4), the relative displacement of the piston can be expressed as:

$$z_{PC} = \sqrt{(l_{rod}^2 - r_c^2 \sin^2 \theta)} - r_c \cos \theta \qquad (3.1)$$

where r_c is the crank length, and l_{rod} denotes the length of the connecting rod.

The velocity of the piston relative to the crank center is subsequently formulated as:

$$\dot{z}_{PC} = \omega_c r_c \sin \theta \left[1 - r_c \cos \theta (l_{rod}^2 - r_c^2 \sin^2 \theta)^{-1/2} \right] \qquad (3.2)$$
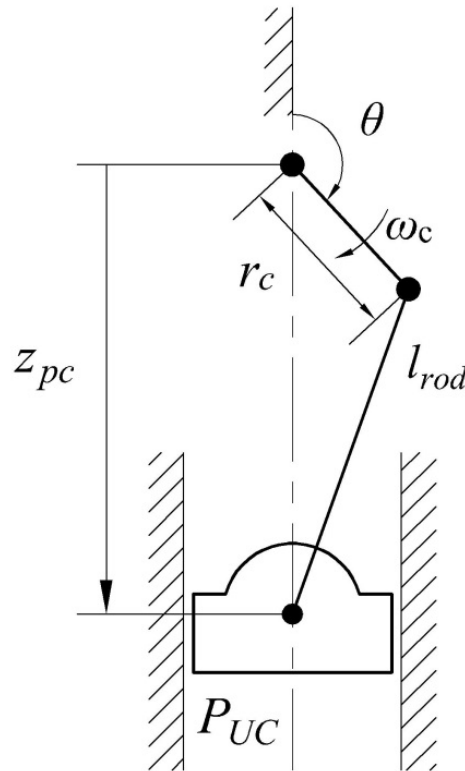
Figure 3.4 : Schematic of the slider-crank mechanism

3.3.3 Air Pressure and Density Variations

The striker with an O-ring separates the guide tube into two chambers: (i) upper chamber bounded by the piston and the striker; and (ii) lower chamber confined by the

striker and lower control disk, as shown in Figure 3.5. The motion of the piston causes considerable variations in the pressure of the air within the upper chamber, which leads to high velocity motion of the striker and subsequent impacts among the tool components. Air flows from the upper and lower chambers occur through the orifices. The mass flow rate of the air, however, depends on the effective orifice area, which is directly related to the relative positions of the striker and the control bushing. Depending upon the position of the striker, the air flow from the lower chamber may occur through both sets of orifices apart from the annular clearance between the striker shaft and the control disks, as shown in Figure 3.5. The flows from the upper chamber, however, are limited to the upper orifices only, irrespective of the striker position. The upper orifice opening, however, also depends upon the position of the control bushing.

Results obtained from a preliminary study (Rakheja et al., 2002b) suggested that the air pressure in the lower chamber remains very close to the atmospheric pressure during the tool operation. This is due to the upward motion of the control bushing under a static feed force, and additional air flows through the annular gap between the striker shaft and the control disks. The lower chamber air pressure is thus assumed to remain constant and equal to the atmospheric pressure.

The relative positions of the striker and the control bushing determine the boundaries of the upper and lower chambers as well as the occurrence of associated air flows. As shown in Figure 3.6, L_{SU} and L_{SL} denote the thicknesses of the striker on the upper and lower chamber sides. Subsequently, $z_{SC}-L_{SU}$ and $z_{SC}+L_{SL}$ define the relative displacements of the upper and lower edges of the striker, respectively.
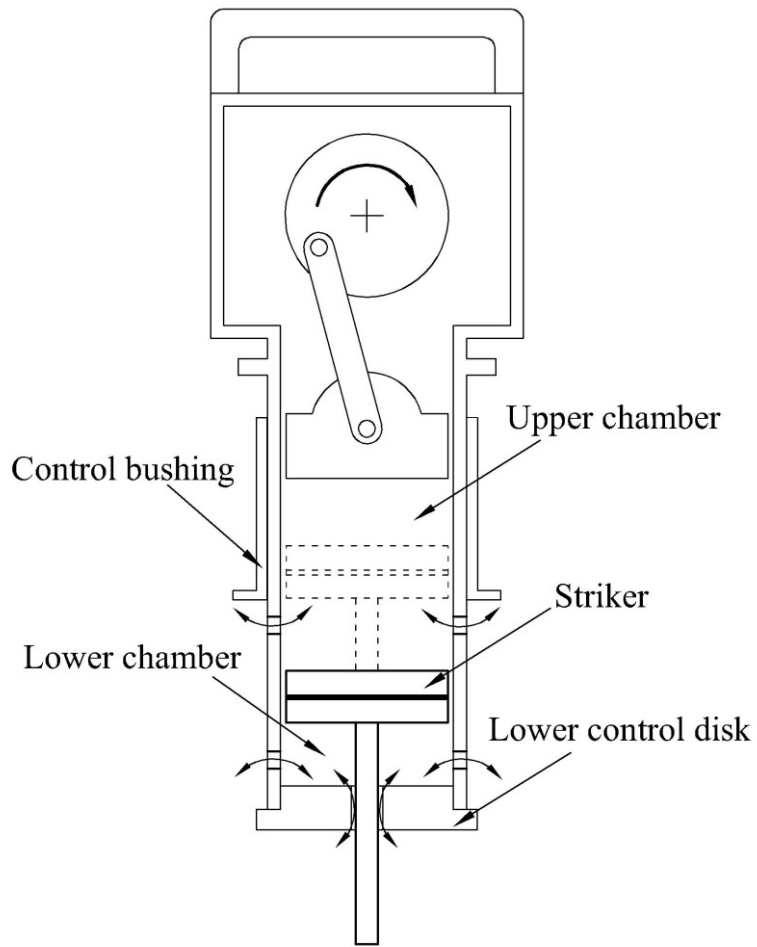
Figure 3.5 : Air flow through the orifices in the upper and lower chambers
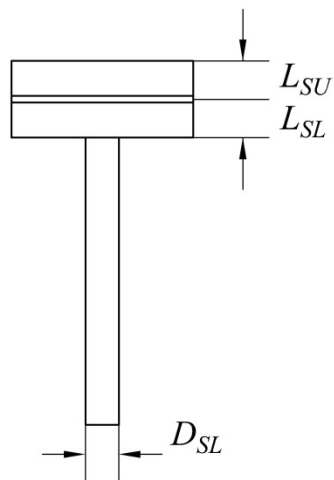
Figure 3.6 : Schematic of the striker

During operation, the control bushing, governing the opening of the orifices, can either sit on the lower control disk or oscillate along the guide tube, as shown in Figure 3.7. It should be noted that the upper control disk is supported on the impact bolt through an O-ring, as seen in Figure 3.7. It is assumed that the loss of contact between the upper control disk and the impact bolt does not occur during the tool operation. Referring to Figure 3.7, the relative displacement of the lower end of the control bushing, z_{CBC}, can be determined from:

$$z_{CBC} = \begin{cases} z_{BC} - L_{UCD}; & z_{BC} \leq (L_{CBC})_{\max} + L_{UCD} \\ (L_{CBC})_{\max}; & z_{BC} > (L_{CBC})_{\max} + L_{UCD} \end{cases} \tag{3.3}$$

where L_{UCD} represents the design length of the upper control disk, and $(L_{CBC})_{max}$ describes the relative distance of the lower end of the control bushing when it sits on the lower control disk. The position of the upper edge of the control bushing is subsequently derived from $z_{CBC} - L_{CB}$, where L_{CB} is the design length of the control bushing.

Let A_{UH} denote the total cross section area of the upper set of orifices and C_{AU} express the fraction of the opening area of the upper orifices. The effective area of the upper orifices is subsequently determined as $C_{AU} A_{UH}$. The fraction C_{AU} approaches unity when the upper orifices are fully open, satisfying both the following conditions for the striker and control bushing positions:

i) When the upper edge of the striker is beneath the lower end of the upper orifices:

$$z_{SC} - L_{SU} \geq L_{UH} + 0.5D_{UH} \tag{3.4}$$

where D_{UH} represents the diameter of the orifice and L_{UH} denotes the relative position of the upper orifices (Figure 3.7).

ii) When the upper edge of the control bushing is beneath the lower end of the upper orifices:

$$z_{CBC} - L_{CB} \geq L_{UH} + 0.5D_{UH} \qquad (3.5)$$

or when the lower edge of the control bushing is above the upper end of the upper orifices:

$$z_{CBC} \leq L_{UH} - 0.5D_{UH} \qquad (3.6)$$

The air flow through the upper orifices will completely diminish ($C_{AU} = 0$) when the striker or the control bushing overlaps the orifices, as determined from one of the two conditions listed below:

i) When the upper edge of the striker is above the upper end of the upper orifices:

$$z_{SC} - L_{SU} \leq L_{UH} - 0.5D_{UH} \qquad (3.7)$$

and the lower edge of the striker is beneath the lower end of the upper orifices:

$$z_{SC} + L_{SL} \geq L_{UH} + 0.5D_{UH} \qquad (3.8)$$

ii) When the upper edge of the control bushing is above the upper end of the upper orifices:

$$z_{CBC} - L_{CB} \leq L_{UH} - 0.5D_{UH} \qquad (3.9)$$

and the lower edge of the control bushing is beneath the lower end of the upper orifices:

$$z_{CBC} \geq L_{UH} + 0.5D_{UH} \qquad (3.10)$$
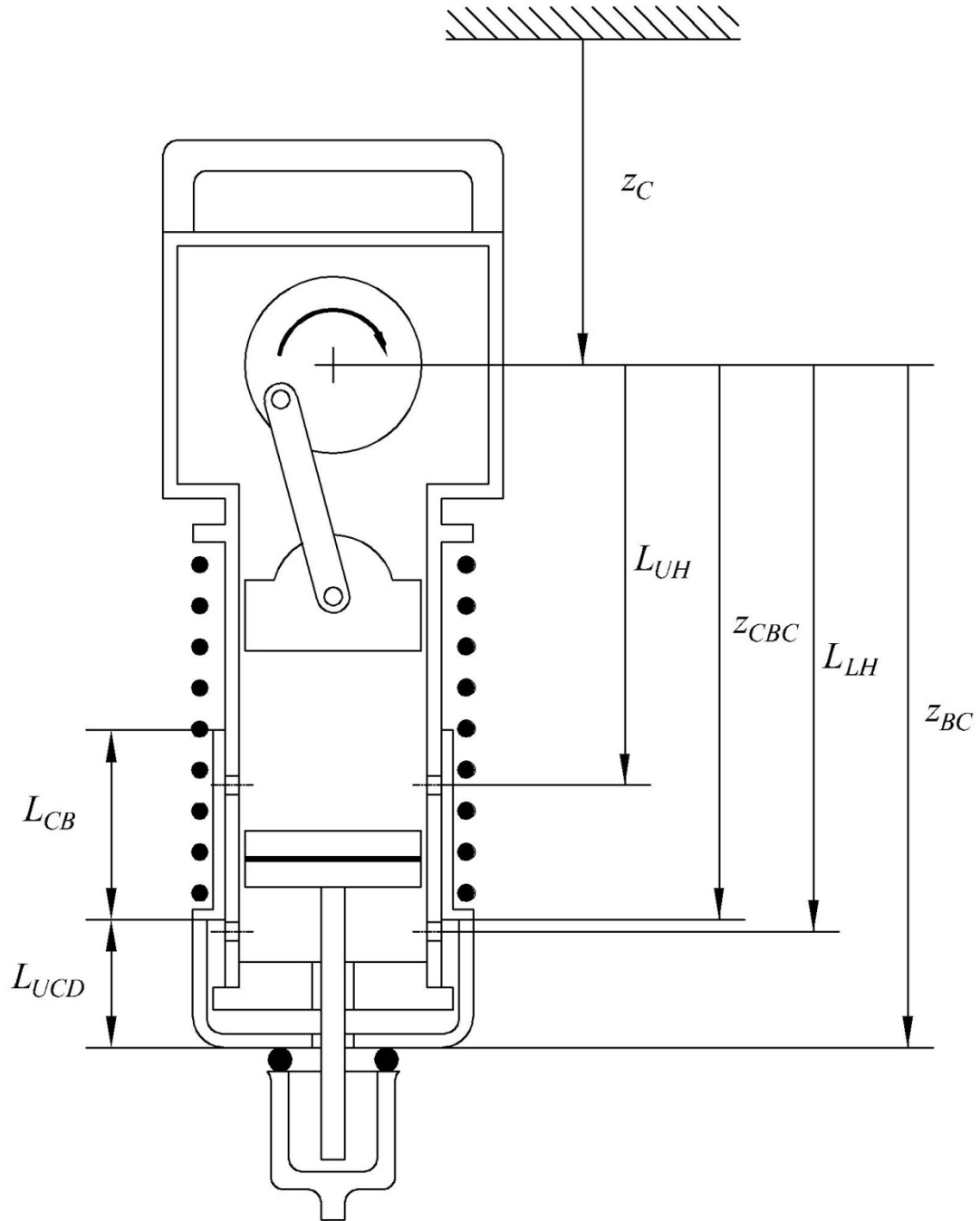
Figure 3.7 : Relative positions of the control bushing and orifices

The violations of the above conditions imply that the upper orifices may be either partly open ($0<C_{AU}<1$), or lie within the lower chamber. When satisfying the partial opening conditions, C_{AU} is determined from the lower of the two fractions, C_{AU1} and C_{AU2},

which are the fractions determined from the relative displacements of the striker and control bushing, respectively, such that:

$$\begin{cases} C_{AU1} = 1 - \dfrac{2\varphi_1 - \sin(2\varphi_1)}{2\pi} & \varphi_1 = \dfrac{\pi}{2} - \arcsin\dfrac{2(z_{SC} - L_{SU} - L_{UH})}{D_{UH}} \\[3mm] C_{AU2} = 1 - \dfrac{2\varphi_2 - \sin(2\varphi_2)}{2\pi} & \varphi_2 = \dfrac{\pi}{2} - \arcsin\dfrac{2(z_{CBC} - L_{CB} - L_{UH})}{D_{UH}} \end{cases} \tag{3.11}$$

Furthermore, the following conditions must also be satisfied for a partial opening of the upper orifices to occur:

$$\left| (z_{SC} - L_{SU} - L_{UH}) / D_{UH} \right| \leq 0.5 \tag{3.12}$$

$$\left| (z_{CBC} - L_{CB} - L_{UH}) / D_{UH} \right| \leq 0.5 \tag{3.13}$$

The variations in the air pressure and mass density could be derived considering the air flows and motions of the piston and the striker. It has been suggested that the upper chamber boundary can be considered adiabatic and the air flows through the orifices can be determined as a reversible adiabatic flow through a nozzle (Rakheja et al., 2002b). The variations in the pressure and density of the air in the upper chamber can be obtained from:

$$\frac{dP_{UC}}{dt} = \begin{cases} \dfrac{\gamma P_{UC}}{\left[z_{SC} - z_{PC} - (L_{SP})_{\min} \right]} \left[\dot{z}_{PC} - \dot{z}_{SC} + V_{UI} C_{AU} \left(\dfrac{P_a}{P_{UC}} \right)^{1-1/\gamma} \right] & P_{UC} < P_a \\[5mm] \dfrac{\gamma P_{UC}}{\left[z_{SC} - z_{PC} - (L_{SP})_{\min} \right]} \left[\dot{z}_{PC} - \dot{z}_{SC} - V_{UE} C_{AU} \left(\dfrac{P_a}{P_{UC}} \right)^{1/\gamma} \right] & P_{UC} \geq P_a \end{cases} \tag{3.14}$$

$$\frac{d\rho_{UC}}{dt} = \begin{cases} \dfrac{\rho_{UC}}{\left[x_{SC} - x_{PC} - (L_{SP})_{min}\right]}\left[\dot{x}_{PC} - \dot{x}_{SC} + V_{UI}C_{AU}\dfrac{\rho_a}{\rho_{UC}}\left(\dfrac{P_{UC}}{P_a}\right)^{1/\gamma}\right] & P_{UC} < P_a \\[20pt] \dfrac{\rho_{UC}}{\left[x_{SC} - x_{PC} - (L_{SP})_{min}\right]}\left[\dot{x}_{PC} - \dot{x}_{SC} - V_{UE}C_{AU}\left(\dfrac{P_a}{P_{UC}}\right)^{1/\gamma}\right] & P_{UC} \geq P_a \end{cases}$$

(3.15)

where ρ_a is the mass density of air at the atmospheric pressure P_a, and ρ_{UC} is the density

of the air in the upper chamber corresponding to its instantaneous pressure P_{UC}. $(L_{SP})_{min}$

denotes the minimum distance between the hinge point of the piston and the seal groove

of the striker, and γ is the adiabatic constant. V_{UI} and V_{UE} are the velocities of the air

flows entering and leaving the upper chamber, respectively, given by (Rakheja et al.,

2002b):

$$V_{UI} = \frac{A_{UH}}{A_{UC}}\sqrt{\frac{2\gamma P_a}{(\gamma-1)\rho_a}\left[1 - \left(\frac{P_{UC}}{P_a}\right)^{1-1/\gamma}\right]}$$

(3.16)

$$V_{UE} = \frac{A_{UH}}{A_{UC}}\sqrt{\frac{2\gamma P_{UC}}{(\gamma-1)\rho_{UC}}\left[1 - \left(\frac{P_a}{P_{UC}}\right)^{1-1/\gamma}\right]}$$

(3.17)

The highly nonlinear variations in the pressure and flow of the compressible fluid

may induce convergence errors, especially when the upper chamber pressure approaches

the atmospheric pressure or the control orifice area varies rapidly. The solutions of theses

equations are thus obtained using very small integration time step of 1×10^{-6} s and

absolute tolerance of 1×10^{-14}.

3.3.4 Modeling of Tool Components

Tool Body

During operation, the forces imposed on the tool body may comprise: tool weight; hand forces imposed on the handles; spring force that determines control bushing's motion; friction forces between the components and the tool body; and the contact forces between the tool body and the tool bit, the lower control disk and the upper control disk. Since the lower control disk is firmly fixed to the tool body and the upper control disk is supported by the impact bolt, the upper-lower control discs impact is converted to the impact between the impact bolt and the tool body. Moreover the forces due to the air pressure variations in the upper and lower chambers also affect the tool body dynamics. Primarily analysis suggested the absence of impacts between the tool bit and the tool body during the tool operation. The friction force arising within the piston in the guide tube is also neglected. As a result, the equation describing the motion of the tool body can be expressed as:

$$
\begin{aligned}
M_C \ddot{z}_C = & M_C g - F_{CB} + F_{sh} + F_{dh} - F_S + F_{FS} + F_{FT} \\
& -\left(P_{UC} - P_a\right) A_{UC}
\end{aligned}
\tag{3.18}
$$

where M_C denotes the lumped mass of the tool body including the drive unit, and $\ddot{z}_C$ is its absolute acceleration. Let g denote the acceleration due to gravity, and F_{CB} is the contact force due to the impact bolt, as described in section 3.5. F_{sh} and F_{dh} are the static and dynamic hand forces imparted on the tool handle, respectively. The biomechanical model of the hand-arm system, presented in Chapter 2, is employed to derive the dynamic hand-force. Considering the two driving points used in the biomechanical model, the static and dynamic hand forces are expressed by combination of the palm and finger forces from Eqs. (2.7-2.9), (2.16-2.18) and (2.19-2.20), as seen in Figure 3.8 (a):

$$F_{sh} = F_{spalm} - F_{sfinger} = F_{push} \tag{3.19}$$

$$F_{dh} = F_{dpalm} + F_{dfinger} \tag{3.20}$$

The vast majority of the biodynamic hand-arm vibration (HAV) models, however, consider a single driving point, as shown in Figures 3.8 (b). In such cases, F_{spalm} refers to the push force ($F_{spalm} = F_{push}$), while the dynamic force developed at the hand-handle interface is determined from the biodynamic HAV model.

(a)   (b)
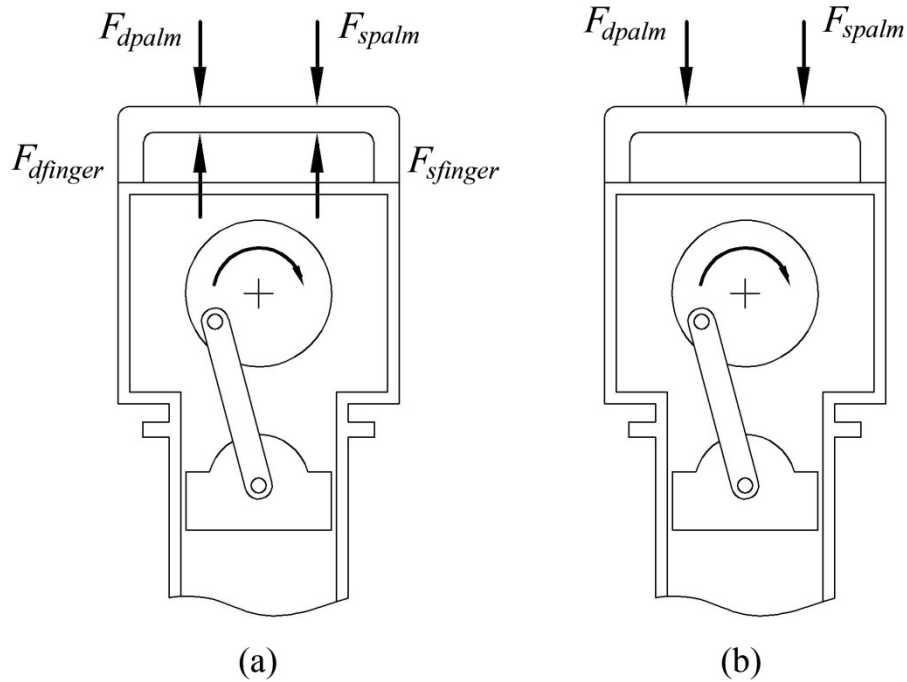
Figure 3.8 : The static and dynamic hand forces imposed on the tool handle (a) by the biomechanical model; and (b) by the biodynamic model

The notation F_S in Equation 3.18 describes the restoring force due to the coil spring, which controls the motion of the control bushing for air flow control. The spring force may be expressed as:

$$F_S = \begin{cases} (F_S)_{min} + k_S \left[(L_{CBC})_{max} - z_{CBC} \right] & (L_{CBC})_{max} > z_{CBC} \\ 0 & (L_{CBC})_{max} = z_{CBC} \end{cases} \qquad (3.21)$$

where k_S is the stiffness of the spring and $(F_S)_{min}$ expresses the initial resorting force. It should be noted that the inertial force due to the control bushing is neglected due to its very low mass.

In Eq. (3.18), F_{FS} and F_{FT} are the friction forces due to striker seal and the tool bit clamped in the tool bit holder, which are modeled as viscous forces, such that:

$$F_{FS} = c_{FS} \dot{z}_{SC} \qquad (3.22)$$

$$F_{FT} = c_{FT} \dot{z}_{TC} \qquad (3.23)$$

where c_{FS} and c_{FT} are the effective viscous damping coefficients.

The last term in Eq. (3.18) describes the force due to the upper chamber air pressure acting on the piston.

<u>Striker</u>

In a similar manner, the forces acting on the striker include its weight, the force due to the pressure variations in the upper chamber, the viscous friction between the striker and the guide tube, and the contact force between the striker and the impact bolt. The equation governing the striker motion is thus expressed as:

$$M_S \ddot{z}_S = M_S g + (P_{UC} - P_a) A_{UC} - F_{FS} - F_{SB} \qquad (3.24)$$

where M_S is the mass of the striker and $\ddot{z}_S$ is its absolute acceleration. F_{SB} describes the contact force between the striker and the impact bolt, which is derived in section 3.5.

Impact bolt

Assuming small masses due to the upper control disk and control bushing, the motion of the impact bolt is governed by its weight, the restoring force transmitted by the control bushing, and the contact forces between the striker and the impact bolt (F_{SB}), the tool body and the impact bolt (F_{CB}), and the tool bit and the impact bolt F_{BT}. The equation describing the motion of the impact bolt is subsequently formulated as:

$$M_B \ddot{z}_B = M_B g + F_S + F_{SB} + F_{CB} - F_{BT} \qquad (3.25)$$

where M_B is the mass of the impact bolt and $\ddot{z}_B$ denotes its absolute acceleration. The contact force between the impact bolt and the tool bit (F_{BT}) is further formulated in section 3.5.

Tool Bit

The forces acting on the tool bit include its weight, the contact force between the bolt and tool bit, the viscous friction between the tool bit and the tool body, and the contact force between the tool bit and the work-piece. The equation describing the motion of the tool bit is thus expressed as:

$$M_T \ddot{z}_T = M_T g + F_{BT} - F_{FT} - F_{TG} \qquad (3.26)$$

where M_T is the mass of the tool bit and $\ddot{z}_T$ denotes its acceleration. F_{TG} is the cutting force developed at the tool bit-workpiece interface, which is described in section 3.4.

3.4 Development of the Tool Tip-Workpiece Contact Model

Apart from the diversity among the tool types, tool maintenance state and working speed, the wide variations in the properties of the work-piece strongly affect the dynamic

75

performances of the coupled hand-tool system. For percussive chipping hammers, the vast majority of the treated materials, such as rock, concrete and metal, could cause highly nonlinear interactions between the tool bit and the workpiece. Substantial energy due to the impacts among the tool components is transmitted to the tool bit, which induces rapid stress variations in the workpiece leading to failure of the treated material.

Development of the coupled hand-chipping hammer system model necessitates modeling of the tool bit-workpiece interactions. However, only a few studies have attempted contact models to characterize the interactions between the tool bit and the workpiece, particularly for a percussive tool. Rakheja et al. (2002b) proposed a two-DOF contact model to characterize the tool bit contact with the steel balls in the standardized energy dissipater (ISO 8662-2, 1992). The tool bit was assumed to create a rigid core in the workpiece at the vicinity of the tool tip and transmit vibrations to a plastic substratum supported by an elastic substratum. The plastic substratum was idealized by a Kelvin-Voigt model, while the elastic substratum was represented by a high stiffness linear spring. Moreover, the mass of the work-piece was ignored and separation was permitted between the tool tip and the plastic zone. However, considerable deviations were observed between the simulation results and the measured data in terms of acceleration responses of the tool body. Golycheva et al. (2003; 2004) integrated a coupled hand-chipping hammer system model with a single-DOF contact model of a treated concrete to analyze the dynamic performances of the coupled system. This model idealized the treated concrete by a parallel combination of a spring and a viscous damper, which permitted separation between the tool tip and the work-piece. The validity of the model through measurements of a tool, however, was not attempted.

76

The elastic-plastic model, proposed by Rakheja et al. (2002b), is similar to the widely reported soil compaction models (Adam and Kopf, 2000; Anderegg and Kaufmann, 2004; Mooney et al., 2005; Kordestani, 2010). The soil compaction model, however, is realized by formulating the elastic and the plastic substrata in the reverse order. In this study, a soil-compaction model structure is considered to characterize the interactions between the tool tip and the steel balls within the energy dissipator, as shown in Figure 3.9 (b). It should be noted that the contact model is formulated for the standardized energy dissipater (ISO 8662-2, 1992), which was used in the experiments. The steel balls in the dissipater are compressed by the anvil attached to the tool tip, which can be considered as an elastic substratum, while the buffering effect due to the relatively ample space among the steel balls is idealized by a plastic substratum comprising a parallel combination of a relatively softer spring and a high viscous damping.

In the laboratory test, the selected percussive tool was operated under relatively high magnitude feed forces (78 and 108 N) and the tool bit was guided by a fixed flange (Adewusi, 2009). A flat anvil was attached to the tool bit, as shown in Figure 3.9 (a). The guided flange and the anvil could help ensure steady contact with the steel balls. The proposed tool tip-workpiece contact model was thus considered adequate for characterizing the continuous contact, as idealized in Figure 3.9 (b). The contact force transmitted to the tool tip-workpiece interface, F_{TG}, can be obtained from:

$$F_{TG} = K_E \left[z_{TC} + z_C - (L_{BC})_{\min} - (L_{TB})_{\min} - z_E \right]$$
(3.27)

where K_E represents the stiffness of the elastic substratum. $z_T = z_{TC} + z_C$ is the absolute displacement of the tool bit, and z_E expresses the displacement of the interface between

the plastic and elastic substrata. $(L_{BC})_{min}$ and $(L_{TB})_{min}$ denote the minimal distances between the impact bolt and the tool body, and the tool bit and the impact bolt at their contact, respectively.

Similarly, the force transmitted to the plastic substratum is formulated as:

$$F_{TG} = K_P z_E + C_P \dot{z}_E \tag{3.28}$$

where C_P and K_P are the viscous damping and stiffness of the plastic substratum, respectively.

Equating Eqs. (3.27) and (3.28) yields a differential equation describing the velocity of the interface between the plastic and elastic substrata, such that:

$$\dot{z}_E = K_E \left[z_{TC} + z_C - (L_{BC})_{min} - (L_{TB})_{min} \right] / C_P - (K_E + K_P) z_E / C_P \tag{3.29}$$

(a)   (b)
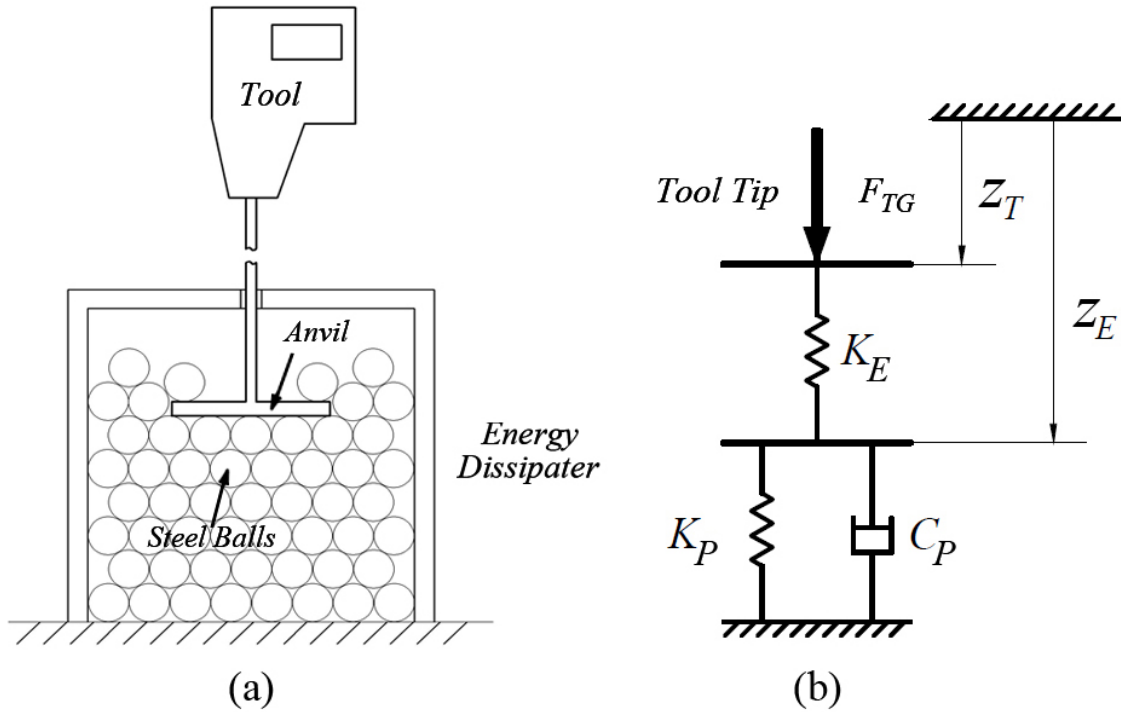
Figure 3.9 : (a) A schematic of the tool mounted in an energy dissipator; and (b) idealized tool tip-workpiece contact model

3.5 Component Contact Pair Models

The complete feature of the selected percussive tool relies on a series of impacts among the tool components. The magnitudes of the contact forces acting on different impact pairs could be extremely high, similar to that acting at the tool tip (Rakheja et al., 2002b). Furthermore, the magnitude of the force arising at each impact pair is strongly dependent upon the impact duration. Irrespective of the curvature of the contacting surfaces, an elastic spring may be considered well-suited to yield a reasonable contact force and deformation for a perfectly elastic collision. However, the vast majority of the collisions involve appreciable energy loss, which is likely attributed to the internal friction of the colliding materials. A visco-elastic material model may thus be considered more desirable to characterize variations in the force, velocity and deformation during a collision involving energy loss (Johnson, 1985; Karasudhi, 1990; French, 1997). The impacts among the tool components could also yield energy loss, especially for the impact bolt-tool body contact pair. Each impact pair is characterized by a single-DOF contact model, where the model parameters are identified from the impact duration and the coefficient of restitution using the method described by Rajalingham and Rakheja (2000).

Consider a collision between the two rigid bodies with masses m_A and m_B, respectively, as shown in Figure 3.10. Let x_A and x_B define the displacement coordinates of the two bodies, and L be the initial distance between the two masses at the beginning of the contact. During a collision, the compression of the linear spring and the damper, expressed as, $x = L - (x_B - x_A)$, is related to the deformation of the contact pair. The contact force, acting on mass B, can be subsequently obtained from:

$$F_{AB} = K_{AB}(L + x_A - x_B) + C_{AB}(\dot{x}_A - \dot{x}_B) \tag{3.30}$$

where C_{AB} and K_{AB} describe the visco-elastic properties of the contact model, respectively.
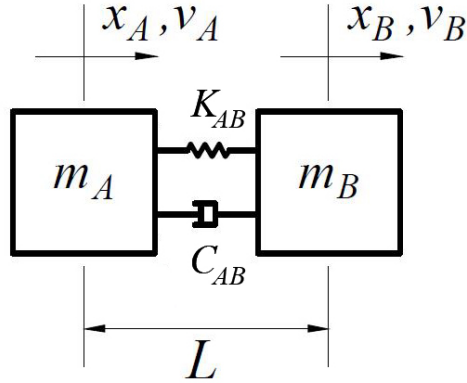
Figure 3.10 : Model illustrating visco-elastic collision between two rigid bodies

Based on the Newton's third law of motion, the relationship between the interaction forces developed on the two masses, F_{BA} and F_{AB}, can be expressed as:

$$F_{BA} + F_{AB} = m_A\ddot{x}_A + m_B\ddot{x}_B = 0 \tag{3.31}$$

Upon substituting for $\ddot{x}_B = -(m_A/m_B)\ddot{x}_A$ and letting $\ddot{x} = \ddot{x}_A - \ddot{x}_B$, Eq. (3.30) yields:

$$F_{BA} = m\ddot{x} = -K_{AB}x - C_{AB}\dot{x} \tag{3.32}$$

where $m = (m_A m_B)/(m_A + m_B)$ denotes the equivalent mass of the system model. It should be noted that the contact model is valid only when the spring-damper combination is under compression.

At the instant of the collision, the initial states of the contact model are assumed as $x(0) = 0$ and $\dot{x}(0) = V_{app}$, where V_{app} denotes the velocity at which mass A approaches

mass B. The solution of Eq. (3.32) depends on the damping ratio of the model, and can be expressed as:

$$x(t) = \begin{cases} \dfrac{V_{app}e^{-\zeta\omega_n t}\sin(\sqrt{(1-\zeta^2)}\omega_n t)}{\sqrt{(1-\zeta^2)}\omega_n} & \zeta < 1 \\[3mm] V_{app}te^{-\omega_n t} & \zeta = 1 \\[3mm] \dfrac{V_{app}e^{-\zeta\omega_n t}\sinh(\sqrt{(\zeta^2-1)}\omega_n t)}{\sqrt{(\zeta^2-1)}\omega_n} & \zeta > 1 \end{cases} \quad (3.33)$$

where ω_n is the natural frequency and ζ is the damping ratio of the system model. For the sake of convenience, let $\zeta_u = cos\alpha_1$ in case of the under-damped system, and $\zeta_o = cosh\alpha_2$, for the over-damped system. The velocity and acceleration responses of the system model can be subsequently derived from Eq. (3.33), such that:

$$\dot{x}(t) = \begin{cases} -\dfrac{V_{app}e^{-\cos\alpha_1\omega_n t}}{\sin\alpha_1}\sin(\omega_d t - \alpha_1) & \cos\alpha_1 < 1 \\[3mm] V_{app}e^{-\omega_n t}(1-\omega_n t) & \zeta = 1 \\[3mm] -\dfrac{V_{app}e^{-\cosh\alpha_2\omega_n t}}{\sinh\alpha_2}\sinh(\omega_d t - \alpha_2) & \cosh\alpha_2 > 1 \end{cases} \quad (3.34)$$

$$\ddot{x}(t) = \begin{cases} \dfrac{V_{app}e^{-\cos\alpha_1\omega_n t}(\omega_d^2 + \cos^2\alpha_1\omega_n^2)}{\omega_d}\sin(\omega_d t - 2\alpha_1) & \cos\alpha_1 < 1 \\[3mm] V_{app}e^{-\omega_n t}(\omega_n^2 t - 2\omega_n) & \zeta = 1 \\[3mm] \dfrac{V_{app}e^{-\cosh\alpha_2\omega_n t}(\omega_d^2 + \cosh^2\alpha_2\omega_n^2)}{\omega_d}\sinh(\omega_d t - 2\alpha_2) & \cosh\alpha_2 > 1 \end{cases} \quad (3.35)$$

where ω_d is the frequency of the damped oscillations of the contact model.

The determination of the contact model parameters for each contact pair in terms of stiffness and damping coefficient is extremely challenging. The collision, however, could be characterized through measuring the impact duration and the restitution coefficient.

81

Considering that the acceleration ($\ddot{x}$) of the equivalent mass (m), in Eq. (3.35), diminishes to zero at the end of the impact during compression, the duration of impact (τ) could be solved as:

$$\tau = \begin{cases} 2\alpha_1/(\omega_n \sin \alpha_1) & \cos \alpha_1 < 1 \\ 2/\omega_n & \zeta = 1 \\ 2\alpha_2/(\omega_n \sinh \alpha_2) & \cosh \alpha_2 > 1 \end{cases} \tag{3.36}$$

The velocity of separation ($V_{sep} = \dot{x}(\tau) = \dot{x}'_A - \dot{x}'_B$) of the contact model tends to decrease after the impact. The coefficient of restitution (ε), describing the relationship between the separation and approaching velocities, is defined as:

$$\varepsilon = \frac{\dot{x}'_B - \dot{x}'_A}{\dot{x}_A - \dot{x}_B} = -\frac{V_{sep}}{V_{app}} \tag{3.37}$$

where $\dot{x}'_A$ and $\dot{x}'_B$ denote the absolute velocities of mass A and mass B, respectively, following the separation. Upon substituting for $t = \tau$ from Eq. (3.36) into Eq. (3.34), the velocity of separation (V_{sep}) can be derived. The coefficient of restitution can be subsequently obtained as:

$$\varepsilon = \begin{cases} e^{-2\alpha_1/\tan \alpha_1} & \cos \alpha_1 < 1 \\ e^{-2} & \zeta = 1 \\ e^{-2\alpha_2/\tan \alpha_2} & \cosh \alpha_2 > 1 \end{cases} \tag{3.38}$$

The contact forces, developed at each contact pair, can be obtained from Eq. (3.30). The contact force between the striker and the impact bolt is obtained considering the relative motions between the impact pair and the impact condition, such that:

$$F_{SB} = K_{SB}\left(z_{SC} - z_{BC} + \left(L_{BS}\right)_{min}\right) + C_{SB}\left(\dot{z}_{SC} - \dot{z}_{BC}\right)$$ (3.39)

In a similar manner, the contact force between the impact bolt and the tool bit is obtained as:

$$F_{BT} = K_{BT}\left(z_{BC} - z_{TC} + \left(L_{TB}\right)_{min}\right) + C_{BT}\left(\dot{z}_{BC} - \dot{z}_{TC}\right)$$ (3.40)

The contact force between the tool body and the impact bolt is also derived from:

$$F_{CB} = K_{CB}\left(\left(L_{BC}\right)_{min} - z_{BC}\right) - C_{SB}\dot{z}_{BC}$$ (3.41)

where K_{SB} and C_{SB}, K_{BT} and C_{BT}, and K_{CB} and C_{CB} denote the visco-elastic properties for the striker-impact bolt, impact bolt-tool bit, and tool body and impact bolt contact pairs, respectively. $(L_{BS})_{min}$, $(L_{TB})_{min}$ and $(L_{BC})_{min}$ are the lower limits of the distances between the impact bolt and the striker, the tool bit and the impact bolt, and the impact bolt and the tool body at the instant of the contact, respectively, as shown in Figure 3.11.
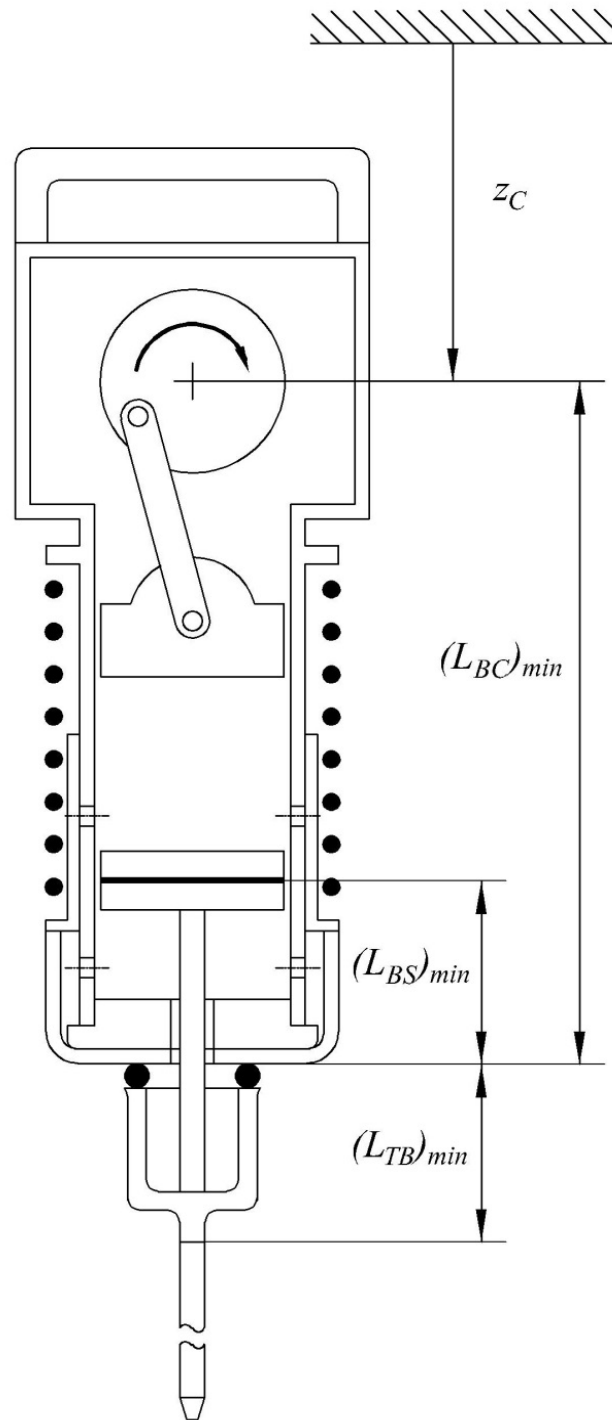
Figure 3.11 : Minimum distances between different contact pairs at the instant of the contact

Owing to the nature of the collision, Eqs. (3.39) to (3.41) are considered valid when

the spring-damper combination of the contact model is under compression. Consequently,

the contact force for each contact pair occurs only when the following conditions are satisfied, while the violation of these conditions suggests the occurrence of the contact loss.

i) The contact force between the striker and the impact bolt:

$$z_{BC} - z_{SC} < (L_{BS})_{min} \qquad (3.42)$$

ii) The contact force between the impact bolt and the tool bit:

$$z_{TC} - z_{BC} < (L_{TB})_{min} \qquad (3.43)$$

iii) The contact force between the tool body and the impact bolt:

$$z_{BC} < (L_{BC})_{min} \qquad (3.44)$$

3.6 Laboratory Measurements

A laboratory test was conducted at the institut de recherché Robert-Sauvé ensanté et en sécurité du travail du Quebec laboratory to characterize the biodynamic responses of the human hand-arm system, while operating a chipping hammer in an energy dissipater (Adewusi, 2009). The selected percussive chipping hammer (BOSCH 11313 EVS) was guided in a steel ball energy dissipator as described in ISO 8662-2 (1992), as seen in Figure 3.12. In the setup, the tool bit is attached to an anvil, which is assumed to remain in contact with the steel balls, as shown in Figure 3.9. Two uni-axial accelerometers (B&K type 4393) were mounted on the tool bit and the primary tool handle, respectively. These transducers were calibrated and aligned to record the acceleration responses along the tool's dominant vibration direction.
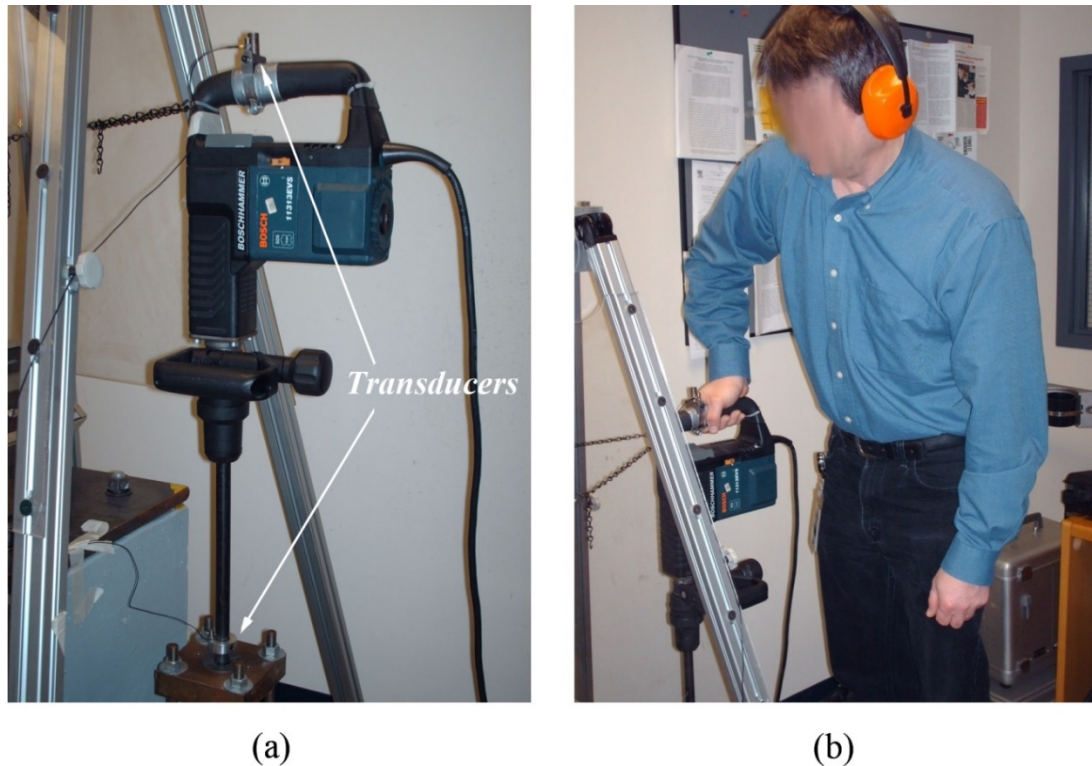
Figure 3.12 : (a) Experimental set-up illustrating the chipping hammer mounted in an energy dissipator; and (b) the hand-arm posture of the subject (Adewusi, 2009)

The measurements of the tool body and tool bit accelerations were conducted with an adult male subject operating the percussive chipping hammer, while grasping the primary handle with one hand with bent-arm posture (elbow angle ≈ 90 degrees and shoulder abduction angle ≈ 30 degrees), as shown in Figure 3.12 (b). Three measurement trials were performed with the subject applying two different levels of push force (78 N and 118 N), which was measured using a force platform. The tool was operated at two different speeds (1830 and 2625 bpm). The push force, measured by the force platform, was displayed to the operator so as to monitor and control the applied force. The grip force imparted by the operator on the tool handle, however, was not measured, since it would involve substantial modifications and instrumentation of the tool handle. In this study, the laboratory measured data are utilized to characterize the impact durations so as

to obtain estimates of visco-elastic properties of each contact pair. The measured data are also used to examine the validity of the coupled hand-tool-workpiece model.

3.7 Parameter Identification

For the tool tip-steel balls contact model, the elastic and plastic stratum parameters were identified through trial and error so as to achieve the peak measured acceleration of the tool bit. The measured data revealed substantial variations in the peak acceleration responses measured during the three trials at the higher speed of 2625 bpm, while those measured at the lower speed revealed more consistent peak accelerations. The parameter identification was thus limited to the data obtained at the lower speed. Figures 3.13 and 3.14 illustrate the time-histories of acceleration measured at the tool tip and the tool body, respectively. Table 3.1 lists the contact model parameters that resulted in reasonably good agreement with the peak measured accelerations. Owing to the highly nonlinear contact properties and the lack of reliable measured data, the validity of the contact model could be examined only in a qualitative sense.

Table 3.1 : Parameters of the tool tip-workpiece contact model

Parameter	Symbol	Value
Elastic zone stiffness (N/m)	K_E	1.05E7
Plastic zone stiffness (N/m)	K_P	6.5E5
Plastic zone damping (Ns/m)	C_P	2500

It needs to be emphasized that the acceleration responses of the impact pairs could not be measured directly. The impact durations of the impact pairs thus could not be identified from direct measurements.
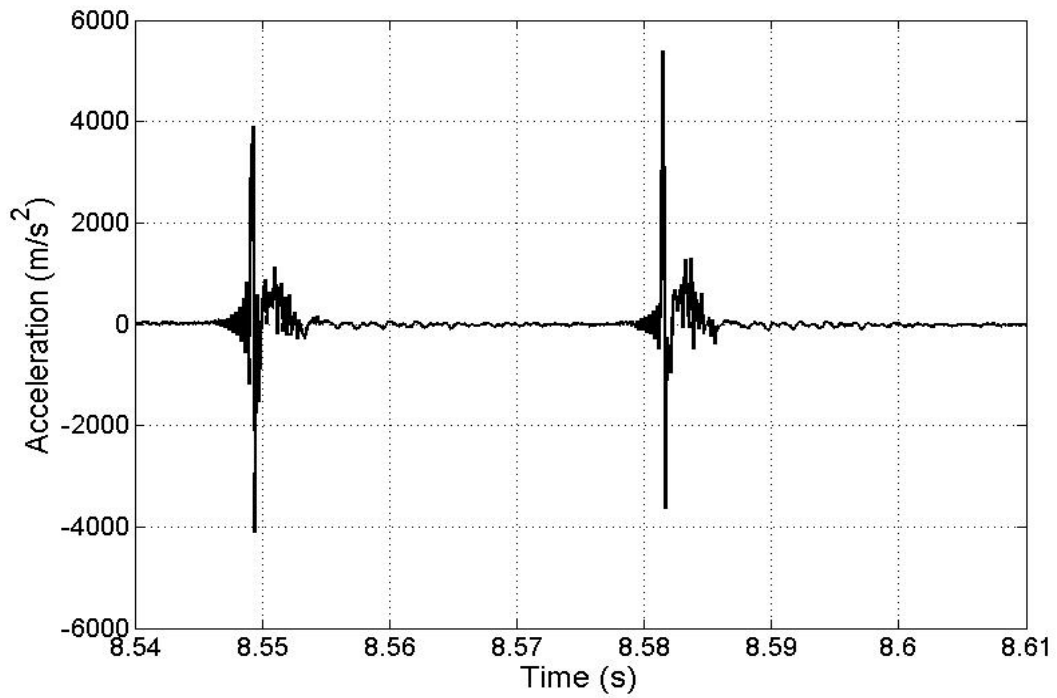
(a)
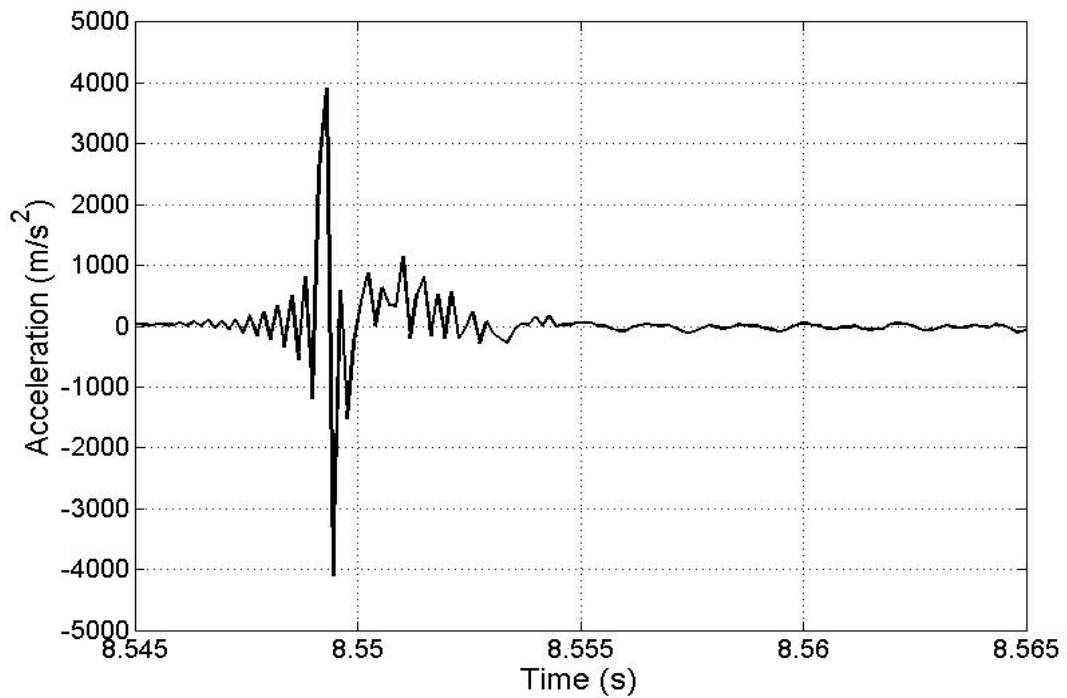
(b)

Figure 3.13 : (a) Time-history of tool bit acceleration measured during two subsequent
blows; and (b) acceleration time-history zoomed around the impact
(1830 bpm and 78 N push force)

88
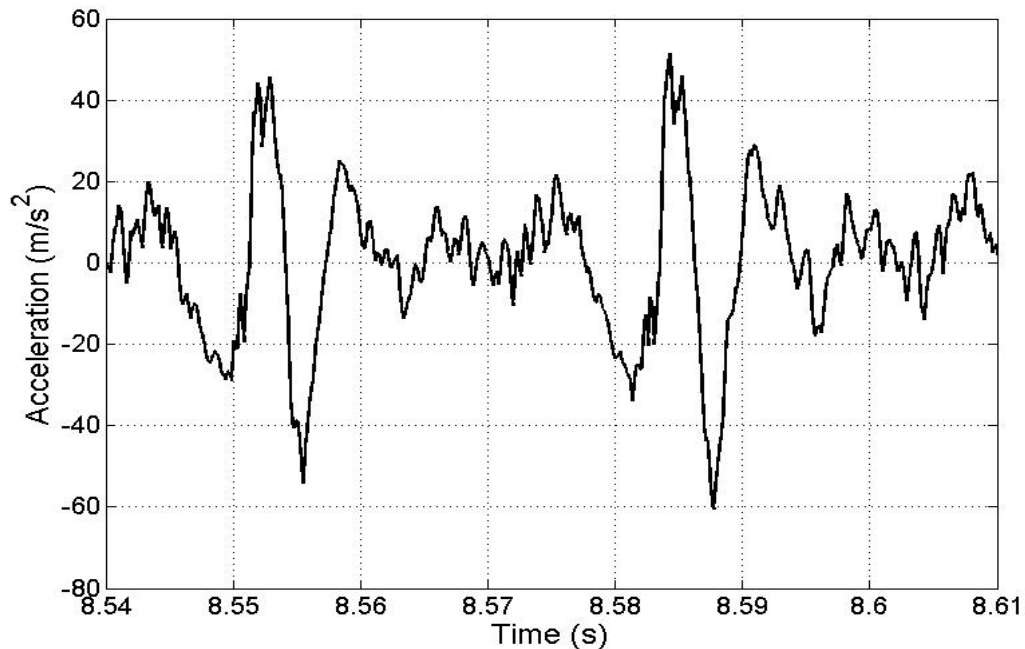
Figure 3.14 : Time-history of acceleration measured at the tool handle
(1830 bpm and 78 N push force)

The acceleration responses of the tool bit and the tool body, however, are the result

of impacts among the selected component contact pairs. The available data could thus be

used to estimate the impact duration. In this study, preliminary estimates of impact

durations for each impacting pair are obtained from the measured data corresponding to a

single blow. As shown in Figure 3.13, the tool bit acceleration response exhibits two

large peaks, preceded and followed by low-magnitude oscillations. The tool bit and

handle acceleration responses show the fundamental frequency near 30.5 Hz, which

corresponds to its operating speed of 1830 bpm. The large magnitude peaks, observed in

the acceleration responses of the tool bit, can be mostly attributed to the impacts between

the impact bolt and the tool bit, while the lower amplitude oscillations, preceded the

primary peaks are attributed to the pre-impacts between the striker and the impact bolt

(Figure 3.13). On the other hand, the bifurcations, observed in the large magnitude peaks

of the acceleration response of the tool body, are attributed to the contacts between the impact bolt and the tool body (Figure 3.14). The mean measured impact durations are summarized in Table 3.2.

Table 3.2 : Mean measured impact durations for different component contact pairs

Impact pair	Impact duration, τ (s)
Striker and impact bolt	2.81e-4
Impact bolt and tool bit	4.64e-4
Impact bolt and tool body	1.38e-3

Rakheja et al. (2002b) reported durations of 0.3, 0.45 and 1.5 ms for the impacts between the striker and the impact bolt, the impact bolt and the tool bit, and the impact bolt and the tool body, respectively. These are comparable with the mean values extracted from the measured time histories.

Owing to wide variations in the properties of different materials, the coefficient of restitution is also expected to vary considerably. In this study, the coefficients of restitution for individual contact pairs are determined based on those reported by Rakheja et al. (2002b), which are summarized in Table 3.3. It should be noted that the coefficient of restitution of the impact bolt-tool body contact pair is considerably lower than those of the rigid metal impacting pairs, which could be attributed to the presence of the O-ring between the impact bolt and the lower control disk.

Table 3.3 : Determined coefficient of restitutions for different contact pairs

Impact pair	Coefficient of restitution ε
Striker and impact bolt	0.95
Impact bolt and tool bit	0.95
Impact bolt and tool body	0.55

3.7.1 Component Contact Pairs Model Parameter Identification

The measured data revealed high magnitude impact forces over very short impact durations. The contact model corresponding to the underdamped condition is thus considered appropriate. Equation (3.38) is subsequently manipulated to yield the damping ratio, $\zeta_u = cos\alpha_1$, in the following form:

$$\cos\alpha_1 = -\frac{\ln\varepsilon\sin\alpha_1}{2\alpha_1} \tag{3.45}$$

Upon substituting for $\sin\alpha_1 = 2\alpha_1/(\tau\omega_n)$ from Eq. (3.36) and defining the damping constant, $C_{AB} = 2m\omega_n\cos\alpha_1$, the damping constant of the impact pair is subsequently obtained from Eq. (3.45), in terms of the contact duration τ and the coefficient of restitution ε:

$$C_{AB} = -\frac{2m\ln\varepsilon}{\tau} \tag{3.46}$$

Upon substituting for $\sin a_1 = 2a_1/(\tau\omega_n)$ and considering the stiffness, $K_{AB} = m\omega_n^2$, the stiffness of a contact pair can be derived from Eq. (3.45), such that:

$$K_{AB} = \frac{m(\ln\varepsilon)^2}{\tau^2\cos^2\alpha_1} \tag{3.47}$$

where α_1 can be expressed as a function of τ and ε:

$$\alpha_1 = arc\cos(-\frac{\ln\varepsilon}{\omega_n\tau}) \tag{3.48}$$

As seen in Eq. (3.36), τ is a function of α_1 for the under-damped system. Equations (3.46) to (3.48), however, contain transcendental functions and cannot be solved in the

closed-form. Moreover, due to the presences of natural logarithm, the system stiffness and damping coefficients may exhibit extreme sensitivity to variations in ε. Alternatively, the impact duration and coefficient of restitution may be expressed as functions of stiffness and damping constants. It is thus possible to determine the stiffness and the damping constant for each contact pair by minimizing the error between the target and assumed impact duration and coefficient of restitution.

According to Eqs. (3.36) and (3.38), the assumed impact duration (τ_a) and coefficient of restitution (ε_a) derived from the assumed stiffness (K_a) and damping constant (C_a), can be formulated as:

$$\begin{cases} \tau_a = \dfrac{2\alpha_1}{\sin\alpha_1 \omega_n} = \dfrac{2\alpha_1}{\sin\alpha_1}\sqrt{\dfrac{m}{K_a}} \\ \varepsilon_a = e^{-2\alpha_1/\tan\alpha_1} \end{cases} \tag{3.49}$$

where α_1 is derived from Eq. (3.48) considering $C_a/2m = -\ln\varepsilon_a/\tau_a$ (Eq.3.46), such that:

$$\alpha_1 = arc\cos(\dfrac{C_a}{2\sqrt{K_a m}}) \tag{3.50}$$

By minimizing the error between the target and assumed impact duration and coefficient of restitution within a small tolerance level, the stiffness and the damping constants can be subsequently obtained, such that:

$$\Delta_\tau = f_{\min}(\tau - \tau_a) \tag{3.51}$$

$$\Delta_\varepsilon = f_{\min}(\varepsilon - \varepsilon_a) \tag{3.52}$$

where f_{min} denotes the error minimization function. The procedure to determine the stiffness and damping coefficients for the contact pairs is illustrated in Figure 3.15. Using

92

the values of τ and ε estimated from the measured data, and absolute tolerance of 1e-15, the error minimization process resulted in the stiffness and damping parameters for each contact pair. The results are presented in Table 3.4.
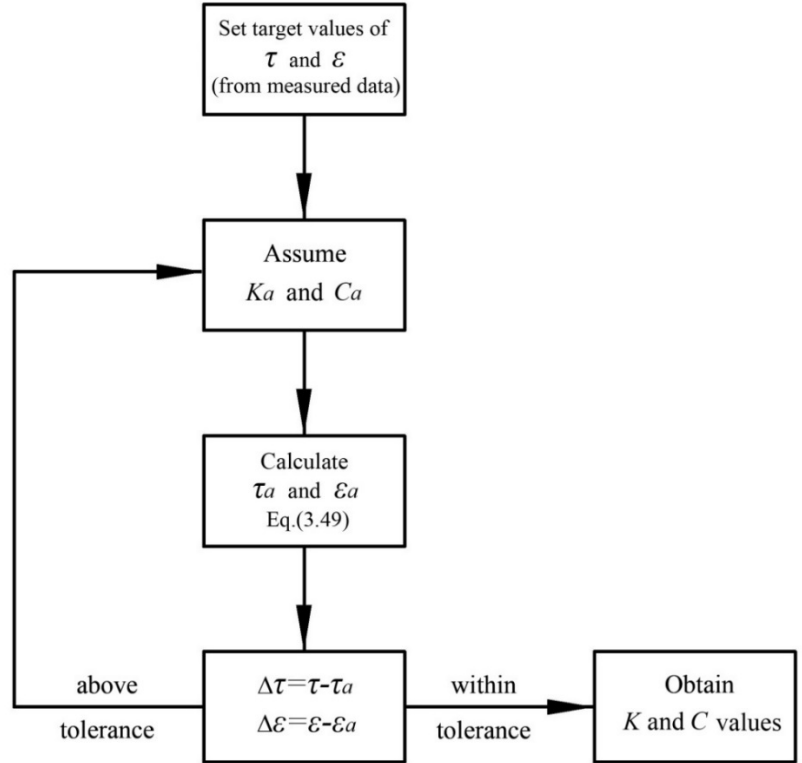
Figure 3.15 : Procedure for determining stiffness and damping parameters for the contact pair

Table 3.4 : Stiffness and damping parameters of different contact pairs

Contact pair	Stiffness (kN/m)	Damping (Ns/m)
Striker and impact bolt	K_{SB}=10646.4	C_{SB}=33.9
Impact bolt and tool bit	K_{BT}=6832.7	C_{BT}=32.7
Impact bolt and tool body	K_{CB}=634.5	C_{CB}=148.1

3.7.2 Validation for the Contact Pairs

The component contact models are evaluated by assuming an approach velocity (V_{app}) of 5 m/s to determine the deformation and velocity responses due to contacts

between the striker and the impact bolt, the impact bolt and the tool bit, and the tool body and the impact bolt. Figures 3.16 to 3.18 illustrate the responses of the impact pairs.

The results show that the peak relative deformations due to impacts between the striker and the impact bolt (0.47 mm), and the impact bolt and tool bit (0.71 mm) are reasonably small, which can be attributed to the high rigidity of the components and the relatively low equivalent masses of these two impact pairs (Figures 3.16 and 3.17). Moreover, the corresponding velocity responses are nearly symmetric, and the change in the velocity during the impact is also reasonably small for these two impact pairs, which conform to their relatively higher coefficients of restitution. However, the deformation due to the contact between the impact bolt and tool body, is substantially higher in the order of 2 mm (Figure 3.18). The velocity responses of the tool body and the impact bolt pair are asymmetric due to the relatively lower coefficient of restitution. The separation velocity (V_{sep}) of the impact bolt-tool body contact pair is also relatively small around 2.75 m/s, suggesting considerable energy loss attributed to the soft O-ring between the impact bolt and the lower control disk. This is also partly attributable to the relatively higher equivalent mass of the impact bolt-tool body contact pair.

Table 3.5 summarizes the impact durations observed from the simulation results for the three contact pairs together with the target values. The results show slight deviations between the simulation and target values. The duration of the impact between the impact bolt and the tool body, obtained from the simulation, is particular higher (6.0%) than the corresponding target value. Such deviations can be mostly attributed to the numerical approximations, and the approximated impact durations and coefficients of restitution.
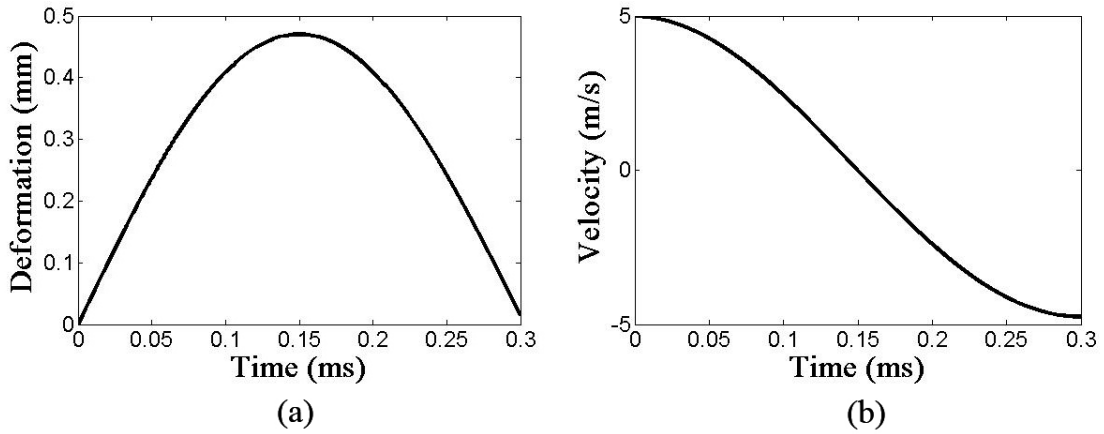
Figure 3.16 : (a) Relative deformation; and (b) velocity responses of the striker and the impact bolt pair
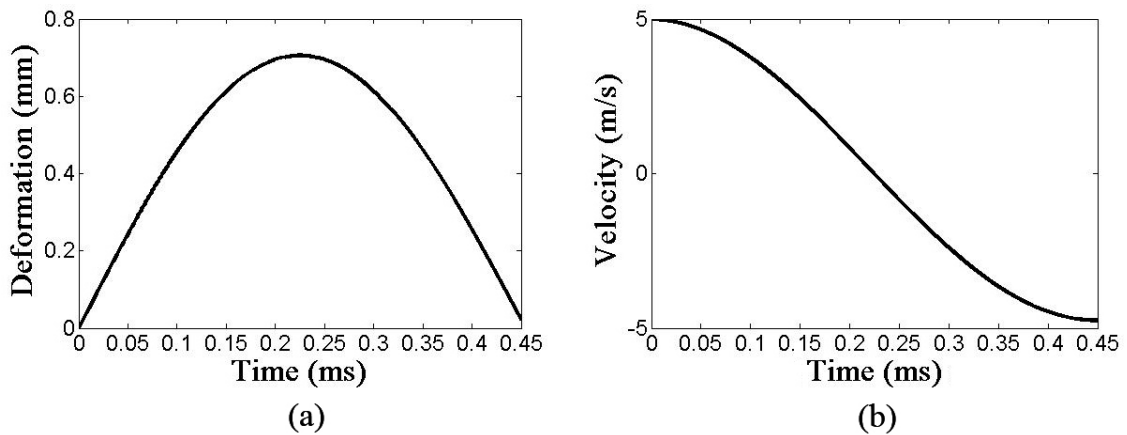
Figure 3.17 : (a) Relative deformation; and (b) velocity responses of the impact bolt and the tool bit pair
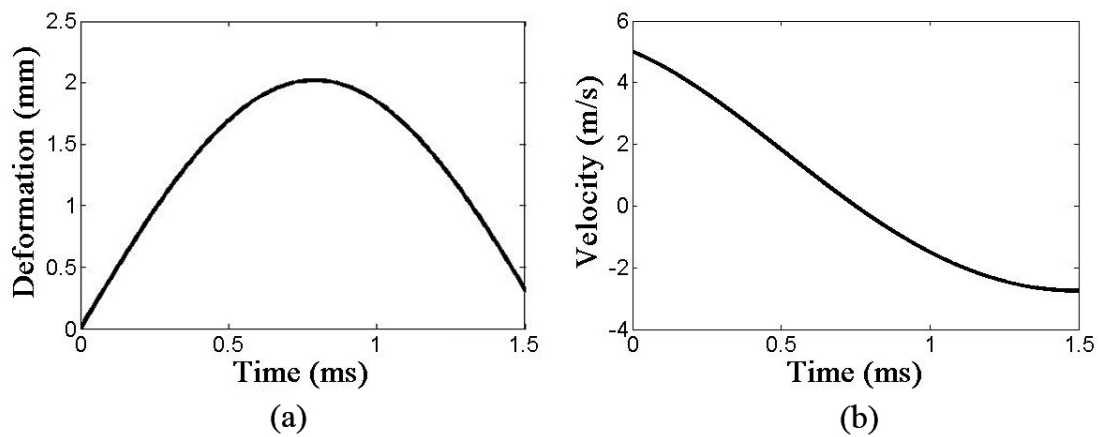
Figure 3.18 : (a) Relative deformation; and (b) velocity responses of the tool body and the impact bolt pair

Table 3.5 : Comparisons of the target and the simulated impact durations for each impact pair

Contact pair	Target (s)	Simulation (s)	Error
Striker and impact bolt	3.0e-4	3.03e-4	1.0%
Impact bolt and tool bit	4.5e-4	4.55e-4	1.3%
Impact bolt and tool body	1.5e-3	1.59e-3	6.0%

3.8 Summary

A dynamic model of a percussive chipping hammer is systematically developed considering different component impact pairs. The high-magnitude impacts among the three contact pairs are modeled considering the tool geometry and linear contact theory. The model parameters of the contact pairs are derived from the available laboratory-measured data through error minimization, which are subsequently validated via simulations. A two-DOF contact model is also proposed in this chapter to characterize the interactions between the tool tip and the workpiece. The biomechanical hand-arm and gloved hand-arm models, developed in Chapter 2, are integrated to the tool model to derive the coupled system models for parametric analyses in the following chapter.

CHAPTER 4

VALIDATION AND ANALYSIS OF INTEGRATED SYSTEM MODELS

4.1 Introduction

The nature of hand-transmitted vibration (HTV) from operation of power tools mainly depends upon the type of power tool and the task (Nemani, 2005; Mallick, 2008; 2010). The variations in many design and operating factors, such as hand forces and handle designs, may also affect the characteristics of HTV (Iwata et al., 1972; Pyykkö et al., 1976; Hartung et al., 1993). A number of studies have reported that workers operating percussion type tools are more prone to suffer from a high prevalence of vibration white finger (VWF) than the other vibrating tool operators (Gurram, 1993; Nemani, 2005). This is primarily due to high magnitude of vibration of the percussive type tools. The need for control of percussive tool-generated vibrations has thus been widely emphasized. Apart from applications of anti-vibration gloves or handle isolators, the designs of low-vibration percussive tools would be more desirable for limiting the vibration exposure at the source (Rakheja et al., 2002b), which necessitates developments in reliable dynamic models of the coupled hand-tool-workpiece system.

The analysis of a coupled hand-tool-workpiece system model can yield a better understanding of the factors affecting the nature of HTV and thus the guidance on the desirable vibration attenuation mechanisms. In this study, the dynamic models of the human hand-arm system (HAS) and the percussive chipping hammer operating within a steel ball energy dissipator, developed in the previous chapters, are integrated for the analysis of the coupled system model. The model validity is also examined through comparisons of the model results with the laboratory measured data in terms of the

97

acceleration responses at the tool handle and the tool bit. Selected operating factors (tool speed, hand-forces and the properties of the workpiece) are parametrically studied to evaluate their influences upon the vibration characteristics of the tool and the HAS. Furthermore, the influences of variations in the diameter of the upper chamber orifices and the masses of the tool body, the striker, the impact bolt and the tool bit on the HTV are explored through parametric sensitivity analyses in order to achieve tool design guidance. The effectiveness of an anti-vibration glove is also investigated by assessing the distributed vibration responses in the gloved-hand model developed in the previous chapter.

4.2 Comparisons of Different Hand-Arm Vibration (HAV) Models Integrated to the Tool Model

It has been shown that the selected biomechanical bent-arm model (Adewusi, 2009), representing the anatomical structure of the human HAS with 90 degrees elbow angle and 0 degree shoulder abduction, and two driving-points (finger-handle and palm-handle interfaces), yields reasonably good predictions of biodynamic responses in terms of DPMI and vibration transmissibility. This model also resulted in relatively low deformations under static push forces. Even though this model does not correspond to the posture employed in the experimental study, the model is considered better suited for the investigation of coupled hand-tool-workpiece system compared to the other models, which generally yield unreasonably high deformations under static push forces (Rakheja et al., 2002c).

In this study, the dynamic responses of the tool model are evaluated considering the coupling with three different hand-arm system models. These include the bent-arm

biomechanical model, the single-DOF hand-arm model effective in the 20-100 Hz frequency range (Reynolds and Soedel, 1972) and the four-DOF hand-arm model described in ISO 10068 (1998). The responses of the three coupled hand-tool models are evaluated and compared to gain some insights into the applicability of the hand arm vibration (HAV) models. The coupled model simulations are performed using integration time step of 8e-6 s and absolute tolerance of 1e-14, while the tool speed is considered to be constant (1830 bpm). Furthermore, the net static hand force exerted by the hand on the tool handle was considered as 75 N for all the models.

The simulation results in each case are compared with the available measured data to examine the validity of the coupled hand-tool system in a qualitative manner. It should be noted that the available measured data were limited to only tool bit and tool handle accelerations, which are shown in Figures 4.1 and 4.2, respectively. The measurements at the tool bit clearly show the fundamental frequency near 30.5 Hz, which corresponds to the operating speed of 1830 bpm. The measurements at the tool handle also show the presence of this fundamental frequency in addition to the other spectral components that may be attributed to different impact pairs of the tool. It needs to be stated that the reported measured data revealed substantial differences among the three trials even at the lower speed of 1830 bpm, as it is evident in Tables 4.1 and 4.2. Such differences were considerably large at a higher speed. These may be attributable to variations in the hand posture, feed forces and impact forces within the energy dissipator, and possible loss of contact between the tool tip and the steel balls. The last two trials, however, revealed acceptable consistency, which were subsequently considered to obtain mean un-weighted

(a_{rms}) and weighted (a_{wrms}) handle r.m.s. accelerations, and the mean peak tool bit acceleration along the z_h-axis.
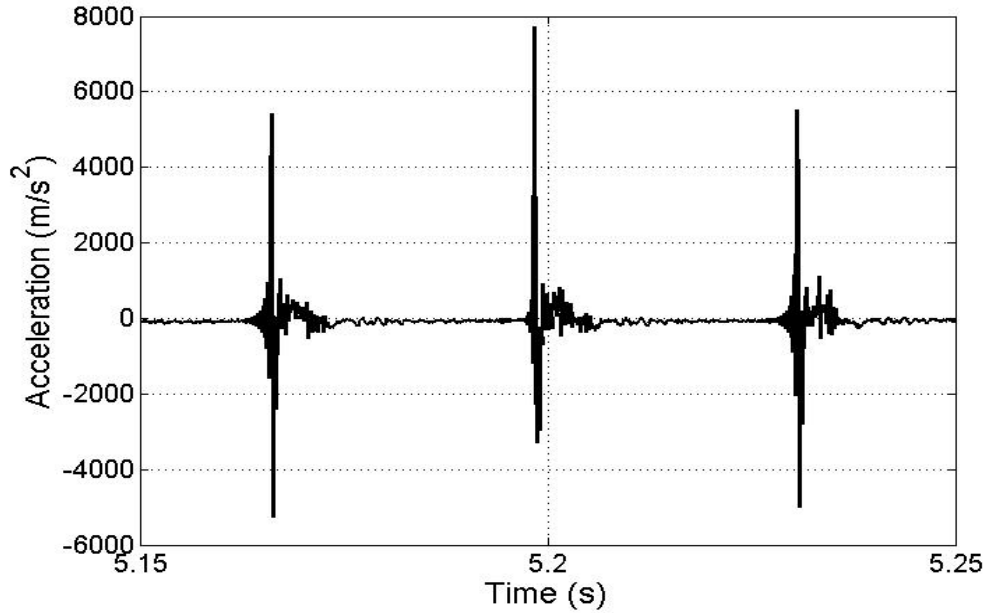
Figure 4.1 : Time-history of acceleration measured at the tool bit
(1830 bpm and 78 N push force)
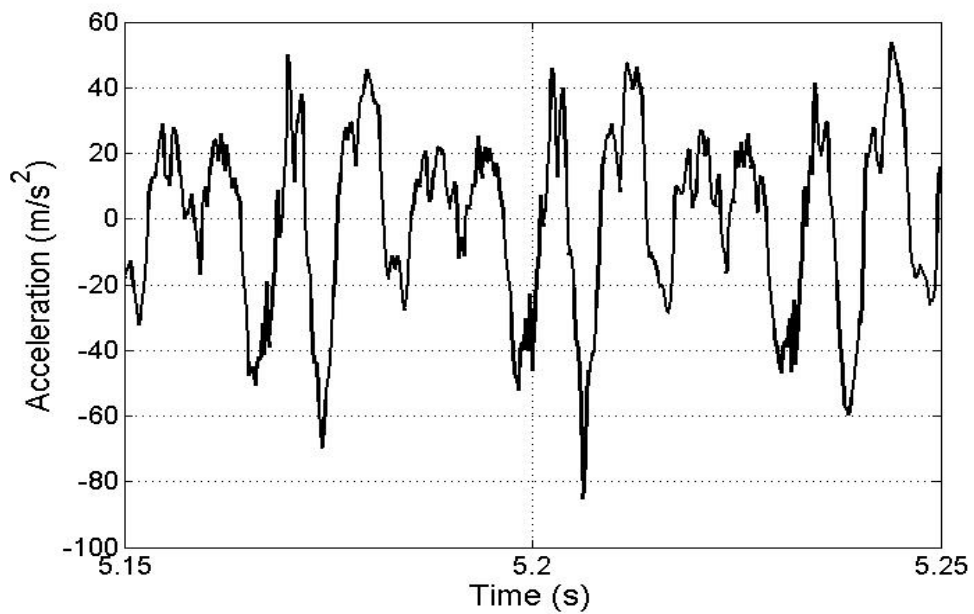
Figure 4.2 : Time-history of acceleration measured at the tool handle
(1830 bpm and 78 N push force)

Table 4.1 : Peak tool bit acceleration magnitudes of the percussive tool measured in the lab (Adewusi, 2009)

Trial	Downward (m/s^2)	Upward (m/s^2)
Trial 1	5927	4203
Trial 2	7445	5334
Trial 3	7960	5405

Table 4.2 : Peak un-weighted handle acceleration, and un-weighted and frequency-weighted r.m.s. handle accelerations of the percussive tool measured in the lab (Adewusi, 2009)

Trial	Peak un-weighted handle acceleration		a_{rms} (m/s^2)	a_{wrms} (m/s^2)
	Downward (m/s^2)	Upward (m/s^2)		
Trial 1	61.98	68.78	18.16	2.75
Trial 2	75.93	108.3	26.83	5.25
Trial 3	62.98	85.05	27.55	5.77

4.2.1 Single-DOF HAV Model

The single-DOF HAV model reported by Reynolds and Soedel (1972) was integrated to the tool model described in Chapter 3. The simulation results of the coupled hand-tool model were obtained in terms of accelerations of the tool body and the tool bit, as shown in Figures 4.3 and 4.4, respectively. The results show somewhat comparable peak acceleration of the tool bit with the measured data (Figure 4.1), while the peak handle acceleration is substantially lower. The positive peak acceleration of the handle, corresponding to the extension of the HAV model (tool's downward motion), is particularly lower (20.37 m/s^2) compared to the measured peak acceleration, which is in excess of 60 m/s^2. Moreover, the accelerations of the tool body and the tool bit show notable discontinuities, as seen in Figures 4.3 and 4.4. These are likely due to the low

resonance frequency (30.0 Hz) of the model, which is very close to the operating speed of

the tool (30.5 Hz).
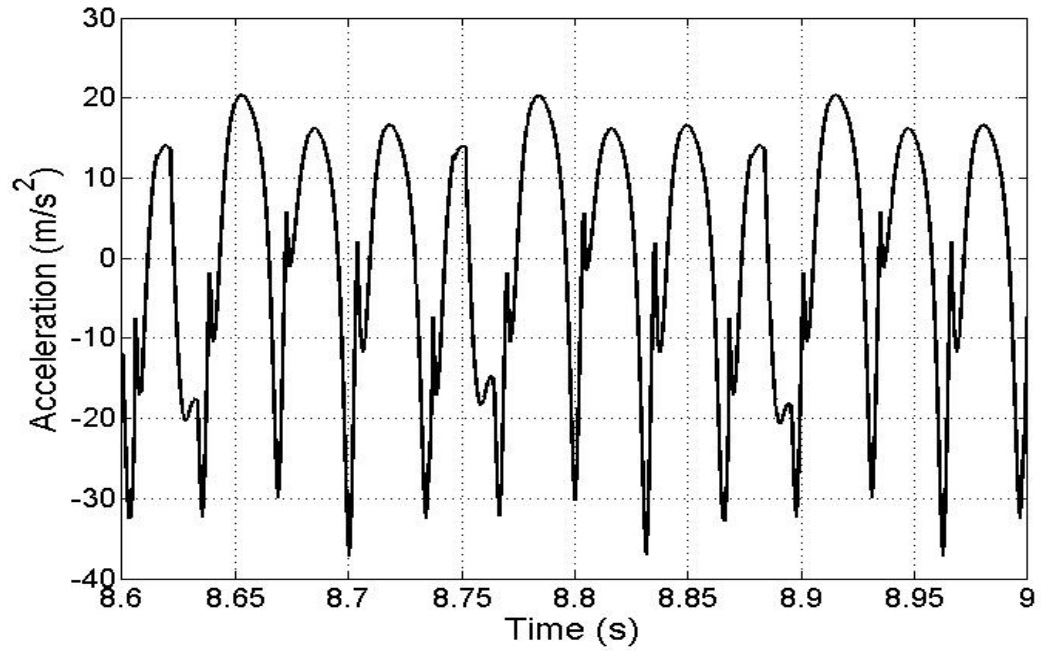
(a)
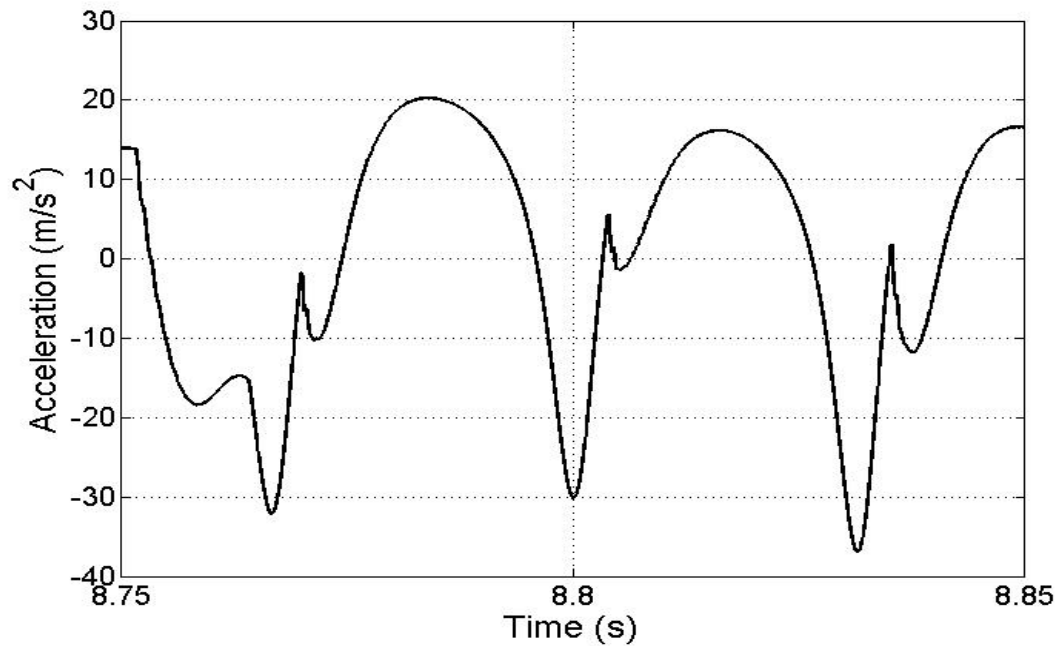
(b)

Figure 4.3 : (a) Acceleration response of the tool body of the percussive tool coupled with
the single-DOF HAV model; and (b) zoomed acceleration response
(1830 bpm and 75 N push force)
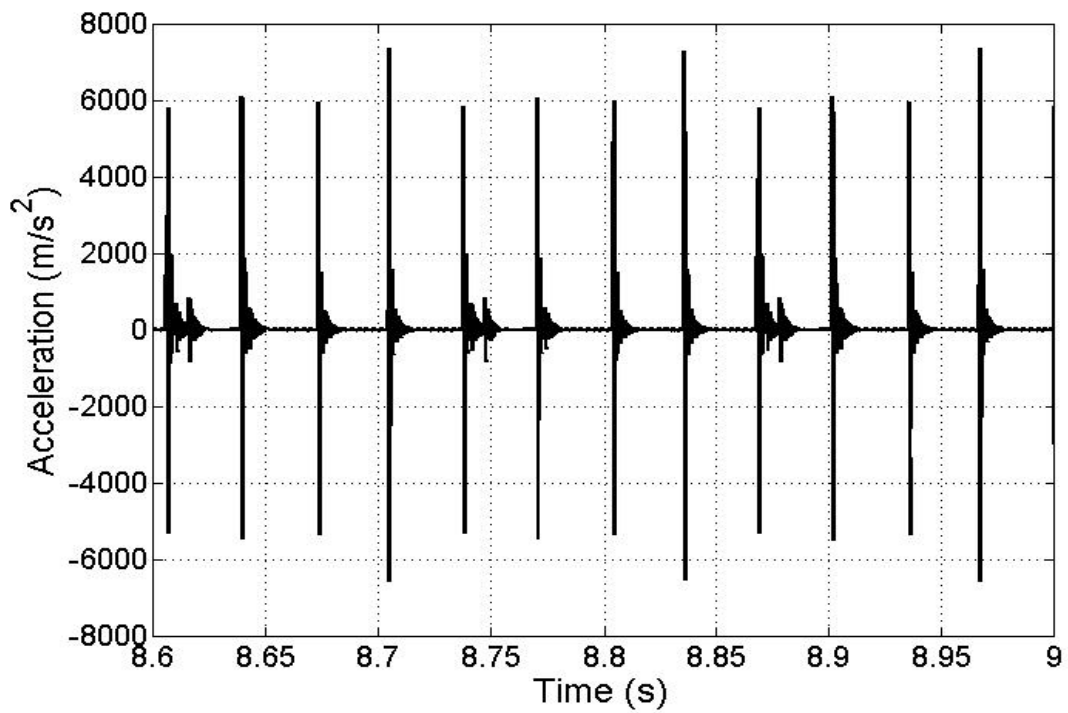
(a)
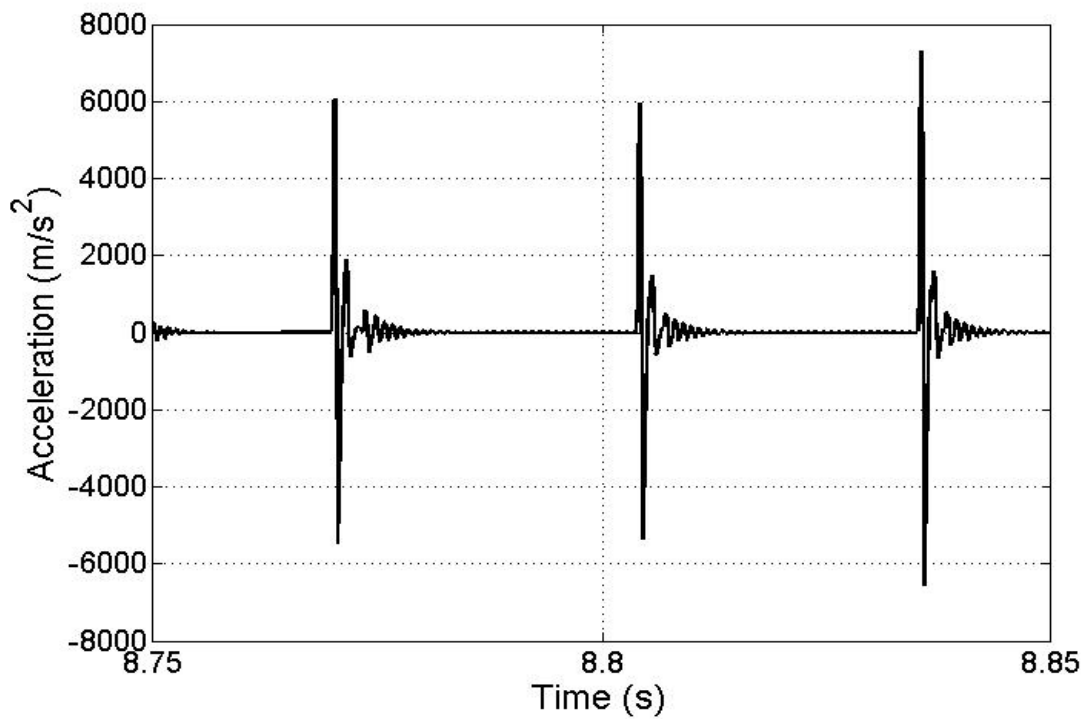
(b)

Figure 4.4 : (a) Acceleration response of the tool bit of the percussive tool coupled with the single-DOF HAV model; and (b) zoomed acceleration response
(1830 bpm and 75 N push force)

4.2.2 Four-DOF HAV Model

The tool-bit and tool-body acceleration responses were obtained through simulation of the tool model coupled with the four-DOF HAV model reported in ISO-10068 (1998). Figures 4.5 and 4.6 illustrate the time-histories of the resulting accelerations of the tool body and the tool bit, respectively. The peak acceleration responses of the tool bit are comparable to the measured data, while the fundamental frequency is identical to the operating speed of 1830 bpm. The acceleration peaks of the tool body, however, are substantially lower than those observed in the measured data. This is most likely attributed to lack of consideration of the lower chamber pressure variations and the lower resonance frequencies of the HAV model. Furthermore, it has been reported that this model, owing to its very low stiffness values, would yield excessive static deflection under a low to medium level hand push force (Rakheja et al., 2002c).
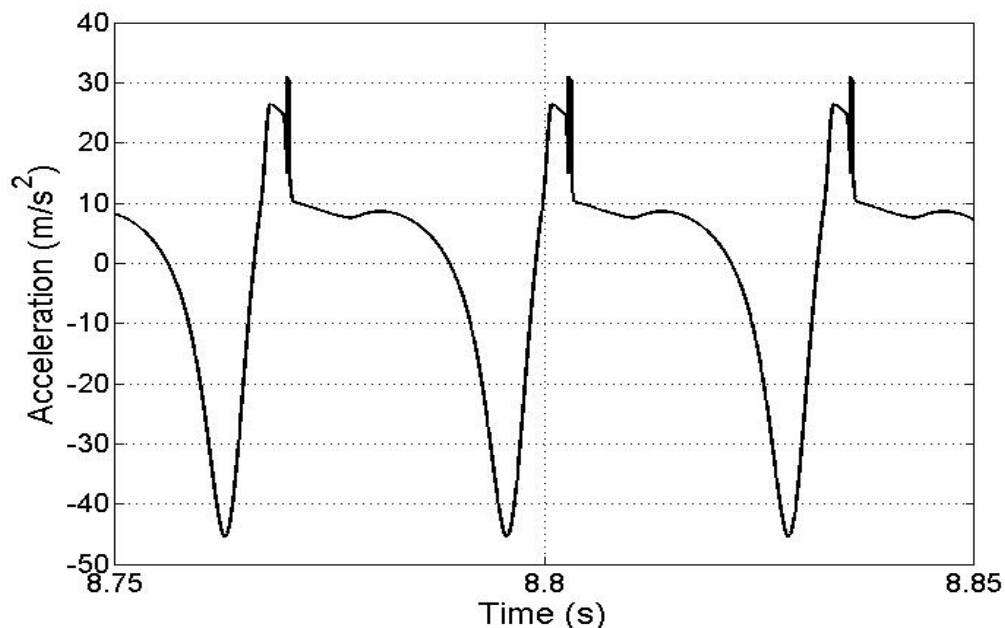
Figure 4.5 : Acceleration response of the tool body of the percussive tool coupled with the four-DOF HAV model (1830 bpm and 75 N push force)
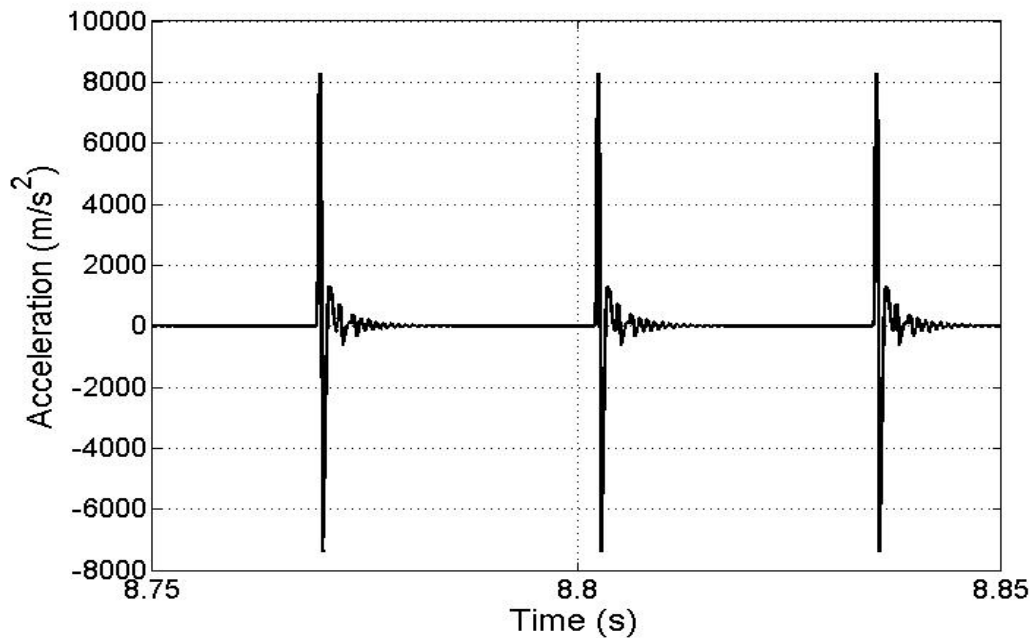
Figure 4.6 : Acceleration response of the tool bit of the percussive tool coupled with the four-DOF HAV model (1830 bpm and 75 N push force)

4.2.3 Six-DOF Biomechanical HAV Model

Figures 4.7 and 4.8 illustrate the tool body and tool bit acceleration responses of the tool model coupled with the six-DOF bent-arm HAV model. The tool bit acceleration response exhibits peak magnitudes similar to those attained with the four-DOF HAV model. Further, the peak magnitudes are comparable with the measured peaks (Figure 4.1). The magnitudes of tool body acceleration peaks, however, are significantly lower than the measured peaks, as observed for the single- and four-DOF HAV models. The fundamental frequency of the acceleration responses is identical to the operating speed.
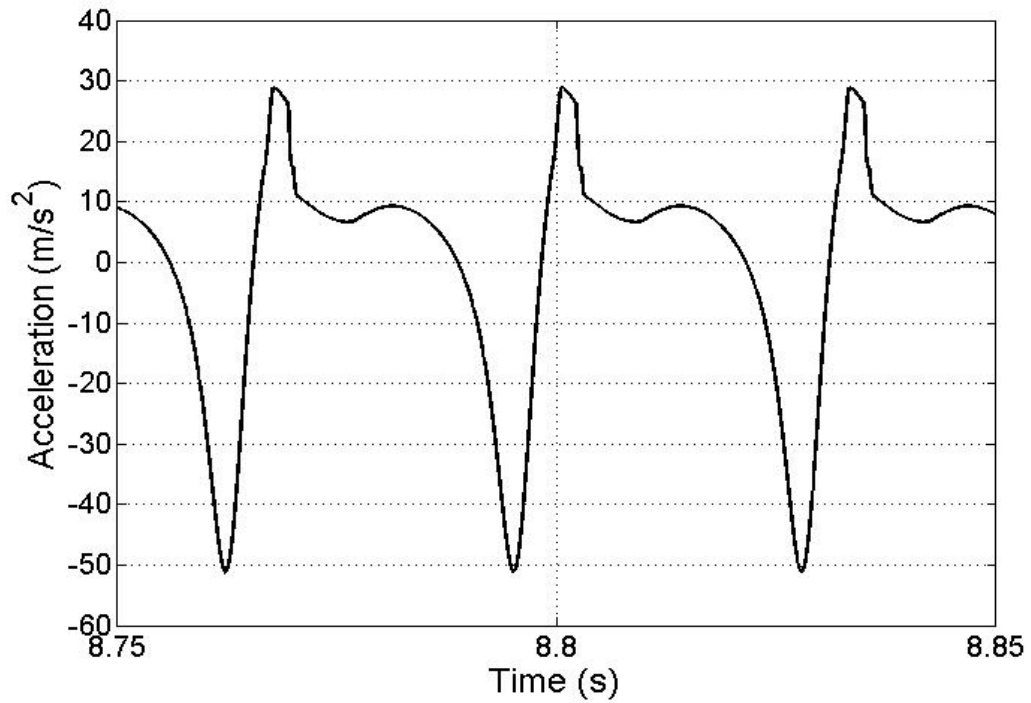
Figure 4.7 : Acceleration response of the tool body of the percussive tool coupled with the six-DOF HAV model (1830 bpm and 75 N push force)
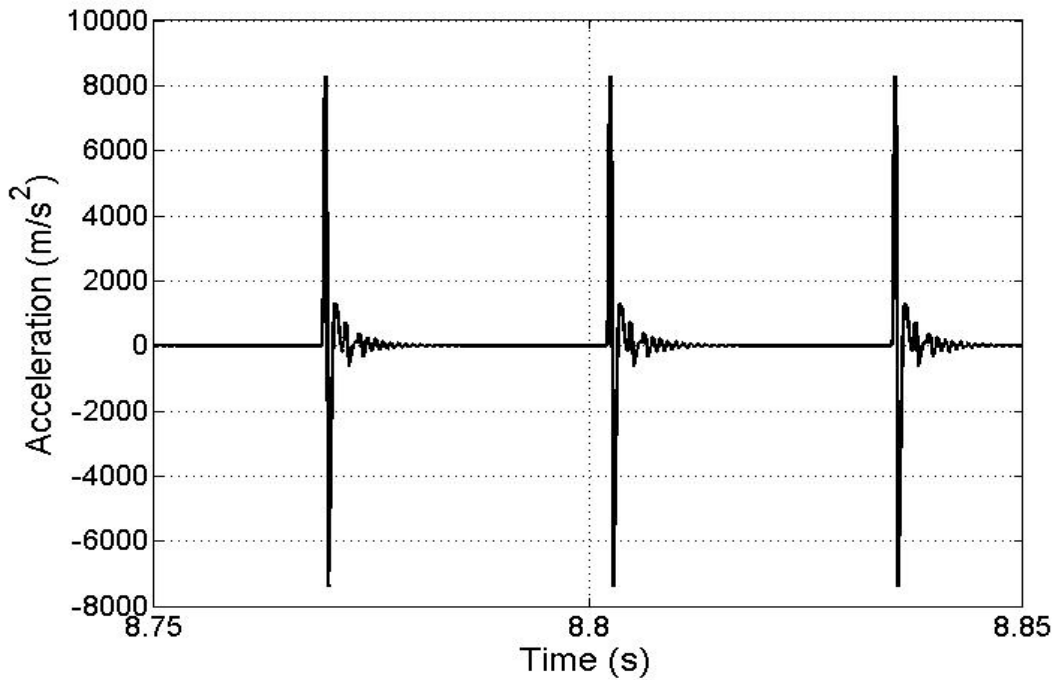
Figure 4.8 : Acceleration response of the tool bit of the percussive tool coupled with the six-DOF HAV model (1830 bpm and 75 N push force)

4.2.4 Discussions

As seen in Figures 4.3, 4.5 and 4.7, the tool model coupled the three different hand-arm models yields lower peak handle (tool body) acceleration responses compared to those observed from the measured data. The four-DOF HAV model yields the highest positive acceleration peaks ($31.03 \ m/s^2$) corresponding to downward motion of the tool. The six-DOF biomechanical HAV model, on the other hand, yields the highest negative acceleration peaks ($51.16 \ m/s^2$), while its positive peak handle acceleration during the downward acceleration motion of the tool, however, is substantially lower compared to the measured peak acceleration. These differences can be attributed to the variations in the structure and parameters of the selected hand-arm models as discussed in Chapter 2.

Table 4.3 summarizes the peak handle acceleration responses of the tool model with three different HAV models. All the hand-arm models yield highly asymmetric acceleration responses of the tool handle. This asymmetry is also evident in the measured data (Figure 4.2 and Table 4.2), which is likely caused by the air pressure variations in the controlled chambers and the loss of contact of the tool bit with the steel balls in the energy dissipater. The human hand-arm system also exhibits asymmetric behavior in compression and rebound, while the reported models are generally linear and thus do not describe the asymmetric responses. The measured data show peak accelerations during downward and upward tool motions of $69.46 \ m/s^2$ and $96.68 \ m/s^2$ (Table 4.3), respectively. The differences between the peak tool body acceleration responses of the coupled tool-hand models and the measured data are partly believed to be caused due to lack of consideration of variations in the lower chamber pressure.

Table 4.3 : Comparisons of peak handle acceleration responses of the percussive tool coupled with different hand-arm vibration models with the mean measured values

Model type	Downward (m/s^2)	Error (%)	Upward (m/s^2)	Error (%)
Measured data	69.46	-	96.68	-
Single-DOF hand-arm model	20.37	70.7	37.22	61.5
Four-DOF hand-arm model	31.03	55.3	45.46	53.0
Six-DOF hand-arm model	28.87	58.4	51.16	47.1

The coupled hand-tool models, however, yield somewhat comparable tool bit peak acceleration responses, which are summarized in Table 4.4. These observations suggest that the modeling of the contact between the tool bit and the workpiece may be considered reasonable for the energy dissipator used in the study. However, it should be noted that the single-DOF HAV model yields notable discontinuities in the acceleration responses, although it reveals the least deviations from the measured peak accelerations, as seen in Figures 4.3 and 4.4. It should be also noted that the low-magnitude oscillations, preceding the primary peaks in the tool-bit acceleration response, are not evident in the model results. These differences are likely due to limitations of the tool tip-workpiece contact model, since it does not permit separation between the tool tip and the steel balls, as described in Chapter 3.

The comparison of the peak tool bit acceleration responses of the coupled hand-tool models suggests that the tool model can provide reasonably good prediction of the tool bit responses. The lower handle acceleration responses suggest the need for developing more effective and perhaps nonlinear models of the hand-arm system, as well as consideration of the variations in the lower chamber pressure.

Table 4.4 : Comparisons of peak tool bit acceleration responses of the percussive tool
model coupled with different HAV models with the mean measured values

Model type	Downward (m/s^2)	Error (%)	Upward (m/s^2)	Error (%)
Measured data	7702.50	-	5369.50	-
Single-DOF hand-arm model	7349.46	4.6	6586.28	22.7
Four-DOF hand-arm model	8101.12	5.2	7193.93	34.0
Six-DOF hand-arm model	8297.81	7.7	7398.40	37.8

Table 4.5 summarizes the un-weighted and frequency-weighted r.m.s. accelerations due to handle vibration responses of the three coupled hand-tool models together with those obtained from the measured data. The un-weighted r.m.s. handle accelerations of all of the coupled hand-tool models, are substantially lower than that of the measured data, as it is also evident from the peak acceleration responses. The single-DOF hand-arm model resulted in largest deviations (42.4% and 58.6%) from the measured un-weighted and frequency-weighted r.m.s. values, while the four-DOF and six-DOF hand-arm models reveal lower deviations. It should be noted that the frequency-weighted r.m.s. acceleration values of all the models are lower than the un-weighted values. This is due to characteristics of the W_h-weighting filter (ISO 5349-1, 2011), which tends to attenuate vibration at frequencies above 12.5 Hz.

Among the three HAV models considered in this study, the biomechanical HAV model is considered better suited for the development of the coupled hand-tool-workpiece model as it also permits the analysis of distributed vibration dosages in the substructures of the human HAS under the bent-arm posture and the assessment of gloved HAS using the two driving points (fingers and palm).

Table 4.5 : Comparisons of un-weighted and frequency-weighted r.m.s. handle acceleration responses of different hand-tool system models with the measured values

Model type	a_{rms} (m/s^2)	Error (%)	a_{wrms} (m/s^2)	Error (%)
Measured data	27.19	-	5.51	-
Single-DOF hand-arm model	15.65	42.4	8.74	58.6
Four-DOF hand-arm model	17.49	35.7	7.06	28.1
Six-DOF hand-arm model	18.74	31.1	7.33	33.0

4.3 Analyses of Interactions among the Impact Pairs

The interactions among the different impact pairs of the coupled hand-tool model are analyzed to gain additional insights into the dynamic performances of the tool. The pressure variations in the upper chamber and the acceleration responses of the striker and the impact bolt are obtained for 30 N grip force and 75 N push force applied to the percussive tool model operating at the rate of 1830 bpm.

Figure 4.9 illustrates the variations in the absolute pressure of air in the upper chamber over three consecutive blows. The chamber pressure varies in a steady-state manner from 0.08 to 0.48 Mpa. The striker approaches near 1.4e3 m/s^2 downward acceleration, when the upper chamber pressure approaches its peak value, as seen in Figure 4.10. The striker subsequently impacts the impact bolt leading to high-magnitudes of upward accelerations of the striker (near 3.0e4 m/s^2). The impact bolt, subsequently collides with the tool bit after the first impact with the striker and experiences acceleration peak as high as 2.6e4 m/s^2 in the downward direction followed by high rebound acceleration peak around 2.9e4 m/s^2, as seen in Figure 4.11. Furthermore, the lower-magnitude accelerations of the impact bolt, observed after the primary peaks in the

upward direction, can be attributed to the impacts following the primary contact between the impact bolt and the tool bit.

The primary peaks in the acceleration response of the tool bit are the result of contacts between the impact bolt and the tool bit, and the tool tip and the workpiece. The upward tool body acceleration response, as seen in Figure 4.7, is mostly affected by the variations in the air pressure, while the downward response can be partly attributed to the static push force and the dynamic hand force exerted on the tool handle, and the weight of the tool body. It should be noted that the impact between the impact bolt and the tool body does not occur at the selected speed of 1830 bpm. This can be attributed to lack of consideration of the pressure variations in the lower chamber, and the masses of the upper control disk and the control bushing in the modeling process.
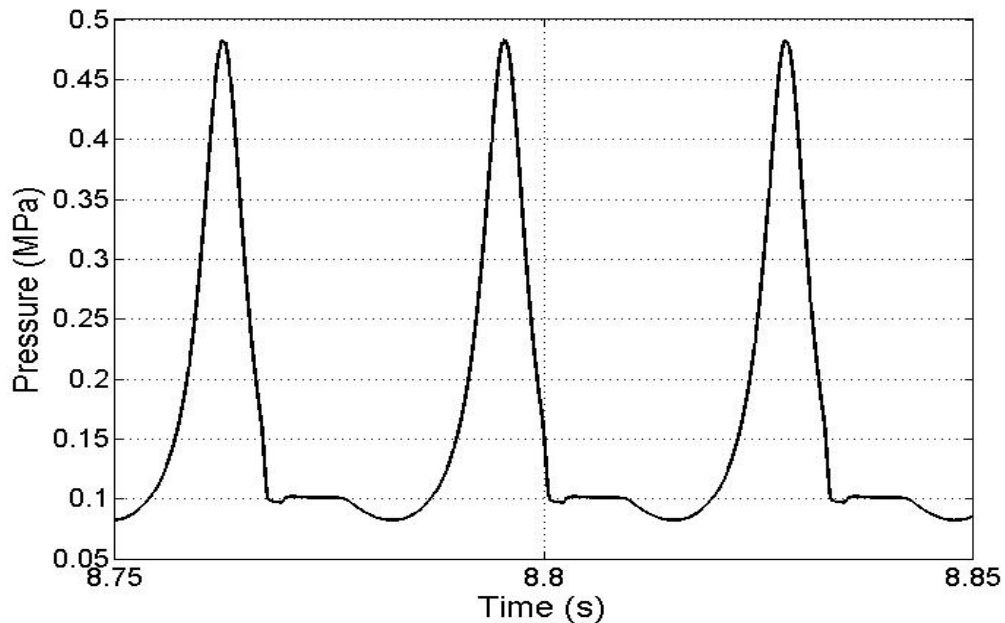
Figure 4.9 : Pressure variations in the upper chamber of the percussive tool coupled with the six-DOF HAV model (1830 bpm, 30N grip and 75N push forces)
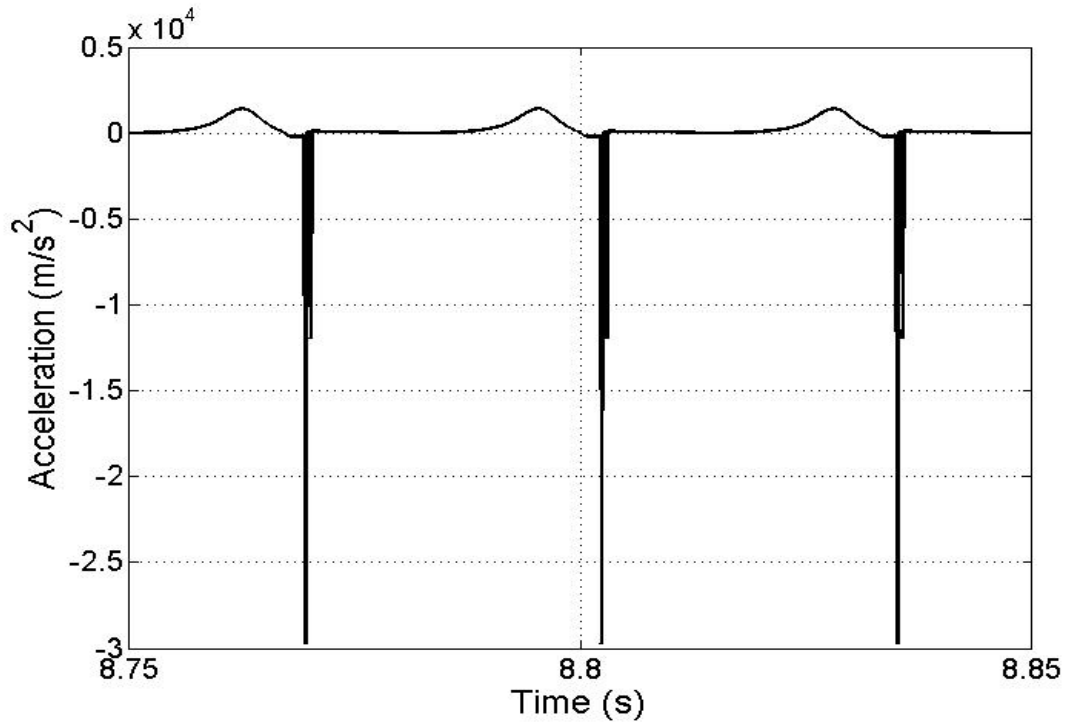
Figure 4.10 : Acceleration response of the striker of the percussive tool coupled with the six-DOF HAV model (1830 bpm, 30N grip and 75N push forces)
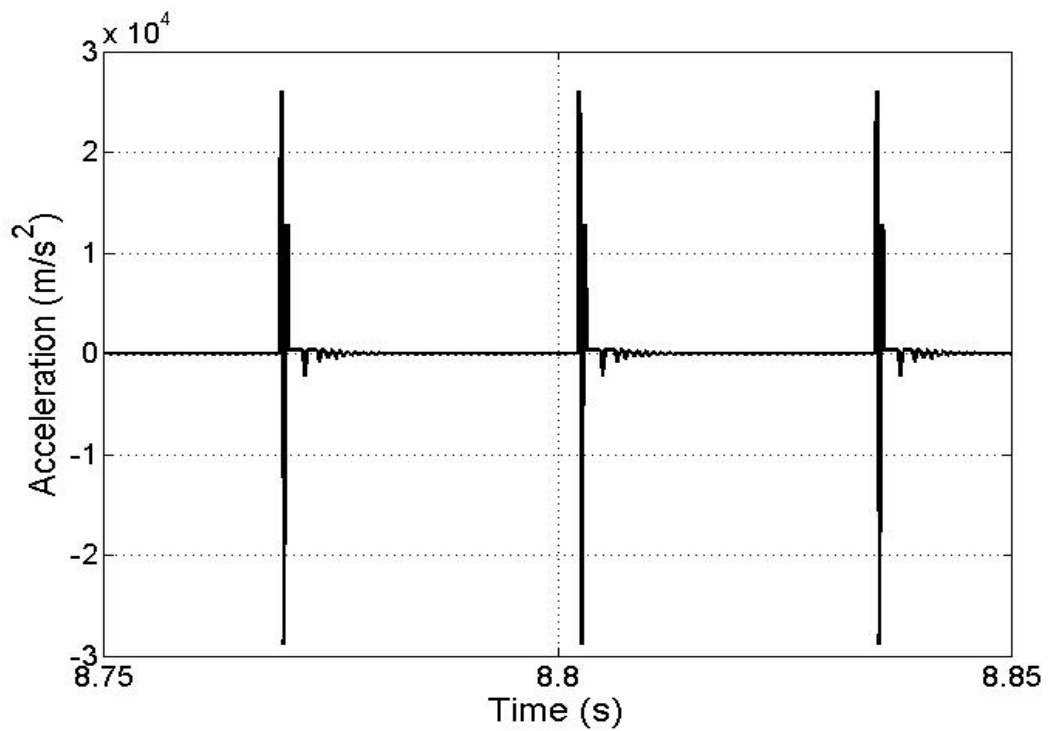
Figure 4.11 : Acceleration response of the impact bolt of the percussive tool coupled with the six-DOF HAV model (1830 bpm, 30N grip and 75N push forces)

4.4 Design Parameter Sensitivity Analyses

Apart from operating a vibrating tool at a suitable speed or maintaining the tool in a good condition, suppression of tool-generated HTV may be achieved using three methods: (i) isolating hands from the vibrating handles though anti-vibration materials or gloves; (ii) isolating tool handles from the vibrating source via handle isolators; and (iii) designs of low-vibration emission power tools or vibration control mechanisms.

Substantial efforts have been made towards the designs of anti-vibration materials and handle isolators, since these can be implemented with greater ease (Gurram et al., 1994; Dong et al., 2005; 2009; Suggs and Abrams, 1983; Oddo et al., 2004; Ko et al., 2011). However, designs of low-vibration hand-held tool may be far more efficient in controlling the vibration at the source. Optimal designs of the power tools, such as tool or components weight, components materials and sizes, may contribute to reduction of vibration at the source. In this study, the analytical model of the chipping hammer is utilized to explore the effects of variations in selected tool design parameters on the tool vibration. These include: (i) the diameter of the orifices in the upper chamber; (ii) the weight of the tool body; (iii) the weight of the striker; (iv) the weight of the impact bolt; and (v) the weight of the tool bit. The effects of the anti-vibration glove parameters on the vibration transmitted to the hand-arm system is further investigated. The simulation results are obtained for constant tool speed of 1830 bpm, while coupled with the biomechanical HAV model with 30 N grip force and 75 N push force.

4.4.1 Diameter of the Upper Chamber Orifices

The variations in the diameter of the upper chamber orifices could affect the pressure buildup in the upper chamber and thus the forces acting on the striker, the

impact bolt, the tool bit and the tool body. In this study, the simulations are performed by varying the orifice diameter from -40% to +50% of the nominal diameter. The 'orifice factor' in Table 4.6 refers to the orifice diameter normalized by the nominal diameter. The table summarizes the effect of orifice diameter on the maximum and minimum upper chamber (U.C.) pressures, and r.m.s. acceleration responses of the tool bit and the tool body.

Table 4.6 : Influence of variations in the orifice diameter on the upper chamber pressure and acceleration responses of the tool bit and the tool body

| Orifice factor | U.C. pressure (Pa) | | r.m.s. accelerations (m/s^2) | | |
	Maximum	Minimum	Too bit	Tool body (un-weighted)	Tool body (weighted)
0.60	493679	80659	982.54	19.23	7.51
0.90	485092	81769	976.89	18.84	7.37
1.00	483007	82049	975.55	18.74	7.33
1.25	479066	82603	972.02	18.56	7.26
1.50	476080	83021	968.12	18.43	7.20

Figure 4.12 further shows the effect of variations in the orifice diameters on the variations in the upper chamber air pressure during two consecutive blows. The results show that decreasing the orifice diameter causes more notable pressure variations in the upper chamber. This is also evident from the differences between the maximum and minimum pressures presented in Table 4.6. The variations in the upper chamber pressure can be attributed to the variations in the position of the orifices relative to the striker and thereby the effective orifice opening. A smaller orifice also causes the upper chamber pressure to drop below the atmospheric pressure as the piston retracts from its bottom most position, as seen in Figure 4.12. Increasing the orifice opening causes the upper chamber pressure to drop to the atmospheric pressure more rapidly as the striker

approaches the impact bolt. Figure 4.13 illustrates the variations in the opening of the orifices in terms of area fraction, C_{AU}.

The higher pressure difference due to lower orifice opening would result in higher striker impact force and thereby higher r.m.s. acceleration of the tool bit, as seen in Table 4.6. The un-weighted and frequency-weighted r.m.s. accelerations of the tool body also increase with lower diameter orifices. The results suggest that increasing the diameter of the upper chamber orifices may yield some degree of vibration control. A large increase in the orifice diameter, however, would adversely affect the cutting force due to reduced pressure buildup.
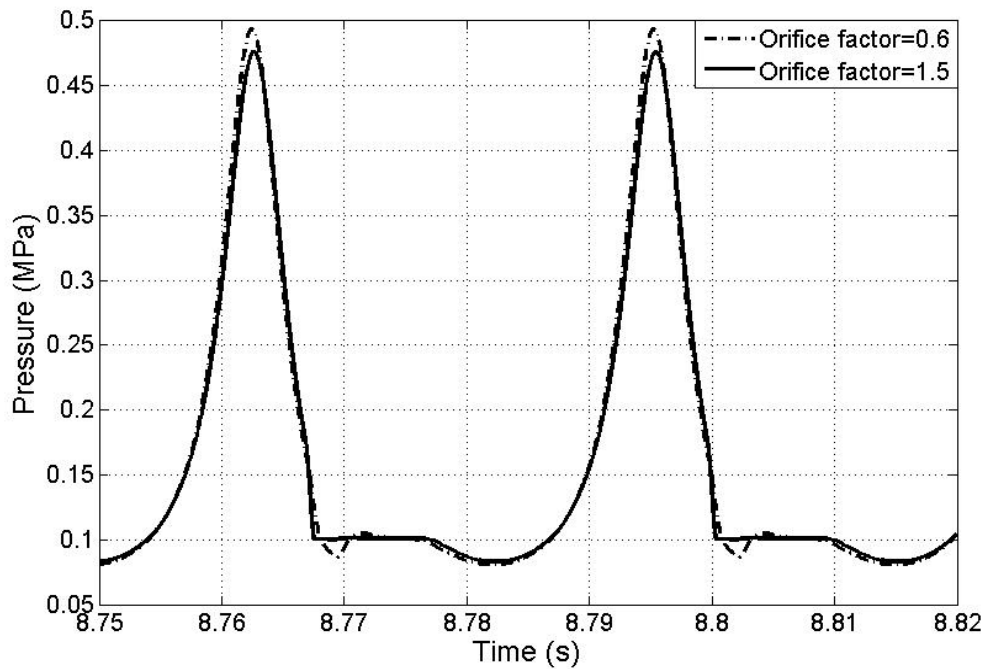
Figure 4.12 : Influence of orifice diameter on the pressure variations in the upper chamber (1830 bpm, 30 N grip and 75 N push)
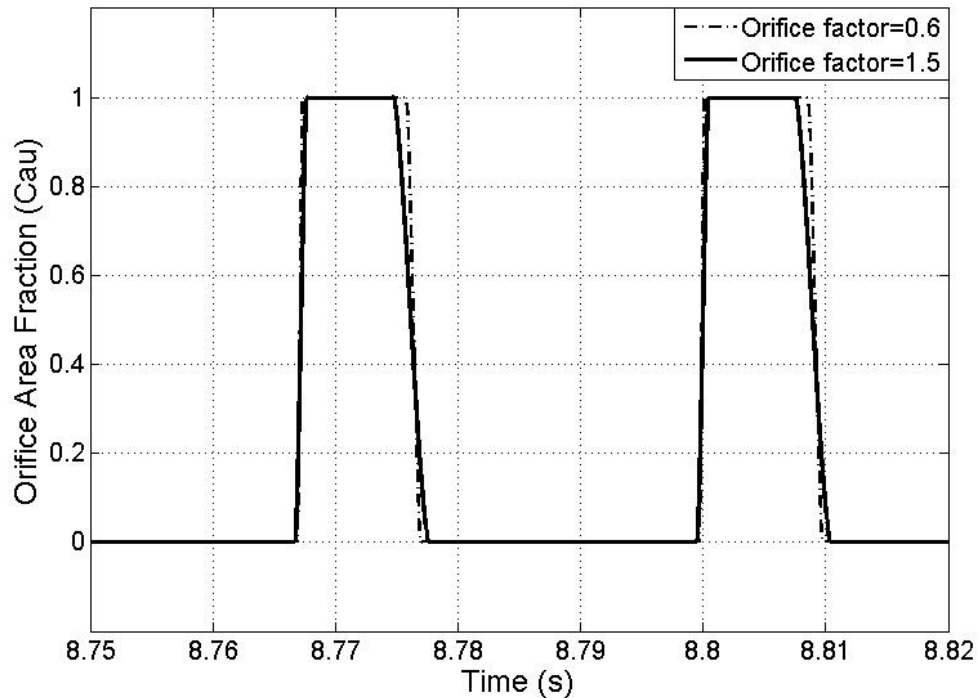
Figure 4.13 : Influence of orifice diameter on the effective opening of the upper chamber orifices (1830 bpm, 30 N grip and 75 N push)

4.4.2 Tool Body Weight

The variations in the weight of the tool body affect the deflection of the spring and thereby the position of the control bushing, which may affect the opening of the upper and lower chamber orifices. Furthermore, the tool body weight directly affects the tool body acceleration, as it is seen in Eq. (3.18). The simulation model developed in this study does not permit the analysis of the effect of the control bushing position on the air flows through the lower chamber orifices, since the lower chamber pressure is assumed to remain constant. The model, however, could be applied to study the inertia effect on the upper chamber orifices opening and the tool body acceleration. The simulations are performed by varying the tool body weight from -25% to +25% of the nominal value,

while the tool speed is 1830 bpm. The 'M_c factor' in Table 4.7 refers to the tool body weight normalized by the nominal value.

Table 4.7 : Influence of variations in the tool body weight on the upper chamber pressure and acceleration responses of the tool bit and the tool body

M_c factor	U.C. pressure (Pa)		r.m.s. accelerations (m/s^2)		
	Maximum	Minimum	Too bit	Tool body (un-weighted)	Tool body (weighted)
0.75	458263	83160	925.11	23.44	9.32
1.00	483007	82049	975.55	18.74	7.33
1.25	630302	66336	1036.05	18.58	6.57

The results in Table 4.7 show substantially higher difference between the maximum and minimum upper chamber pressures, when the tool body weight is increased to 125% of its nominal value, leading to higher r.m.s. acceleration value of the tool bit. This is mostly caused by reduced opening of the upper chamber orifices during each cycle, as seen in Figure 4.14, due to overlapping of the control bushing over the upper chamber orifices.

The un-weighted and weighted r.m.s. accelerations of the tool body, however, decrease with higher tool weight, as seen in Table 4.7. The peak tool body acceleration decreases during the downward stroke, considering for the higher tool weight, as seen in Figure 4.15. The peak tool body acceleration during the downward stroke is approximately 25 m/s^2, which is substantially lower than that observed for the lower tool weight (60 m/s^2 for M_c factor=0.75). The downward acceleration peaks, corresponding to the lower tool body weight, however, exhibit considerable variations. This was suspected to be caused by occasional loss of contact between the control bushing and the upper control disk. The loss of contact would occur during downward

motion of the upper control disk, which results in total relaxation of the spring, as it is evident from the time history of the spring force shown in Figure 4.16. The intermittent loss of contact between the control bushing and the upper control disk during some of the blow cycles causes rapid oscillations in the spring force, leading to relatively higher acceleration peaks.

The results suggest that increasing the tool body weight would be beneficial in not only reducing the tool body acceleration but also in enhancing the cutting force. A higher tool weight, however, would cause greater stresses in the musculoskeletal structure of the operator (Herberts et al., 1984).
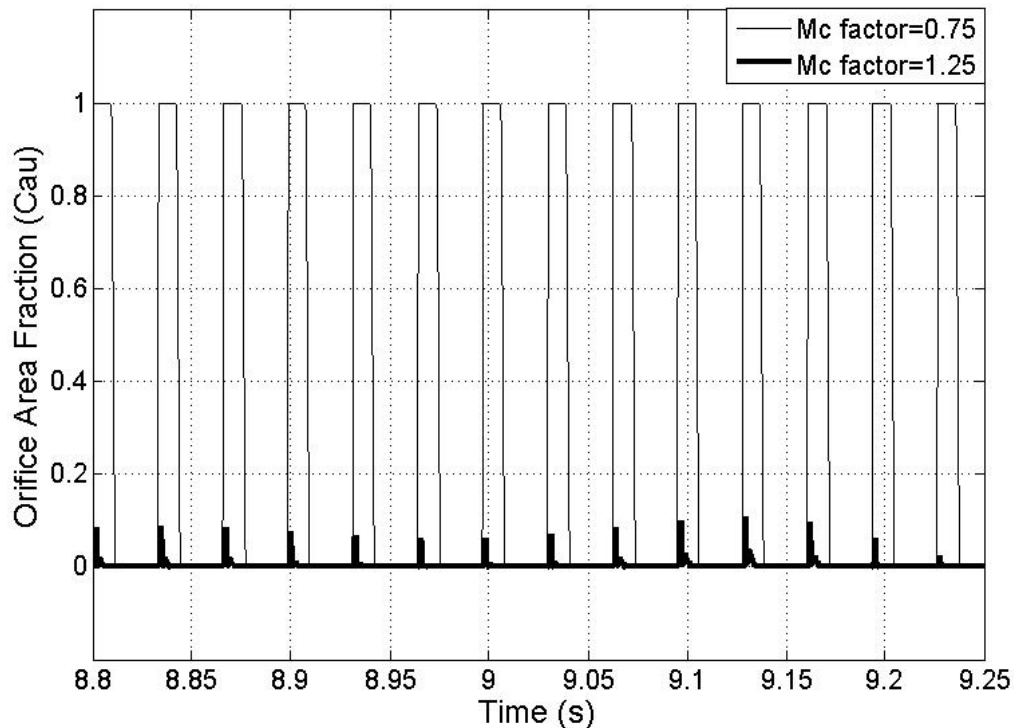

Figure 4.14 : Influence of tool body weight on the effective opening of the upper chamber orifices (1830 bpm, 30 N grip and 75 N push)
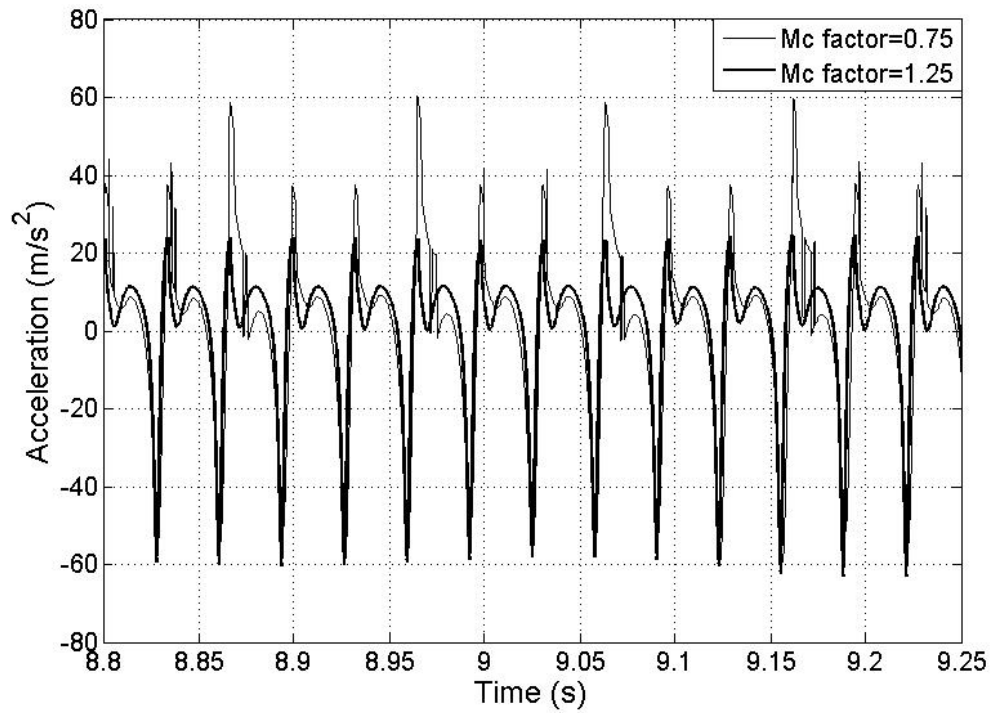
Figure 4.15 : Influence of tool body weight on the acceleration response of the tool body
(1830 bpm, 30 N grip and 75 N push)
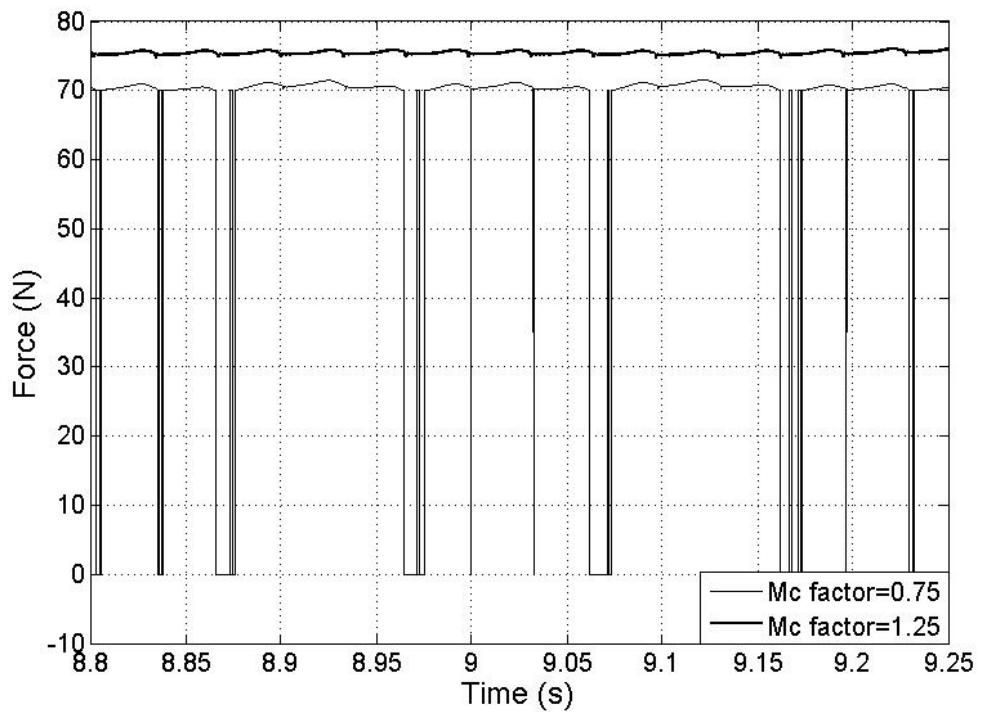
Figure 4.16 : Influence of tool body weight on the response of the spring force
(1830 bpm, 30 N grip and 75 N push)

119

4.4.3 Weights of the Striker, the Impact bolt and the Tool Bit

The weight of the striker may affect the magnitude of the impact forces imparted to the impact bolt and the tool bit. The effect of variations in the striker weight on the upper chamber air pressure and tool responses are thus investigated by varying the striker weight by -20% to +15% about the nominal value. The 'M_s factor', in Table 4.8, refers to the striker weight normalized by the nominal value. An increase in the striker weight also reduces the effective orifices opening and thereby causes higher difference between the maximum and minimum upper chamber pressures, as it is seen in Table 4.8. This causes the tool body and tool bit accelerations to increase.

Table 4.8 : Influence of variations in the striker weight on the upper chamber pressure and acceleration responses of the tool bit and the tool body

| M_s factor | U.C. pressure (Pa) | | r.m.s. accelerations (m/s^2) | | |
	Maximum	Minimum	Too bit	Tool body (un-weighted)	Tool body (weighted)
0.80	478419	82697	955.98	17.84	6.82
1.00	483007	82049	975.55	18.74	7.33
1.15	501403	88517	1055.00	21.03	8.34

Tables 4.9 and 4.10 present the influences of variations in the weights of the impact bolt and the tool bit, respectively, on the maximum and minimum upper chamber pressure, and the r.m.s. acceleration responses. The results are presented for $\pm 10\%$ variations in the weights of the impact bolt and the tool bit about the respective nominal values.

Table 4.9 : Influence of variations in the impact bolt weight on the upper chamber
pressure and acceleration responses of the tool bit and the tool body

| M_b factor | U.C. pressure (Pa) | | r.m.s. accelerations (m/s^2) | | |
	Maximum	Minimum	Too bit	Tool body (un-weighted)	Tool body (weighted)
0.90	478782	83433	986.42	18.58	7.28
1.00	483007	82049	975.55	18.74	7.33
1.10	487069	80374	987.06	18.89	7.39

Table 4.10 : Influence of variations in the tool bit weight on the upper chamber pressure
and acceleration responses of the tool bit and the tool body

| M_t factor | U.C. pressure (Pa) | | r.m.s. accelerations (m/s^2) | | |
	Maximum	Minimum	Too bit	Tool body (un-weighted)	Tool body (weighted)
0.90	488023	80293	1075.97	18.93	7.41
1.00	483007	82049	975.55	18.74	7.33
1.10	478187	83553	891.04	18.56	7.27

The results suggest small effects of the weight variations on the tool body
acceleration responses. An increase in the tool bit weight results in relatively lower tool
bit peak acceleration and thereby lower peak upper chamber pressure. An increase in the
impact bolt mass, on the other hand, causes higher peak pressure and only slight
variations in the r.m.s. acceleration of the tool bit. The variations in both weights also
affect the magnitudes of impact forces and displacements of the tool components (striker,
impact bolt, upper control disk and control bushing) only slightly. These subsequently
affect the effective orifices opening and the air pressure in the upper chamber.

4.4.4 Discussions

Increasing the diameter of the upper chamber orifice, the weights of the tool body
and the tool bit, or decreasing the weights of the striker and the impact bolt could yield

reductions in the magnitude of HTV. Furthermore, the variations in the weights of the tool body and the striker reveal more vibration reductions than those in the weights of the impact bolt and the tool bit. The motions of the tool body and the striker affect the pressure variations in the upper chamber, while the motions of the impact bolt and the tool bit have relatively little influence on the pressure variations in the upper chamber.

It should be noted that increasing the diameter of the upper chamber orifices resulted in relatively smaller vibration attenuation effect compared to those due to variations in the weights of the tool body and the striker. The relatively lower influence of orifice diameter variations is partly believed to be caused due to lack of consideration of the lower chamber pressure variations in the model. Furthermore, it is noted that dynamic motions of the striker, the impact bolt, the tool bit and the tool body affect the air pressure variations in the upper chamber in a highly complex manner, which is mostly due to highly nonlinear variations in the effective opening area of the upper chamber orifices. In this regard, further simulations considering the variations in the lower chamber pressure would be highly desirable.

4.4.5 Anti-Vibration Glove

The gloved hand-arm model, developed in Chapter 2, is used to study the vibration attenuation effectiveness of an air bladder glove, when coupled with the tool model. The tool speed is considered to be constant (1830 bpm), while the biomechanical hand-arm vibration model, corresponding to 30 N grip force and 75 N push force, is applied in the coupled glove-hand-tool-workpiece system model. Simulation results obtained for the coupled model with and without the glove are analyzed in terms of the un-weighted r.m.s. accelerations distributed in the fingers, palm, forearm and the upper arm of the

biomechanical HAV model. The results are also compared to assess the vibration isolation effectiveness of the glove.

The effect of variations in the design parameters of the anti-vibration glove, the visco-elastic properties of the materials attached to the fingers (k_{g1} and c_{g1}) and the palm (k_{g2} and c_{g2}), are also investigated to attain a better understanding on the vibration attenuation performances of the glove. For this purpose, the stiffness of the finger-side isolation material is varied from 0.5 to 4.0 times the nominal stiffness reported by Dong et al. (2009). The stiffness of palm-side isolation material is varied from 0.5 to 1.5 times the nominal stiffness. The damping constants of the finger- and palm-side materials are varied by ±50% about the respective nominal values.

Table 4.11 : Influence of variations in the glove material properties on the un-weighted r.m.s. accelerations distributed at different HAS segments

	Fingers (m/s^2)	Palm (m/s^2)	Forearm (m/s^2)	Upper Arm (m/s^2)
Bare Hand	21.16	18.47	9.42	4.90
Gloved (nominal)	23.17	16.95	9.13	5.02
k_{g1}*0.50	24.59	16.96	9.13	5.02
k_{g1}*1.50	22.61	16.95	9.12	5.02
k_{g1}*2.00	22.32	16.95	9.12	5.02
k_{g1}*4.00	21.91	16.95	9.12	5.02
k_{g2}*0.50	23.38	15.25	8.44	4.76
k_{g2}*1.50	23.06	17.50	9.27	5.01
c_{g1}*0.50	23.28	16.95	9.13	5.02
c_{g1}*1.50	23.06	16.95	9.13	5.02
c_{g2}*0.50	23.22	17.21	9.25	5.08
c_{g2}*1.50	23.13	16.74	9.01	4.96

Table 4.11 summarizes the effect of variations in the glove material properties on the r.m.s. accelerations due to tool vibration transmitted to the fingers, palm, forearm and

the upper arm. The vibration responses of the hand-arm system coupled with the tool without the glove shows lower vibration of the forearm and the upper arm, compared to that of the palm. This is attributed to absorption of vibration into the hand-arm system (Dong et al., 2005c; Adewusi, 2009). The vibration transmitted to the fingers mass tends to be the highest, which is attributed to higher resonance frequency of the fingers compared to the hand-arm system. The addition of the glove results in reduction of vibration transmitted to the palm and the forearm with amplification of vibration at the fingers and the upper arm.

It should be noted the fundamental frequency of the tool-handle vibration is 30.5 Hz. It has been shown that the hand-arm system tends to transmit only low frequency vibration to the upper arm and the whole-body. Gloves are generally designed to achieve relatively lower stiffness of the palm-side vibration isolation material, since the standardized assessment method (ISO 10819, 2013) is based only on the palm-side vibration transmissibility. The finger-side material, on the other hand, exhibits considerably higher stiffness. The high material stiffness coupled with higher natural frequency of the fingers, is the likely cause of amplification of the tool handle vibration to the finger-side of the hand (Dong et al., 2009). The relatively soft palm side material, on the other hand, transmits higher levels of low frequency vibration to the upper arm.

The results suggest only limited vibration attenuation effect by the glove in view of the un-weighted r.m.s accelerations of the palm and forearm, while the anti-vibration glove tends to amplify the vibrations transmitted to the fingers and the upper arm. The results further show that increasing finger-side material stiffness (k_{g1}) yields notable vibration reductions for the fingers, while an increase in material damping (c_{g1}) provides

124

small vibration reduction for the fingers. The un-weighted r.m.s. acceleration of the fingers' mass, however, is still higher than that obtained for the bare hand. It can be concluded that the glove materials do not help attenuation of the handle vibration transmitted to the fingers' mass.

The vibration transmission to the palm, however, can be considerably reduced by decreasing the palm-side glove material stiffness (k_{g2}) and increasing the material damping (c_{g2}). The low stiffness and high damping of the palm-side material also yields notable reductions in the vibrations transmitted to the forearm and the upper arm. Reducing the palm-side stiffness, however, may increase the glove material thickness and thereby affect the hand dexterity in an adverse manner.

4.5 Influences of Tool Operating Factors

The dynamic performances of percussive tools and the HTV exposure may be strongly affected by variations in the operating conditions, such as the properties of workpiece, tool maintenance, operating speed, hand-arm posture and hand forces. It is, however, recognized that control of many of these operating factors would be very difficult due to various constraints posed by the work environment and the productivity demands. This study is thus limited to the effects of variations in the push force, operating speed and the parameters of the tool tip-workpiece contact model on the dynamic performances of the integrated hand-tool-workpiece system model.

4.5.1 Static Push Force

Hand forces, applied to the tool handles for the guidance and control of power tools, play an important role in the dynamic performances of the coupled hand-tool system. The

influences of hand-grip and push forces on the biodynamic responses of the human HAS have been extensively studied through laboratory experiments (Iwata et al., 1972; Pyykkö et al., 1976; Hartung et al., 1993; Kihlberg, 1995). These have shown increases in the resonant frequencies and driving-point impedance of the HAS under increasing grip and push forces.

The effects of hand forces on the tool vibration transmission, however, have not been reported. In this study, the model simulations are performed considering two levels of the hand push force (50 N and 75 N), while the hand grip force is held as 30 N. The HAV model parameters corresponding to the two push-grip force combinations are taken as those reported by Adewusi (2009). Table 4.12 summarizes the effect of hand push force on the model responses in terms of r.m.s. accelerations of the tool tip and the tool body, and peak tool-tip cutting force.

Table 4.12 : Influence of variations in the push force on the peak tool-tip cutting force and acceleration responses of the tool bit and the tool body

| Push force (N) | Peak tool-tip cutting force (N) | r.m.s. accelerations (m/s^2) | | |
		Too bit	Tool body (un-weighted)	Tool body (weighted)
50	3658.76	893.95	17.62	7.21
75	3755.85	975.55	18.74	7.33

Figures 4.17 and 4.18 illustrate the effect of hand push force on the upper chamber orifices opening and the air pressure. The results suggest that decreasing the push force increases the duration of the full opening of the upper chamber orifices and reduces the peak pressure in the upper chamber. The lower air pressure subsequently results in lower magnitude of impacts between the striker and the impact bolt, and the impact bolt and the

126

tool tip, as seen in Figures 4.19 and 4.20, respectively, leading to lower r.m.s. accelerations of the tool bit and tool body, as seen in Table 4.12. This further results in lower peak cutting force of the tool tip and leads to lower impact force of the tool bit against the impact bolt, which may cause intermittent loss of contact of the impact bolt with the upper control disk. In this case, the control bushing tends to seat on the lower control disk and diminishes the spring force exerted on the tool body, as seen in Figure 4.21.

Through laboratory measurements, it has been reported that the handle vibrations of the tool, expressed in terms of un-weighted and frequency-weighted r.m.s accelerations, increase as the push force decreased from 118 N to 78 N under the tool speed of 1830 bpm (Adewusi, 2009). The simulation results, however, show an opposite tendency, while only very little data exists to understand the sources of this discrepancy.
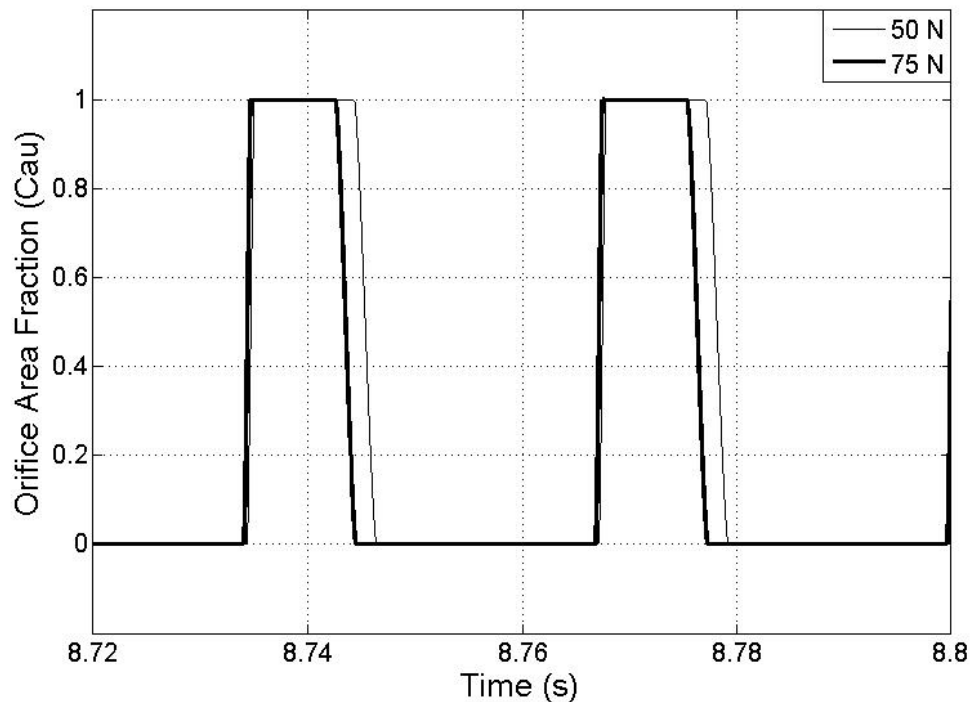
Figure 4.17 : Influence of push force on the effective opening of the upper chamber orifices (1830 bpm and 30 N grip force)
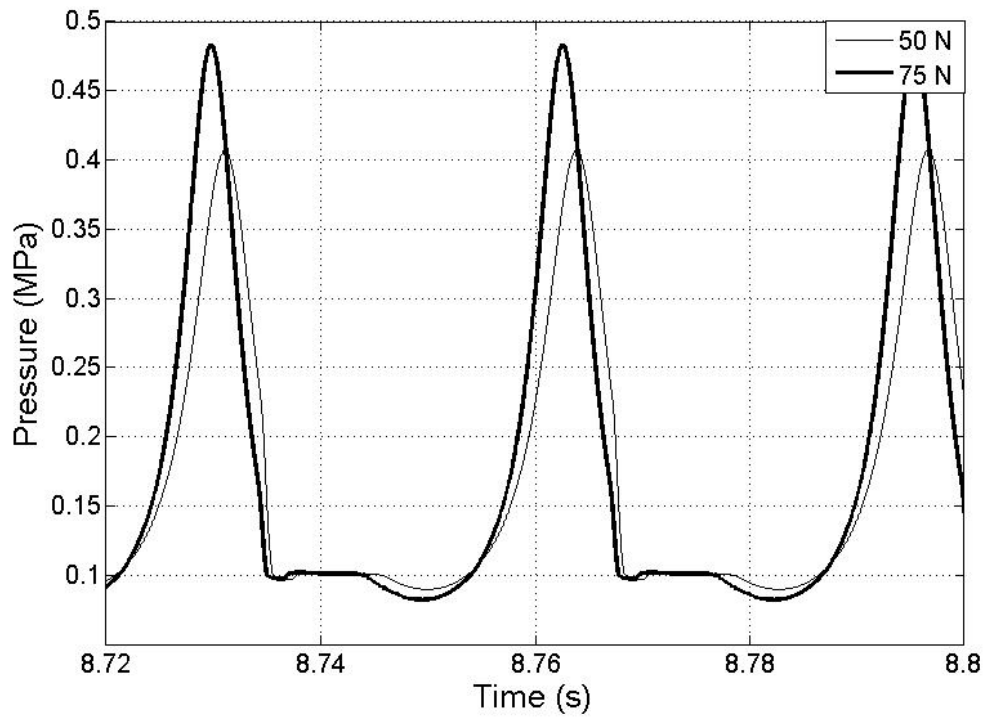
Figure 4.18 : Influence of push force on the pressure variations in the upper chamber
(1830 bpm and 30 N grip force)
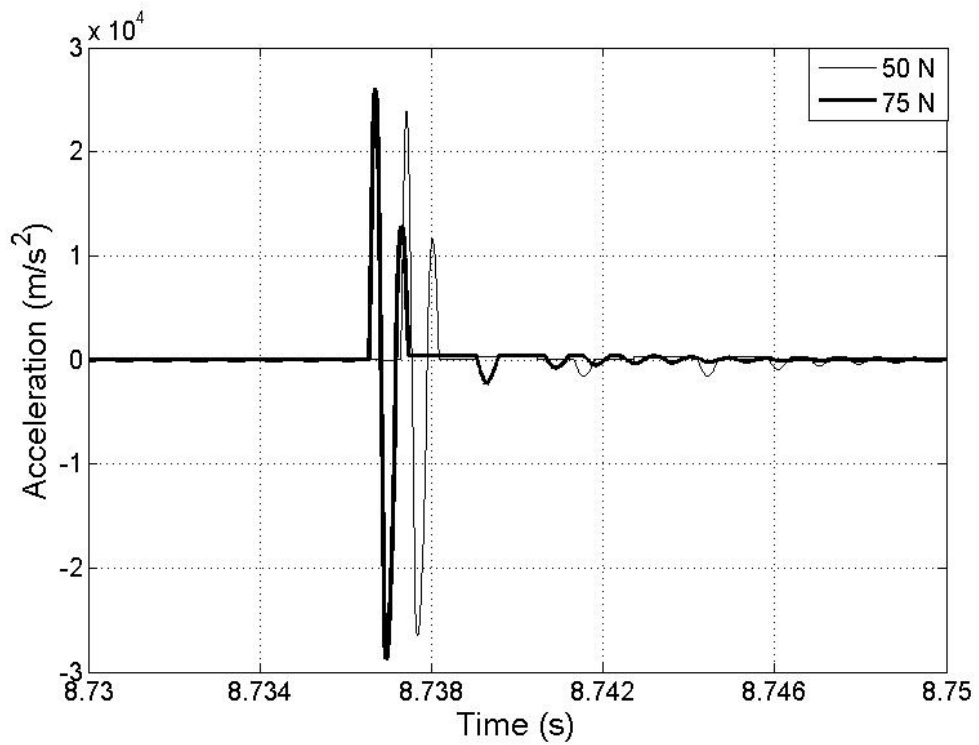
Figure 4.19 : Influence of push force on the acceleration response of the impact bolt
(1830 bpm and 30 N grip force)
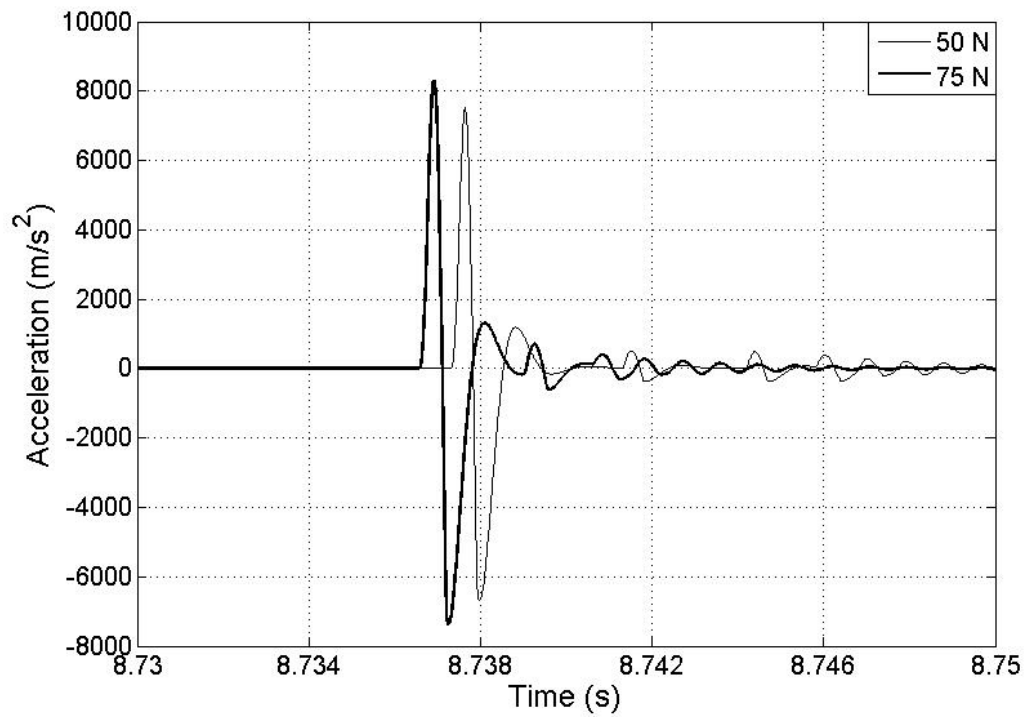
Figure 4.20 : Influence of push force on the acceleration response of the tool bit
(1830 bpm and 30 N grip force)
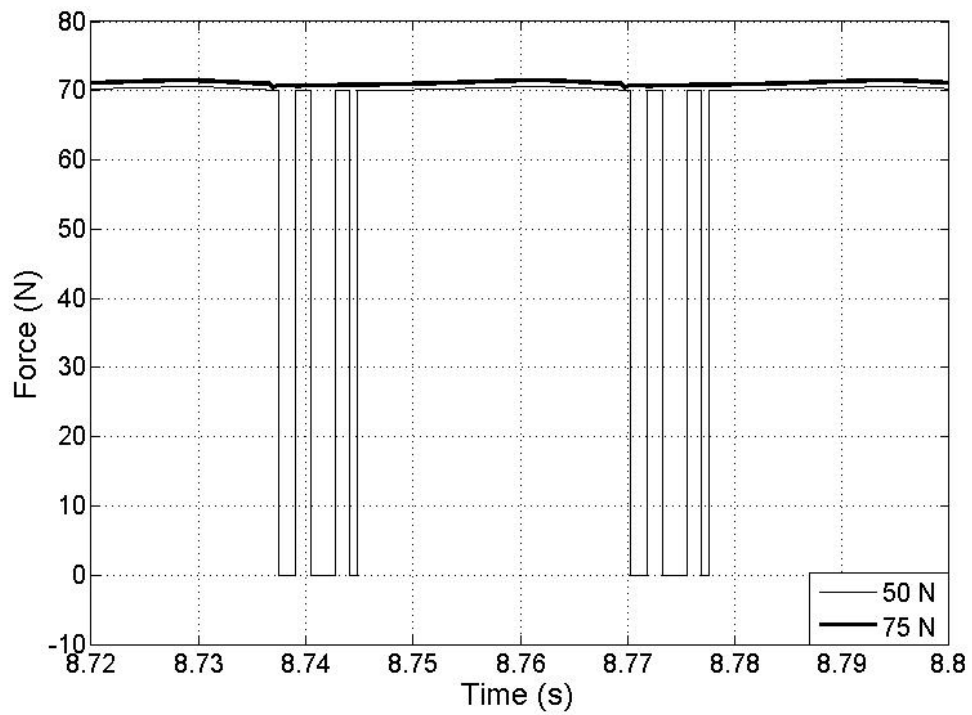
Figure 4.21 : Influence of push force on the response of the spring force
(1830 bpm and 30 N grip force)

4.5.2 Tool Speed

The selected percussion tool (BOSH, 11313 EVS) allows operator to customize the speed from 1300 to 2600 bpm. Increasing the motor speed will likely results in considerably higher pressure variations in the upper chamber and thereby higher impact forces and vibrations of the coupled hand-tool system. In this study, the simulations are performed for three different operating speeds (1300, 1830 and 2600 bpm) denoted as 'low', 'medium' and 'high' speeds, while the HAV model is integrated considering 30 N grip and 75 N push forces. The results, summarized in Table 4.13, clearly show that increasing the tool speed causes substantially higher tool vibration and the peak cutting force. This is due to higher upper chamber pressure at higher speeds, as seen in Figure 4.22. Under the high speed (2600 bpm), the peak air pressure in the upper chamber increases substantially and approaches 1.0 Mpa, which would lead to far more significant impacts among tool components. The peak accelerations of the tool bit and the peak tool-tip cutting force thus increase significantly, as seen in Figure 4.23 and Table 4.13.

Table 4.13 : Influence of variations in the tool speed on the peak tool-tip cutting force and acceleration responses of the tool bit and the tool body

Speed (bpm)	Peak cutting force (N)	Peak tool bit acceleration (m/s^2)		r.m.s. accelerations of tool body (m/s^2)	
		Downward	Upward	Un-weighted	Weighted
1300	1522.65	2999.54	2781.96	10.13	7.15
1830	3755.85	8297.81	7398.40	18.74	7.33
2600	6040.62	13712.84	11065.86	43.58	11.77

The un-weighted and frequency-weighted accelerations of the tool body are observed to increase by 330.2% and 64.6%, respectively, when the tool speed is increased from 1300 to 2600 bpm, which is directly attributed to higher impact forces and

considerably higher pressure variations in the upper chamber. This is also clearly evident from the time-histories of the tool body acceleration responses, as shown in Figure 4.24. Furthermore, the upper control disk tends to lose contact with the control bushing under the high tool speed (2600 bpm). This causes intermittent rapid variations in the spring force exerted on the tool body, as seen in Figure 4.25. The rapid variations in the spring force also result in sharp discontinuities in the tool body acceleration responses, as shown in Figure 4.24.
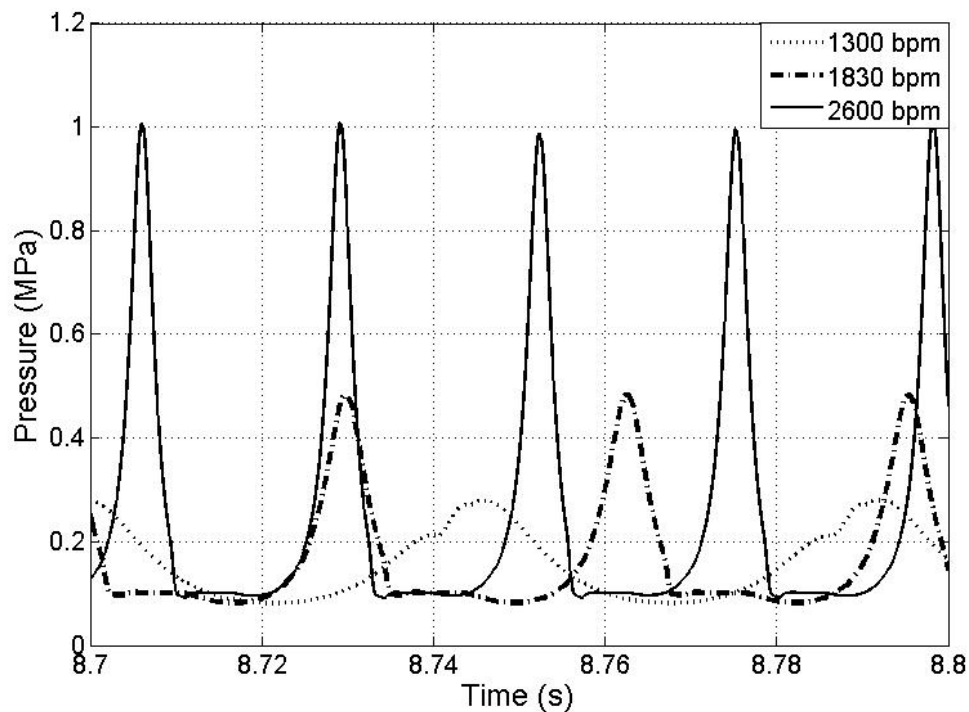
Figure 4.22 : Influence of tool speed on the pressure variations in the upper chamber (30N grip and 75N push forces)
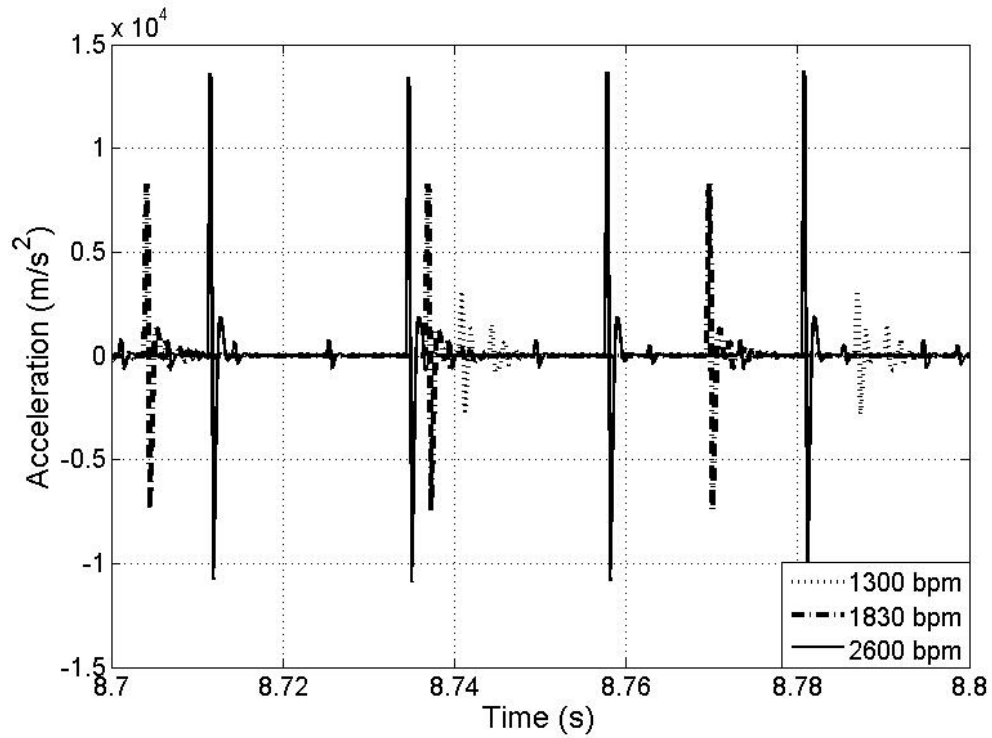
Figure 4.23 : Influence of tool speed on the acceleration response of the tool bit
(30N grip and 75N push forces)
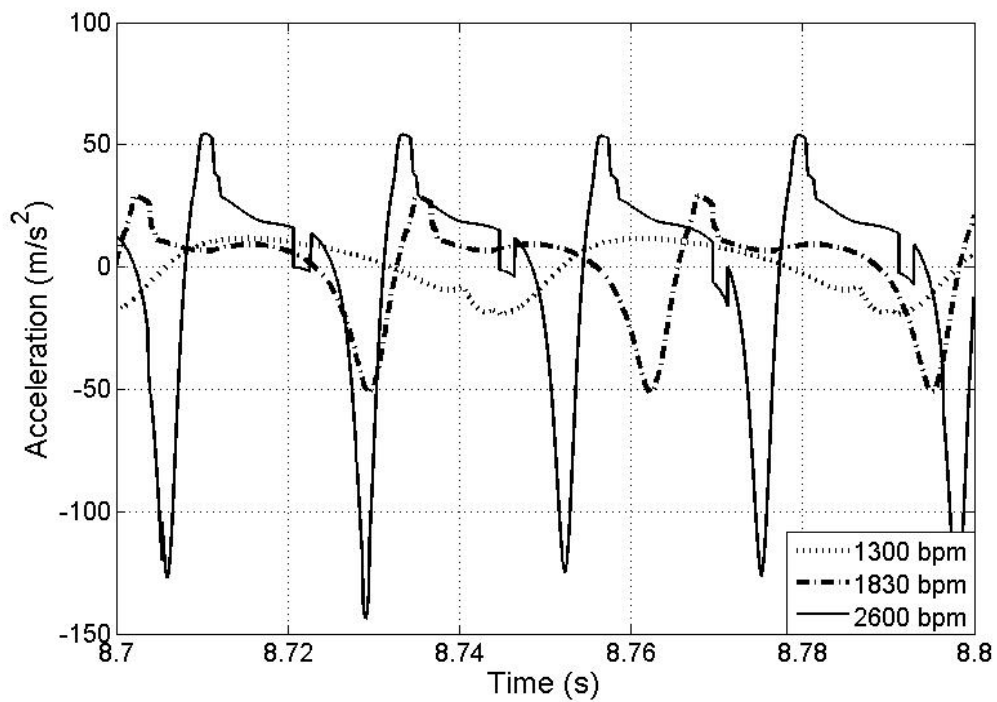
Figure 4.24 : Influence of tool speed on the acceleration response of the tool body
(30N grip and 75N push forces)

132
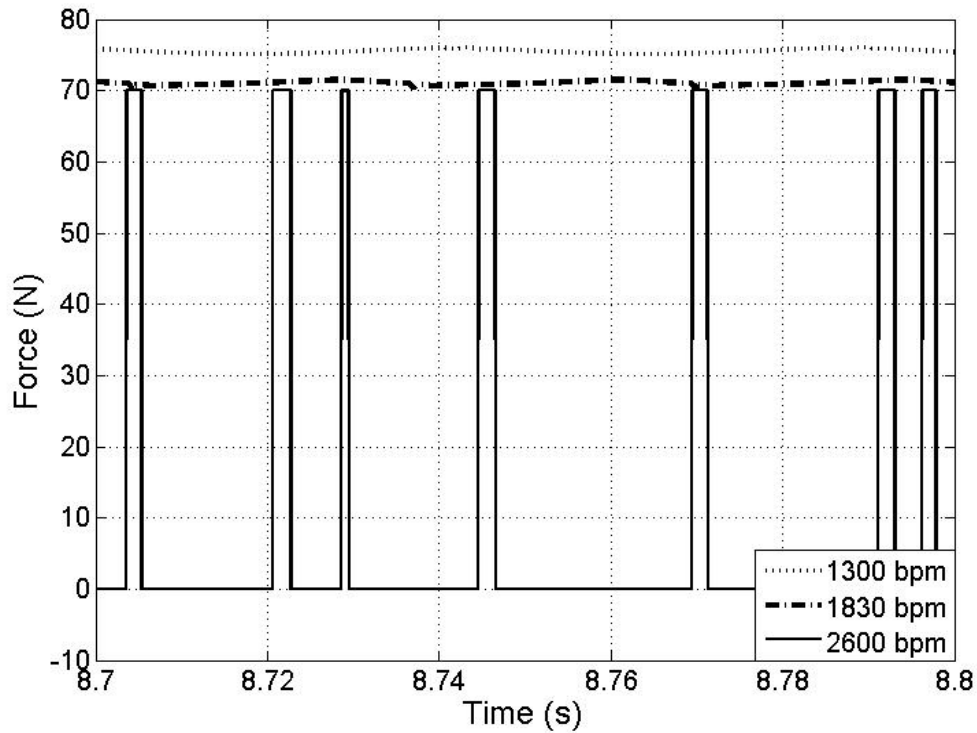
Figure 4.25 : Influence of tool speed on the response of the spring force
(30N grip and 75N push forces)

4.5.3 Tool Tip-Workpiece Contact Model

The diversity among different types of workpiece may significantly affect the work quality, tool durability and the dynamic performances of the coupled hand-tool system. However, very few studies have been attempted to evaluate the influences of different types of workpiece on the dynamics of coupled hand-tool system, which is likely due to limited knowledge of the properties of work materials and the contact model.

In this study, simulations of the coupled hand-tool-workpiece system model are performed to study the influences of different contact model parameters that may be related to different workpiece properties. These include the elastic zone stiffness (K_E), and stiffness and damping properties (K_P and C_P) of the plastic substratum of the workpiece (steel balls). Table 4.14 illustrates the effect of the variations in K_E, K_P and C_P

133

on the acceleration responses of the coupled hand-tool model, by varying K_E, K_P and C_P from -25% to +25% of the respective nominal values.

Table 4.14 : Influence of variations in the parameters of the tool tip-workpiece contact model on the acceleration responses of the tool bit and the tool body

Parameter	Factor	Peak tool bit acceleration (m/s^2)		r.m.s. accelerations (m/s^2)		
		Downward	Upward	Tool bit	Tool body (un-weighted)	Tool body (weighted)
K_E	0.75	8635.39	7002.84	1025.97	18.83	7.37
	1.00	8297.81	7398.40	975.55	18.74	7.33
	1.25	8013.78	7640.55	931.63	18.66	7.30
K_P	0.75	8300.15	7359.74	971.39	18.74	7.33
	1.00	8297.81	7398.40	975.55	18.74	7.33
	1.25	8296.49	7437.26	980.06	18.74	7.33
C_P	0.75	8424.27	6508.90	931.42	18.78	7.35
	1.00	8297.81	7398.40	975.55	18.74	7.33
	1.25	8213.94	8075.22	1028.46	18.71	7.32

Table 4.14 shows that increasing the elastic zone stiffness (K_E) would lead to higher upward and lower downward peak accelerations of the tool bit. The higher elastic zone stiffness further lower the oscillations following the primary peaks, leading to lower r.m.s. acceleration of the tool bit. An increase in the plastic zone stiffness (K_P) also leads to higher upward and lower downward peak accelerations of the tool bit, while it slightly increases the magnitudes of oscillations following the primary peaks and the r.m.s. acceleration of the tool bit. These can be attributed to the relatively lower stiffness of plastic zone and the structure of the tool tip-workpiece contact model. Similar trends are also observed from the acceleration responses of the tool bit by increasing the damping (C_P) of the plastic zone, as seen in Table 4.14.

On the other hand, the variations in the parameters of the contact model yields relatively lower influences on the r.m.s. accelerations of the tool body. These can be attributed to the slight variations in the impact forces and displacements of the tool components. The simulation results suggest that the acceleration responses of the tool bit are more sensitive to the parameter variations in the contact model than those of the tool body.

4.6 Summary

The dynamic responses of the percussive tool model are evaluated considering the coupling with three different hand-arm system models. It is showed that the percussive tool model, coupled with the biomechanical hand-arm vibration model, can yield somewhat reasonable dynamic performances compared with the available measured data. Parametric sensitivity analyses are performed by varying the diameter of the upper chamber orifices and the weights of tool components to explore a design guidance for low vibration emission tool. The effectiveness of an anti-vibration glove is also investigated by assessing the distributed vibration responses in the gloved-hand model. Moreover, the effects of variations in the push force, operating speed and the parameters of the tool tip-workpiece contact model on the dynamics of the integrated hand-tool-workpiece system model are also investigated. Conclusions and suggestions are further stated in the following chapter for future work.

CHAPTER 5

CONCLUSIONS AND RECOMMENDATIONS FOR FUTURE WORK

5.1 Major Contributions of the Study

The main focus of this research dissertation is to investigate the dynamic responses of a hand-held percussive tool integrated with the human hand-arm system (HAS) model, while operating within a steel ball energy dissipator. The major contributions include the developments of the integrated hand-tool-workpiece and glove-hand-tool-workpiece system models, together with identifications of the contact pair models. Parametric sensitivity analyses were performed by varying selected design parameters and operating factors, in order to gain insight into design guidance towards a low vibration tool and for identification of favorable operating conditions. Moreover, this study also focused on the vibration attenuation effectiveness of an anti-vibration glove so as to seek design guidance on vibration isolation materials employed in the glove. The major highlights and contributions of this study are summarized below:

- A push force-dependent biomechanical model of the hand-arm system in the bent-arm posture was evaluated in terms of natural frequencies, deflections under different static feed forces, driving point mechanical impedance (DPMI) and vibration transmissibility, for integration to the tool model;

- A nonlinear dynamic model of a percussion demolition hammer was developed to characterize its vibration performances along the z_h-axis. The validity of the tool model was examined using available laboratory-measured data, which was further used to identify the parameters of the major contact pair models;

- A two degrees-of-freedom contact model was developed to describe the dynamic interactions between the tool tip and the steel-ball energy dissipator;

- An eight-DOF integrated gloved-hand model was developed to study the vibration performances of an anti-vibration glove along the z_h-axis.

5.2 Conclusions

- The biomechanical model of the hand-arm system provided a low static deflection of the hand-arm (40.75 mm) under a 50 N push force, while the total deflection under 75 N push force was considerably higher (187.06 mm). The model provided reasonably good predictions of the biodynamic responses of the human hand-arm system in terms of DPMI and vibration transmissibility;

- The hand-arm vibration model, reported in ISO 10068 (1998), yielded excessive deflections of the hand-arm and is not adequate for integration to the tool model;

- Three linear contact models, describing the contacts between the striker and impact bolt, the impact bolt and the tool bit, and the impact bolt and the tool body, yielded relatively good dynamic performances in view of components deformations and rebound velocity responses;

- The contact pair models revealed reasonably good predictions of the impact durations. The highest deviation was in the order of 6% for the impact between the impact bolt and tool body;

- The percussive tool model coupled with the four- and six-DOF hand arm vibration models revealed reasonably good agreements between the predicted tool bit acceleration and the laboratory measured data;

- Varying the diameter of the upper chamber orifices, the weights of the impact bolt and the tool bit could lead to some degree of vibration attenuation, while the variations in the weights of the tool body and the striker revealed relatively greater vibration reductions for the coupled hand-tool model;

- The anti-vibration glove could reduce the tool vibration transmitted to the palm and the forearm only slightly, while it transmitted higher vibration to the fingers, when compared to the bare hand;

- The effectiveness of an anti-vibration glove could be enhanced by increasing the stiffness of the glove material at the finger side, and decreasing the stiffness and increasing the damping of the glove material at the palm side;

- The dynamic performances of the proposed hand-tool system were strongly affected by the variations in tool speed and push force, while the variations in the tool tip-workpiece contact model primarily affected the dynamics of the tool bit only.

5.3 Recommendations for Future Studies

- It is desirable to develop a more appropriate biomechanical hand-arm vibration model to reflect the dynamic performances of the human hand-arm system corresponding to typical work postures and ranges of hand-grip and push forces;

- Laboratory and field measurements are vital to accurately describe the dynamic responses of the coupled hand-tool system under practical ranges of hand forces in order to identify the contact model parameters;

- The proposed tool model should be refined to incorporate the effect of the air pressure and density variations in the lower chamber;

138

- Consideration of the inertia effects due to the masses of different components of the percussive chipping hammer, such as the slider-crank mechanism, the upper control disk and the control bushing, could help realized a more effective model;

- Further refinements are desirable in the component contact pair models through accurate measurements of the impact duration and coefficient of restitution. This is particularly important for the interactions among the impact bolt, the control disks and the tool body; and

- A refined tool tip-workpiece contact model is also essential for simulating the separation of tool tip from the workpiece.

REFERENCE

Abrams C.F. and Suggs C.W. *Chain Saw Vibration: Isolation and Transmission through the Human Arm*. Transactions of the ASAE (1969): 423-425

Abrams C.F. and Suggs C.W. *Development of a Simulator for Use in the Measurement of Chain Saw Vibration*. Applied Ergonomics 8.3 (1977): 130-134.

Abrams C.F. *Modeling the Vibrational Characteristics of the Human Hand by the Driving Point Mechanical Impedance Method*. Ph.D. Thesis. North Carolina State University, 1971.

Adam D. and Kopf F. *Sophisticated Compaction Technologies and Continuous Compaction Control*. European Workshop Compaction of Soils and Granular Materials. (2000): 207-220.

Adam D. and Kopf F. *Theoretical Analysis of Dynamically Loaded Soils*. European Workshop Compaction of Soils and Granular Materials (2000): 3-16.

Adewusi S.A. *Distributed Biodynamic Characteristics of the Human Hand-arm System Coupled with Vibrating Handles and Power Tools*. PhD thesis, Montreal: Concordia University, 2009.

Adewusi S.A., Rakheja S., Marcotte P. and Boutin J. *Vibration Transmissibility Characteristics of the Human Hand-arm System under Different Postures, Hand Forces and Excitation Levels*. Journal of Sound and Vibration 329 (2010): 2953-2971.

Agate J.N., Druett H.A. and Tombleson J.B.L. *Raynaud's Phenomenon in Grinders of Small Metal Castings*. British Journal of Industrial Medicine 3.3 (1946):167-174.

Anderegg R. and Kaufmann K. *Intelligent Compaction with Vibratory Rollers: Feedback Control Systems in Automatic Compaction and Compaction Control*. Transportation Research Record (2004): 124-134.

ANSI S2.70. *Guide for the Measurement and Evaluation of Human Exposure to Vibration Transmitted to the Hand*. American National Standard, Acoustical Society of America, Melville, New York, USA. 2006.

Babitsky V.I. *Hand-held Percussion Machine as Discrete Non-Linear Converter*. Journal of Sound and Vibration 214.1 (1998): 165-182.

Banister P.A. and Smith F.V. *Vibration Induced White Fingers and Manipulative Dexterity*. Br J Ind. Med 29 (1972): 264-267.

Bannister R., Sever P. and Gross M. *Cardiovascular Reflexes and Biochemical Responses in Progressive Autonomic Failure*. Brain 100 (1977): 327-344.

Behrens V., Taylor W., Wilcox T., Miday R., Spaeth S. and Burg J. *Vibration Syndrome in Chipping and Grinding Workers*. Journal of Occupational Medicine 26.10 (1984): 769-773.

Bovenzi M. *A Longitudinal Study of Vibration White Finger, Cold Response of Digital Arteries, and Measures of Daily Vibration Exposure*. International Archives of Occupational and Environmental Health 83.3 (2010): 259-273.

Bovenzi M. *Exposure-Response Relationship in the Hand-Arm Vibration Syndrome: An Overview of Current Epidemiology Research*. Int. Arch Occup. Environ Health 71 (1998): 509-519.

Bovenzi M., Fiorito A., and Volpe C. *Bone and Joint Disorders in the Upper Extremities of Chipping and Grinding Operators*. Int. Arch Occup. Environ. Health 59 (1987): 189-198

Bovenzi M., Franzinelli A. and Strambi F. *Prevalence of Vibration-Induced White Finger and Assessment of Vibration Exposure among Travertine Workers in Italy*. Int. Arch. Occup. Environ. Health 61.1-2 (1988): 25-34.

Bovenzi M., Lindsell C.G. and Griffin M.J. *Acute Vascular Responses to the Frequency of Vibration Transmitted to the Hand*. Occup. Environ Med 57.6 (2000): 422-430.

Bovenzi M., Petronio L. and Marino F.D. *Epidemiological Survey of Shipyard Workers Exposed to Hand Arm Vibration*. International Archives Of Occupational and Environmental Health 46 (1980): 251-256.

Bovenzi, M. *Medical Aspects of the Hand-Arm Vibration Syndrome*. International Journal of Industrial Ergonomics 6 (1990): 61-73.

Brammer A.J. *Exposure of the Hand to Vibration in Industry*, National Research Council Canada, Publication (1984) No. NRCC 22845.

Brammer A.J. *Influence of Hand-Grip on the Vibration Amplitude of Chain-Saw Handles*. Proc. International Occupational Hand-Arm Vibration Conference. Cincinnati, Ohio, USA, (1975): 179-186.

Brammer A.J. and Taylor W. *Vibration Effects on the Hand and Arm in Industry*. New York: John Wiley & Sons, 1982.

Brown A.P. *The Effects of Anti-vibration Gloves on Vibration-induced Disorders: A Case Study*. Journal of Hand Therapy 3.2(1990):94-100.

Brubaker R.L., Mackenzie C.J.G. and Hutton S.G. *Vibration Induced White Finger among Selected Underground Rock Drillers in British Columbia*. Scandinavian Journal of Work Environment & Health 12.4 (1986): 296-300.

Bureau of Labor Statistics. Department of Labor. *Nonfatal Cases Involving Days Away From Work: Selected Characteristics. Injuries, Illnesses and Fatalities*. USA, 05.27, 2004.

Chatterjee D.S., Petrie A. and Taylor W. *Prevalence of Vibration Induced White Finger in Fluorspar mines in Weardale*. British Journal of Industrial Medicine 35 (1978): 208-218.

Cherian T., Rakheja S. and Bhat R.B. *An Analytical Investigation of an Energy Flow Divider to Attenuate Hand-transmitted Vibration*. International Journal of Industrial Ergonomics 17

(1996): 455-467.

Daikoku M. and Ishikawa F. *Mechanical Impedance and Vibration Model of Hand-Arm System*. Proceedings of 5th International Conference on Hand-Arm Vibration. Kanzawa, Japan, 1990.

Dandanell R. and Engstrom K. *Vibration from Riveting Tools in the Frequency Range 6 Hz-10 MHz and Raynaud's phenomenon*. Scand. J. Work, Environ & Health 12 (1986): 338-342.

Dong J.H. *Distributed Biodynamic Response Analysis of the Hand-Arm System Exposed to Vibration along the Forearm Direction*. M.A.Sc. Thesis. Concordia University, Montreal, 2007.

Dong J.H., Dong R.G., Rakheja S., Welcome D.E. McdowEll T.W. and Wu J.Z. *A Method for Analyzing Absorbed Power Distribution in the Hand and Arm Substructures When Operating Vibrating Tools*. Journal of Sound and Vibration 311.3-5 (2008): 1286-1304.

Dong R. G., Welcome D.E., McDowll T.W., Wu J.Z. and Schopper A.W. *Frequency Weighting Derived from Power Absorption of Fingers-Hand-Arm System under Zh-Axis. Journal of Biomechanics 39.12 (2006): 2311-2324.*

Dong R.G., Dong J.H., Wu J.Z. and Rakheja S. *Modeling of Biodynamic Responses Distributed at the Finger and the Palm of the Human Hand-Arm System*. Journal of Biomechanics 40.10 (2007): 2335-2340.

Dong R.G., McDowell T.W., Welcome D.E., Warren C., Wu J.Z. and Rakheja S. *Analysis of Anti-vibration Gloves Mechanism and Evaluation Methods*. Journal of Sound and Vibration 321 (2009): 435-453.

Dong R.G., Rakheja S., Smutz W.P., Schopper A.W., Welcome D., and Wu J.Z. *Evaluating Anti-vibration Performance of a Glove Using Total Effective Transmissibility*. International Journal of Industrial Ergonomics 30 (2002): 33-48.

Dong R.G., Rakheja S., Smutz W.P., Schopper A.W. and Caporali S. *Dynamic Characterization of the Simulated Tool Handle and Palm-Adapter Used for Assessment of Vibration Performance of Gloves*. Journal of Testing and Evaluation 31.3 (2003): 234-4246.

Dong R.G., Rakheja S., Mcdowel T. W., Welcome D. E., Wu J. Z., Warren C., Barklay J., Washington B. and Schopper A.W. *A Method for Assessing the Effectiveness of Anti-Vibration Gloves Using Biodynamic Responses of the Hand-Arm System*. Journal of Sound and Vibration 282.3-5 (2005a):1101-1118.

Dong R.G., Rakheja S., Schopper A. W., Han B. and Smutz W.P. *Hand-Transmitted Vibration and Biodynamic Response of the Human Hand-Arm; a Critical Review*. Critical Reviews in Biomedical Engineering 29.4 (2001): 391-441.

Dong R.G., McDowell T. W., Daniel E.W., Christopher W., Wu J.Z and Rakheja S. *Analysis of Anti-vibration Gloves Mechanism and Evaluation Methods*. Journal of Sound and Vibration 321 (2009): 435-453.

Dong R.G., McDowell T. W., Welcome D.E., Smutz W.P., Schopper A.W., Warren C., Wu

J.Z. and Rakheja S. *On-the-hand Measurement Methods for Assessing Effectiveness of Anti-vibration Gloves*. Journal of Industrial Ergonomics 3.4 (2003): 283-298.

Dong R.G., Welcome D.E. and Wu J.Z. *Frequency Weightings Based on Biodynamics of Fingers-Hand-Arm System*. Industrial Health 43 (2005b): 485-494.

Dong R.G., Wu J.Z. and Welcome D.E. *Recent Advances in Biodynamics of Hand-Arm System*. Industrial Health 43 (2005c): 449-471.

Emil H., Heinrich D. and Marina S. *Effects of Grip and Push Forces on the Acute Response of the Hand-Arm System under Vibrating Conditions*. Occupational and Environmental Health 64 (1993): 463-467.

Engstrom K. and Dandanell R. *Exposure Conditions and Raynaud's Phenomenon among Riveter in the Aircraft Industry*. Scandinavian Journal of Work, Environment & Health 12.4 (1986): 293-295.

European Parliament and the Council of the European Union. *Directive 2002/44/EC (EU Directive) on the Minimum Health and Safety Requirements regarding the Exposure of Workers to the Risks Arising from Physical Agents (Vibration)*. Official Journal of the European Communities OJ L177, 2002.

Farkkila M.A., Pyykkö I., Starck J.P. and Korhonen O.S. *Hand Grip Force and Muscle Fatigue in the Etiology of the Vibration Syndrome*. New York, NY: 1982.

Fraenkel L., Zhang Y., Chaisson C.E., et al. *Different Factors Influencing the Expression of Raynaud's Phenomenon in Men and Women*. Arthritis Rheum 42 (1999): 306–310.

Fritz M. *An Improved Biomechanical Model for Simulating the Strain of the Hand-Arm System under Vibration Stress*. Journal of Biomechanics 24.12 (1991): 1165-1171.

Fuatsuka M and Ueno T. *Vibration Exposure and Vibration Induced White Finger due to Chain Saw Operation*. J. Occup. Med. 24.4 (1985): 257-264.

Gemne G. and Saraste H. *Bone and Joint Pathology in Workers using Hand-Held Vibrating Tools: An Overview*. Scand. J. Work Environ. Health 13 (1987): 290-300.

Gemne G. and Taylor W. *Hand-Arm Vibration and the Central Autonomic Nervous System*. Journal of Low Frequency Noise and Vibration Special Volume (1983):1-12.

Gemne G., LundstroÈm R. and Hansson J.E. *Disorders Induced by Work with Hand-Held Vibrating Tools*. Arb Halsa 6 (1993): 1-83.

Goel V. K. and Kwan R. *Role of Gloves in Reducing Vibration: Analysis for Pneumatic Chipping Hammer*. American Industrial Hygiene Association Journal 48.1 (1987):249-254.

Golycheva E.V., Babitsky V.I. and Veprik A.M. *Dynamic Correction of Excitation in Hand-held Electro-Pneumatic Percussion Machines*. Journal of Sound and Vibration, 259.4 (2003): 829-843.

Golycheva E.V., Babitsky V.I. and Veprik A.M. *Vibration Protection for an Operator of a*

Hand-held Percussion Machine. Journal of Sound and Vibration 274 (2004): 351-367.

Griffin M.J. *Evaluating the Effectiveness of Gloves in Reducing Hazards of Hand-Transmitted Vibration*. Occupational and Environmental Medicine 55 (1998): 340–348.

Griffin M.J. *Handbook of Human Vibration*. London: Academic Press, 1990.

Griffin M.J. *Minimum Health and Safety Requirements for Workers Exposed to Hand-Transmitted Vibration and Whole-Body Vibration in the European Union: a Review*. Occup. Environ. Med. 61 (2004): 387-397.

Griffin M.J., Bovenzi M. and Nelson C.M. *Dose-Response Patterns for Vibration-Induced White Finger*. J. Occup. Environ. Med. 60 (2003): 16-26.

Griffin M.J., Macfarlane C.R. and Norman C.D. *The Transmission of Vibration to the Hand and the Influence of Gloves*. In: Brammer A.J. and Taylor W. (Eds.) Vibration Effects on the Hand and Arm in Industry. New York: John Wiley and Sons, (1982): 103-116.

Gurram R. *A Study of Vibration Response Characteristics of the Human Hand-Arm System*. Ph.D. Thesis. Concordia University, Montreal, 1993.

Gurram R., Rakheja S. and Gouw G.J. *Biodynamic Response of the Human Hand-Arm System Subject to Sinusoidal and Stochastic Excitations*. International Journal of Industrial Ergonomics 16 (1995): 135-145.

Gurram R., Rakheja S. and Gouw G.J. *Vibration Transmission Characteristics of the Human Hand-Arm and Gloves*. International Journal of Industrial Ergonomics 13.3 (1994): 217-234.

Gurram R., Rakheja S., Boileau P.E. and Gouw G.J. *Development of a Grip Force Dependent Hand-Arm Vibration Model*. Central European Journal of Public Health 40 (1996): 65-68.

Härkönen H. et al. *Symptoms of Vibration Syndrome and Radiographic Findings in the Wrists of Lumberjacks*. Br. J. Ind. Med. 41 (1984): 133-136

Hartung E., Dupuis H. and Scheffer M. *Effects of Grip and Push Forces on the Acute Response of the Hand-Arm System under Vibrating Conditions*. International Archives of Occupational Environment Health 64 (1993): 463-467.

Hayward R.A. *Measures Of Vibrotactile Sensitivity in Persons Exposed to Hand-Arm Vibration*. Scand J Work Environ Health 12 (1986): 423-427.

Herberts P. et al. *Shoulder Pain and Heavy Manual Labor*. Clinical Orthopaedics and Related Research 191 (1984).

Hewitt S. *Assessing the Performance of Anti-vibration Gloves-A Possible Alternative to ISO 10819, 1996*. Annals of Occupational Hygiene 42.4 (1998): 245-252.

Hempstock T.I. and O'connor D.E. *The Measurement of Hand Vibration, in Taylor and Pelmear (eds): Vibration White Finger in Industry*. London: Academic Press (1975): 111-122.

Hjortsberg U., RoseÂn I., Lundborg G. and Balogh I. *Finger Receptor Dysfunction in Dental Technicians Exposed to High-Frequency Vibration*. Scand. J. Work Environ. Health 15 (1989): 339-344.

Hyvärinen J., Pyykkö I. and Sundberg S. *Vibration in Frequencies and Amplitudes in the Aetiology of Traumatic Vasospastic Disease*. Lancet 1 (1973): 791-794.

ISO 10068. *Mechanical Vibration and Shock -- Mechanical Impedance of the Human Hand-Arm System at the Driving Point*. International Organization for Standardization, Geneva, Switzerland, 1998.

ISO 10068. *Mechanical Vibration and Shock -- Mechanical Impedance of the Human Hand-Arm System at the Driving Point*. International Organization for Standardization, Geneva, Switzerland, 2012.

ISO 10819. *Mechanical Vibration and Shock -- Hand-Arm Vibration -- Measurement and Evaluation of the Vibration Transmissibility of Gloves at the Palm of the Hand.* International Standards Organization, Geneva, Switzerland, 2013.

ISO 15230. *Mechanical Vibration and Shock – Coupling Forces at the Man – Machine Interface for Hand-transmitted Vibration.* International Standards Organization, Geneva, Switzerland, 2007.

ISO 5348. *Mechanical Vibration and Shock -- Mechanical Mounting of Accelerometers.* International Standards Organization, Geneva, Switzerland, *1998.*

ISO 5349. *Mechanical Vibration-Guidelines for the Measurement and the Assessment of Human Exposure to Hand-Transmitted Vibration*. International Standards Organization, Geneva, Switzerland, 1986.

ISO 5349-1. *Mechanical Vibration -- Measurement and Evaluation of Human Exposure to Hand-transmitted Vibration -- Part 1: General Requirements*. International Organization for Standardization, Geneva, Switzerland, 2001.

ISO 5349-2. *Mechanical Vibration – Measurement and Evaluation of Human Exposure to Hand-transmitted Vibration -- Part 2: Practical Guidance for Measurement in the Workplace*. International Organization for Standardization, Geneva, Switzerland, 2001.

ISO 8662-1. *Hand-held Portable Power Tools -- Measurement of Vibrations at the Handle -- Part 1: General*. International Organization for Standardization, Geneva, Switzerland, 1988.

ISO 8662-2. *Hand-held Portable Power Tools -- Measurement of Vibrations at the Handle -- Part 2: Chipping Hammer and Riveting Hammers.* International Organization for Standardization, Geneva, Switzerland, 1992.

ISO 8662-11. *Hand-held Portable Power Tools -- Measurement of Vibrations at the Handle -- Part 11: Fastener Driving Tools.* International Organization for Standardization, Geneva, Switzerland, 1999.

Iwata H. *Effects of Rock Drills on Operators. Part I: Vibration of Rock Drills and Air*

Temperature at Pits. Japan Journal of Ind. Health 6 (1968): 28-36.

Iwata H. *Effects of Rock Drills on Operators. Part II: Survey and Examination on Raynaud's Phenomenon*. Industrial Health 6 (1968): 28-46.

Iwata H., Dupuis H. and Hartung E. *Übertragung von Horizontalen Sinusschwingungen auf die Oberen Extremitäten bei Halbpronationsstellung und Reaktion des M. Biceps*. Int. Arch. für Arbeitsmed 30 (1972): 313-328.

Jahn R. and Hesse M. *Applications of Hand-Arm Models in the Investigation of the Interaction between Man and Machine*. Scand. J. Work, Environment & Health 12 (1986): 343-346.

Kihlberg S. *Biodynamic Response of the Hand-Arm System to Vibration from an Impact Hammer and a Grinder*. International Journal of Industrial Ergonomics 16 (1995):1-8.

Lindell H. *Redesign of Hand-Held Impact Machines to Reduce Hand-Arm Vibration*. Canadian Acoustics 39.2 (2011):80-81.

Mallick Z. *Optimization of Operating Parameters for a Back-pack Type Grass Trimmer*. International Journal of Industrial Ergonomics 38.1 (2008): 101-110.

Mallick Z. *Optimization of the Operating Parameters of a Grass Trimming Machine*. Applied Ergonomics 41.2 (2010): 260-265.

Marcotte P., Aldien Y., Boileau P.-E., Rakheja S. and Boutin J. *Effect of Handle Size and Hand–Handle Contact Force on the Biodynamic Response of the Hand–arm System under Zh - axis Vibration. Journal of Sound and Vibration 283.3-5 (2005): 1071-1091.*

Maricq H.R., Carpentier P.H., Weinrich M.C., et al. *Geographic Variation in the Prevalence of Raynaud's Phenomenon: a 5 Region Comparison*. J. Rheumatol. 24 (1997): 879–89.

Maricq H.R., Carpentier P.H., Weinrich M.C., et al. *Geographic Variation in the Prevalence of Raynaud's Phenomenon: Charleston, SC, USA, vs Tarentaise, Savoie, France*. J. Rheumatol. 20: (1993): 70–76.

Martin F. *An Improved Biomechanical Model for Simulating the Strain of the Hand-arm System under Vibration Stress*. Journal of Biomechanics 24.12 (1991): 1165-1171.

Matsumoto K., Itoh N., Kasamatsu T. and Iwata H. *A Study on Subjective Symptoms Based on Total Operating Time of Chain Saw*. Japan Journal of Industrial Health 19.1 (1977): 22-28.

Matsumoto T., Harada N., Yamada S. and Kobayashi S. *On Vibration Hazards of Chipping Hammer Operations in an Iron Foundry*. Japan Journal of Industrial Health 23 (1982): 51-60.

Matsumoto T., Yamada S. and Harada N. *Comparative Study of Vibration Hazards among Operators of Vibrating Tools in Certain Industries*. Arhiv za Higijenu rada Toksikologiju 30 (1979): 701-707.

Meltzer G, Melzig-Thiel R. and Schatte M. *Ein Mathematisches Schwingungsmodell für das Menschliche Hand-Arm-System*. Maschinenbautechnik 29.2 (1980): 54-58.

Meltzer G. *A Vibration Model for the Human Hand-Arm System*. Studies in Environmental Science 13 (1981): 210-221.

Monney M.A., Gorman P.B. and Gonzalez J.N. *Vibration-Based Health Monitoring of Earth Structures.* Structural Health Monitoring 4.2 (2005): 137-152.

Mishoe J.W. and Suggs C.W. *Hand-arm Vibration. Part II. Vibrational Responses of the Human Hand*. Journal of Sound and Vibration 53 (1977): 545-558.

Mishoe J.W. *Dynamic Modeling of the Human Hand Using Driving Point Mechanical Impedance Techniques*. Ph.D. Thesis. Raleigh, N.C.: N.C. State Univ., 1974.

Miwa T. *Studies on Hand Protectors for Portable Vibration Tools*. Industrial Health 2 (1968): 95-105.

Miwa T., Yonekawa Y., Nara A., Kanada K. and Baba K. *Vibration Isolators for Portable Vibrating Tool. Part 1. A Grinder*. Industrial Health 17 (1979): 85-122.

Miyashita K., Shiomi S., Itoh N. et al. *Epidemiological Study of Vibration Syndrome in Response to Total Hand-Tool Operating Time*. British Journal of Industrial Medicine 40 (1983): 92-98.

Nemani L.N.N. *Vibration Analysis of a Hand-Grinder System under Wheel Unbalance Excitation*. M.A.Sc Thesis, Montreal: Concordia University, 2005.

NIOSH. Dept. of Health and Human Services, National Institute for Occupational Safety and Health. *Criteria for a Recommended Standard: Occupational Exposure to Hand-Arm Vibration*. Cincinnati, OH, USA, (1989): 89-106.

NIOSH. Dept. of Health and Human Services, National Institute for Occupational Safety and Health. *Musculoskeletal Disorder and Workplace Factors: A Critical Review of Epidemiological Evidence for Work-Related Musculoskeletal Disorders of the Neck, Upper Extremity, and Low Back.* Cincinnati, OH, USA, (1997): 97-141.

Oddo R., Loyau T., Boileau P.E. and Champous Y. *Design of a Suspended Handle to Attenuate Rock Drill Hand-Arm Vibration; Model Development and Validation*. Journal of Sound and Vibration 275 (2004):623-640.

Oliver T.P., Pethybridge R.J. and Lumley K.P.S. *Vibration White Finger in Dockyard Workers*. Arhiv Za Higijenu Rada Toksikologiju 30 (1979): 683-693.

Palesch Y.Y., Valter I., Carpentier P.H. and Maricq H.R. *Association between Cigarette and Alcohol Consumption and Raynaud's Phenomenon*. Journal of Clin. Epidemiol. 52 (1999): 321–28.

Pelmear P.L. and Wasserman D.E. *Hand-Arm Vibration: A Comprehensive Guide for Occupational Health Professionals*. Beverly Farms, MA, USA: OEM Press, 1998.

Pelmear P.L., Leong D., Taylor W., M. Nagalingam, and Fung D. *Measurement of Vibration of Hand-held Tools: Weighted or Un-weighted?* J. Occup. Med. 31.11 (1989): 902-908.

Pelmear P.L., Taylor W. and Pearson J.C.G. *Raynaud's Phenomenon in Grinders, in Taylor W. and Pelmear P.L. (Eds), The Vibration White Finger in Industry*. London: Academic press, (1974): 21-30.

Piligian G., Herbert R., Hearns M., Dropkin J, Landsbergis P. and Cherniack M. *Evaluation and Management of Chronic Work-Related Musculoskeletal Disorders of the Distal Upper Extremity*. American Journal of Industrial Medicine 37 (2000): 75-93.

Pinto I., Stacchini N., Bovenzi M., Paddan G.S. and Griffin M.J. *Protection Effectiveness of Anti-vibration Gloves: Field Evaluation and Laboratory Performance Assessment*. 9th International Conference on Hand-Arm Vibration, Nancy, France, 2001.

Pitts P. et al., *Hand-arm Vibration Emission of Chainsaws-Comparison with Vibration Exposure*. Derbyshire: HSL, 2004.

Politschuk A.P. and Oblivin V.N., *Methods of Reducing the Effects of Noise and Vibration on Power Saw Operators*. Proc. International Occupational Hand-Arm Vibration Conference. Cincinnati, Ohio, USA, (1971): 230-232.

Pyykkö I., Färkkilä M., Toivanen J., Korhonen O. and Hyvarinen J. *Transmission of Vibration in the Hand-Arm System with Special Reference to Changes in Compression Force and Acceleration*. Scandinavian Journal of Work, Environment & Health 2 (1976): 87-95.

Pyykkö I., Sairanen E., Korhonen O., Farkkila M. et al. *A Decrease in the Prevalence and Severity of Vibration-Induced White Fingers among Lumberjacks in Finland*. Scand. J. Work Environ. Health 4 (1978): 246- 254.

Radwin, R.G. *Neuromuscular Effects of Vibrating Hand Tools on Grip Exertions, Tactility, Discomfort, and Fatigue*, Ph.D. Thesis, The Univ. of Michigan, Michigan, USA, 1986.

Radwin R.G., Armstrong T.J. and Bergeijk E.V. *Hand-Arm Vibration and Work-Related Disorders of the Upper Limb. In: P.L. Pelmear, D.E. Wasserman, Editors*. *Hand-arm Vibration*. Beverly Farms, MA: OEM Press, (1998): 122-152.

Rajalingham C. and Rakheja S. *Analysis of Impact Force Variation during Collision of Two Bodies using a Single-degree-of-freedom System Model*. Journal of Sound and Vibration, 229.4 (2000): 823-835.

Rakheja S., Dong R.G., Welcome D. and Schopper A.W. *Estimation of Tool-specific Isolation Performance of Anti-vibration Gloves*. International Journal of Industrial Ergonomics 30.2 (2002a):71-87.

Rakheja S., Gurram R. and Gouw G.J. *Development of Linear and Nonlinear HAV Models using Optimization and Linearization Techniques*. Journal of Biomechanics 26 (1993): 1253-1260.

Rakheja S., Rajalingham C. and Boileau P.E. *Analysis of Hand-transmitted Vibration of a Hand-held Percussive Tool*. European Journal Mech. & Env. Eng. 47.3 (2002b): 141-156.

Rakheja S., Wu J.Z., Dong R.G. and Schopper A.W. *A Comparison of Biodynamic Models of the Human Hand-Arm System for Applications to Hand-held Power Tools*. Journal of Sound

and Vibration 249.1 (2002c): 55-82.

Reynolds D.D. and Falkenberg R.J. *Three- and Four-degrees of Freedom Models of the Vibration Response of the Human Hand.* Vibration Effects on the Hand and Arm in Industry (1982): 117-132.

Reynolds D.D., Wasserman D.E., Basel R., Taylor W, Doyle T.E. and Asburry W. *Vibration Acceleration Measured on Pneumatic Tools used in Chipping Hammer and Grinding Operations. In Brammer and Taylor (eds), Vibration effects on the hand and arm in industry.* New York, John Wiley & Sons, (1982): 211-224.

Reynolds D.D. and Falkenberg R.J. *A Study of Hand Vibration on Chipping and Grinding Operators. Part II: Four-Degree-of-Freedom Lumped Parameter Model of the Vibration Response of the Human Hand.* Journal of Sound and Vibration 95 (1984): 499-514.

Reynolds D.D. and Soedel W. *Dynamic Response of the Hand-Arm System to a Sinusoidal Input.* Journal of Sound and Vibration 21 (1972): 339-353.

Riera G., Vilardell M., Vaque J., Fonollosa V. and Bermejo B. *Prevalence of Raynaud's Phenomenon in a Healthy Spanish Population.* J. Rheumatol. 20.1 (1993): 66–69.

Robert J., Mereau P., Cavelier C. and Chameaud J. *Occupational Angioneurotic Problems Caused by Hand-Tool Vibrations.* Archives Des Maladies Professionnelles de Medicine du Travail et de Securite Sociale 38 (1977): 437-455.

Seppalainen A.M., Starck J. and Harkonen H. *High-Frequency Vibration and Sensory Nerves. Scandinavian.* J. of Work, Environment & Health 12 (1986): 420-422.

Starck J.P. and Pyykkö I. *Impulsiveness of Vibration as an Additional Factor in the Hazards Associated with Hand-Arm Vibration.* Scand. J. of Work, Environ. & Health (1986): 323-326.

Starck J.P., Farkilla M.A., Aatola S., Pyykkö I. and Markonen O. *Vibration Syndrome and Vibration in Pedestal Grinders.* British Journal of Industrial Medicine 40 (1983): 426-433.

Strydom J.P.D., Heyns P.S. and Niekerk J.L.V. *Development of a Vibration Absorbing Handle for Rock Drills.* The Journal of the South African Institute of Mining and Metallurgy (2002):167-172.

Suggs C.W. and Abrams C.F. Jr. *Vibration Isolation of Power Tool Operators.* Proceedings of the Human Factors and Ergonomics Society Annual Meeting 27.7 (1983): 606-610.

Suggs C.W., Abrams C.F. and Cundiff J.S. *Attenuation of High-frequency Vibration in Cain Saws.* International Journal of Sound and Vibration 2.6 (1968)

Tasker E.G. *Assessment of Vibration Levels Associated with Hand-Held Road-Breakers.* Scand. J. of Work, Environ. & Health (1986): 407-412.

Taylor W. *Biological Effects of the Hand-Arm Vibration Syndrome; Historical Perspectives and Current Research.* Journal of Acoustics Society of America 83 (1988): 415-422.

Taylor W., Wasserman D., Behrens V., Reynold D.D. and Samueloff S. *Effect of Air Hammer on the Hands of Stone Cutters*. *The Limestone Quarries of Bedford Indiana, Revisited.* British Journal of Industrial Medicine, 41 (1984): 289-295.

Taylor W., Wilcox T. and Wasserman D. *NIOSH Health Hazard Evaluation Report*. Wisconsic: Neenah Foundry Company HHE 80 (1981): 187-870.

Tominaga Y. *The Relationship between Vibration Exposure and Symptoms of Vibration Syndrome*. Journal of Science of Labor (1993): 1-14.

Walker D.D., Jones B. and Ogston S. *Occurrence of White Finger in the Gas Industry*. Scand. J. of Work, Environ. & Health 12.4 (1986): 301-303.

Walker D.D., Jones B., Ogston S., Tasker E.G. and Robinson A.J. *A Study of White Finger in the Gas Industry*. British Journal of Industrial Medicine 42 (1985): 672-677.

Watanabe M. *White Hand Disease (Local Vibration Disturbances)*. Hoppo Ringyo 209 (1966): 213-219.

Welcome D.E., Dong R.G., Xu X.S., Warren C and McDowell T.W. *An Evaluation of the Proposed Revision of the Anti-vibration Glove Test Method Defined in ISO 10819 (1996)*. International Journal of Industrial Ergonomics 42(2012):143-155.

Welsh C.L. *The Effect of Vibration on Digital Blood Flow*. British Journal of Surgery 67.10 (1980): 708-710.

Wood L.A., Suggs C.W. and Abrams C.F. *Hand-Arm Vibration. Part III: A Distributed Parameter Dynamic Model of the Human Hand-Arm Syste*m. Journal of Sound and Vibration 57 (1978):157-169.

Ying Hao K., Xin Mei L. and Ripin Z. M., *Tuned Vibration Absorber for Suppression of Hand-Arm Vibration in Electric Grass Trimmer*. International Journal of Industrial Ergonomics 41 (2011): 494-508

Ying Hao K., Xin Mei L. and Ripin Z. M. *The Design and Development of Suspended Handles for Reducing Hand-Arm Vibration in Petrol Driven Grass Trimmer*. International Journal of Industrial Ergonomics 41 (2011): 459-470.

APPENDIX

A_{LC}	6.0067e-4 m^2
A_{Lh}	4.9265e-5 m^2
A_{UC}	8.0174e-4 m^2
A_{UH}	4.9265e-5 m^2
c_{FT}	0.5 Ns/m
c_{FS}	6.5 Ns/m
D_{LH}	3.96 mm
D_{UH}	3.96 mm
$(F_S)_{min}$	70 N
g	9.8 m/s^2
$(L_{BC})_{min}$	0.16257 m
$(L_{BS})_{min}$	0.04539 m
$(L_{CBC})_{max}$	0.14642 m
l_{rod}	0.06198 m
L_{SL}	0.00889 m
L_{SU}	0.00501 m
$(L_{SP})_{min}$	0.0188 m
$(L_{TB})_{min}$	0.05885 m
L_{UH}	0.10913 m
L_{LH}	0.13717 m
M_b	0.19408 kg
M_c	4.35 kg
M_s	0.20262 kg
M_t	0.5455 kg
P_a	1.01e5 Pa
r	0.01608 m
ρ_a	1.293 kg/m^3
γ	1.4